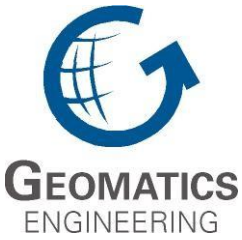

UCGE Reports
Number 20389

Department of Geomatics Engineering

Improving High Sensitivity GNSS Receiver Performance in Multipath Environments for Vehicular Applications

(URL: http://www.geomatics.ucalgary.ca/graduatetheses)

by

Peng Xie

September 2013

UNIVERSITY OF CALGARY

Improving High Sensitivity GNSS Receiver Performance in Multipath Environments for Vehicular Applications

by

Peng Xie

A THESIS

SUBMITTED TO THE FACULTY OF GRADUATE STUDIES

IN PARTIAL FULFILMENT OF THE REQUIREMENTS FOR THE

DEGREE OF DOCTOR OF PHILOSOPHY

DEPARTMENT OF GEOMATICS ENGINEERING

CALGARY, ALBERTA

SEPTEMBER, 2013

Abstract

Generally, standalone GNSS receiver architectures cannot provide a position accuracy suitable for use in vehicular applications in urban canyon scenarios. Specifically, GNSS signals are affected by the surrounding objects, such as high buildings, trees, etc., which will introduce multipath errors. Multipath arises from the reception of reflected or diffracted signals in addition to the line-of-sight (LOS) signal, and is one of the most detrimental error sources in GNSS positioning applications. By using a block processing high sensitivity receiver scheme with more correlators and/or longer coherent integration time, this thesis aims to obtain better positioning performance in the urban canyon areas.

It was reported that signal correlation peaks (e.g., LOS correlation peaks, multipath correlation peaks) may be separated in the Doppler domain by a long coherent integration time. Generally, the dominant peak is utilized in high sensitivity receivers, however, this approach is not always optimal in multipath environments since it is not assured that the dominant peak is the LOS peak. In this regard, a LOS peak identification scheme is proposed in this work, which yields better positioning performance compared to the dominant peak scheme.

Multipath distributions in the urban canyon area are characterized in this work. In particular, the Doppler frequency and code phase delay under different conditions are assessed as a function of vehicle speed and signal power. Results of this characterization is use to configure the receiver to better remove the multipath signals. More specifically, the multipath distribution will eventually affect the search strategy (i.e., search space size, coherent integration time) utilized in the high sensitivity receiver. Multipath directional-dependence phenomenon (i.e., the variation resulting from the direction of travel of the user) is observed during this process; and the multipath

maximum Doppler offset and minimum Doppler offset are derived and verified by the real data, and finally used to detect errors in the receiver's navigation solution.

It is shown that most of the multipath peaks are removed in the receiver after using the proposed algorithm; consequently, pseudorange and Doppler accuracies are improved substantially. Also, different search space sizes and coherent integration times are compared in this work and an empirically-optimal search strategy is developed. Three data sets collected in the urban canyon areas are used to assess the proposed high sensitivity receiver strategy, it is shown that the position accuracies are better than 20 m.

Acknowledgements

It is a pleasure to thank those who made this thesis possible. Foremost, I would like to thank my Supervisor, Dr. Mark Petovello for his guidance, support and continuous encouragement during my studies. His enthusiasm for advanced technologies and abundant knowledge in the field of GNSS always motivated me. Furthermore, I would like to express my gratitude to Dr. Gérard Lachapelle, he led me into the world of GNSS navigation, and it has been a wonderful learning experience.

I would like to express my thanks to Dr. Daniele Borio for his valuable discussions. I would further like to extend my thanks to those friends Srinivas Bhaskar, Billy Chan, Anup Dhital, Jingjing Dou, Zhe He, Ali Jafarnia, Rakesh Kumar, Bo Li, Tao Li, Tao Lin, G.S. Naveen, Tiantong Ren, Melania Susi, Boxiong Wang, Da Wang in the PLAN group for providing a comfortable and co-operative working environment. Their precious suggestions and discussions on my work are appreciated. I would also like to thank the person who edited the thesis for me.

I would like to thank Mohammad Abdizadeh, Dr. Saeed Daneshmand, Shuang Du, Yihe Li and other great friends I played soccer with at Calgary, who gave me a haven away from research to enjoy the summer, even if we sometimes only had four players.

The financial support of General Motors of Canada, the Natural Science and Engineering Research Council of Canada and Alberta Innovates Technology Futures is also acknowledged.

Special thanks to my wife Shiwei for standing beside me throughout my study. Her beautiful smile was always inspiring and refreshing. Finally, and most importantly, I would like to thank my parents, for their unconditional love, encouragement, and understanding through all of my

years from a small town to Beijing, and then to Canada. This work would not have been possible without their support.

Table of Contents

List of Tables

List of Figures

List of Abbreviations and Symbols

Abbreviations

A/D	Analog to Digital
A-GNSS	Assisted-GNSS
BPSK	Binary Phase-Shift Keying
C/A	Coarse/Acquisition
C/N_0	Carrier to Noise Ratio
DLL	Delay Lock Loop
DOP	Dilution of Precision
DR	Dead Reckoning
ELS	Early-Late-Slope
FLL	Frequency Lock Loop
GNSS	Global Navigation Satellite System
GPS	Global Positioning System
GSNRx	GNSS Software Navigation Receiver
HS	High Sensitivity Global Positioning System
SS	Signal Sensor
IF	Intermediate Frequency
IMU	Inertial Measurement Unit
INS	Inertial Navigation System
L1	L1 Frequency Band Centred at 1575.42 MHz
LHCP	Left-Hand Circularly Polarized
LOS	Line of Sight

MEMS	Micro Electro-Mechanical Systems
MEDLL	Multipath Estimating Delay Lock Loop
MET	Multipath Elimination Technology
MMT	Multipath Mitigating Technique
NCO	Numerically Controlled Oscillator
NI	National Instruments
OCXO	Oven Controlled Crystal Oscillator
PLAN	Position, Location And Navigation
PLL	Phase Lock Loop
PRN	Pseudorandom Noise
Q	Quadra-phase Correlator Output
RHCP	Right Hand Circularly Polarized
RF	Radio Frequency
RMS	Root Mean Square
SPAN	Synchronized Position Attitude Navigation
STD	Standard Deviation
SV	Space Vehicle
TTFF	Time-To-First-Fix
VDFLL	Vector Delay/Frequency Lock Loop
VDLL	Vector Delay Lock Loop
VFLL	Vector Frequency Lock Loop

Symbols

A	Signal Amplitude
B	Front-end bandwidth
b	Receiver clock bias
$D(t)$	Navigation data bit
d	Receiver clock drift
f	Carrier frequency
f_D	Doppler frequency
f_{IF}	Intermediate frequency
f_{LOS}	LOS signal Doppler frequency
f_{MP}	Multipath signal Doppler frequency
f_R	Frequency resolution
Δf_{LOS}	Line-of-sight signal Doppler offset
Δf_{MP}	Multipath signal Doppler offset
$\vec{H}_{MP}$	Multipath signal vector
L	C/A code chip length
LOS_{Region}	LOS region
m	Confidence level
MP_{Region}	Multipath region
$P_{\text{Protection}}$	Cross-correlation protection
$\vec{P}_S$	Satellite position vector

$\vec{P}_R$	Receiver position vector
P	Variance-covariance matrix
$R(\ )$	Correlation function
T	Chip duration time
$\vec{V}_R$	Receiver velocity vector
$\vec{V}_S$	Satellite velocity vector
$x(t)$	Spread spectrum code
Y_I	Inphase reference signal
Y_Q	Quadrature reference signal
θ	Carrier phase
τ	Code phase
τ_{LOS}	Line-of-sight signal code phase delay
τ_{MP}	Multipath signal code phase delay
σ_{LOS}	Line-of-sight signal uncertainty
σ_{MP}	Multipath signal uncertainty
λ	Signal wavelength
α	Satellite azimuth
β	Satellite elevation
δ	Signal power loss
η	Empirical constant factor

Chatper One: Introduction

Global Navigation Satellite Systems (GNSS) have been widely used in many applications. However, GNSS are not necessarily an ideal option for wireless positioning in adverse environmental conditions. Specifically, the GNSS signal is affected by the surrounding objects, such as high buildings, trees, etc., which introduce positioning errors. Multipath arises from the reception of reflected or diffracted signals in addition to the line-of-sight (LOS) signal (Ward *et al*., 2006), and is one of the most detrimental error sources in GNSS positioning applications. This is especially true in urban canyon environments where the LOS signal is highly corrupted by multipath signals from surrounding objects. Furthermore, often signal strength can be attenuated in these scenarios. The multipath errors can range from several metres to a few tens of metres in pseudorange measurements and up to a few centimetres in carrier phase measurements (Ward *et al*., 2006). In the presence of multipath, most GNSS receivers suffer degradation in position accuracy, moreover, it cannot be removed by differential GNSS processing as the multipath errors are not spatially correlated (Phelts and Enge, 2000; Weinbach *et al*., 2009).

In the multipath environment the signal strength degradation can be caused by the surrounding objects, thus the carrier to noise density ratio (C/N_0) can reach as low as 10 to 20 dB-Hz (MacGougan *et al*., 2002). If this is the case, high sensitivity receivers are required to track satellite signals. High sensitivity receivers have been developed specifically for the urban canyons, indoors, or in forests to extend GNSS positioning availability. The art of designing high sensitivity receivers is to make the signal correlation component big and/or clean when the received signal is weak (Van Diggelen, 2009), which essentially relies on a longer integration time (Bickerstaff *et al*., 2006), or more correlators (Van Diggelen, 2009). In so doing, degraded signals are accumulated together and can then be used to generate receiver measurements. Block

processing employs a large number of correlators, which can be categorized as a high sensitivity tracking strategy. Basically, the idea of block processing is to generate a grid of correlator outputs using coherent/non-coherent integration, and to use all of the values to track the signal. For illustration purpose, correlation map and correlation peak are defined first in this chapter. However, high sensitivity receiver design will be detailed in Chapter Two.

Correlation Map ("search space"): Defines a group of correlators for a given satellite obtained using a range of locally generated code phase and Doppler frequency values. All correlators on the map have the same integration time.

Correlator Peak ("Peak"): Local maxima observed in a correlation map. Local maxima arise for two main reasons; first, if a signal is present, the maximum value of the signal correlation component will be a local maximum, and; second, in the absence of a signal, many local maxima will be seen as a result of noise.

In the block processing strategy, generally the assumption is that the LOS signal is stronger than the multipath signals. To this end, usually the correlator with largest power (*i.e.*, dominant peak) is selected as the LOS signal and the signal parameters (*i.e.*, code phase and carrier Doppler) are estimated directly from the correlator output (O'Driscoll et *al*., 2011; Lin *et al*., 2011). However, in some scenarios it is not assured that the dominant peak is the LOS peak. For example, it is possible that the LOS signal is attenuated by the high buildings in the urban canyon scenario and the receiver acquires a strong reflected signal from a building. In this case, the initial assumption is invalid and the dominant peak is not the LOS peak. Thus, the most accurate peak should be identified, and will be assumed as the LOS peak. Figure 1.1 shows an example of the block processing receiver outputs under the multipath environment, where a set of correlators are

employed in both code phase domain and Doppler domain. A LOS signal component (at the centre) and a multipath signal component are observed in the correlation map.

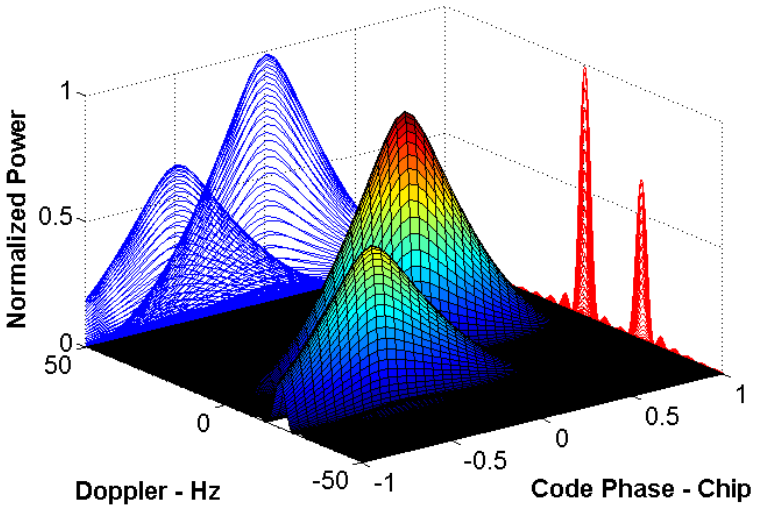

Figure 1.1: Correlation Map under the Multipath Environment

Previous research shows that generally LOS signal and multipath signal have different Doppler frequencies. Further to this, the correlation peak (e.g., LOS correlation peak, multipath correlation peak, etc.) can be separated in the frequency domain by a long coherent integration time (Soloviev *et al.*, 2008; O'Driscoll *et al.*, 2011; Xie *et al.*, 2011), which motivates this research to separate signals in the block processing receiver for vehicular applications. With this in mind, the main concern of this research is to identify the most accurate peak (or assumed LOS peak) in the correlator block. In so doing, better receiver performance would be expected after separating the LOS peak from multipath peaks. It should be noted that the main concern of this work is not to track more satellites than the general high sensitivity receiver, but, to obtain better measurements. The novel part of this research is to propose a strategy to extract more accurate signal information in the multipath environments.

This thesis is focused on the design and implementation of a block processing high sensitivity receiver. The thesis expands on previous research on the high sensitivity receiver design and the multipath signals are intensively assessed. Also, the performance of the proposed high sensitivity receiver strategy is evaluated under various operational environments. This chapter presents literature review in the field of GNSS system and multipath mitigation techniques. The limitations of methodologies reviewed are described and some methods of expanding upon these are proposed.

1.1 Background

1.1.1 Global Navigation Satellite System

Global Navigation Satellite Systems (GNSS) are all-weather, worldwide, continuous coverage, satellite-based radio navigation systems. Currently, the U.S. Global Positioning System (GPS) and the Russian Global Navigation Satellite System (GLONASS) are mostly commonly used GNSS and each provides nearly uniform, worldwide accuracy. Moreover, the Chinese Compass system (Beidou) has begun offering services to customers in the Asia-Pacific region and plans to begin serving global customers from 2020 onwards; and the Europe's Galileo navigation system will provide a highly accurate, guaranteed global positioning service under civilian control upon its completion. GNSS receivers provide pseudorange, carrier Doppler and carrier phase measurements, and ultimately the position and velocity of the receiver. Further to this, GNSS receivers are available at reasonable prices (Farrell, 2008).

GNSS signal characteristics are well known and widely available in the literature (Van Dierendonck, 1992; Parkinson *et al.*, 1996; Kaplan and Hegarty, 2006). Several signals are transmitted by the recent GPS satellites, e.g., L1, L2, and L5 (Kaplan and Hegarty, 2006). In this research, only GPS L1 C/A signals are considered for weak signal processing (the same concept

can also be applied to other signals). The L1 signal centered at 1575.42 MHz is modulated by a civilian signal (Coarse Acquisition, or C/A), and two military signals. The broadcasted L1 C/A signal is of the form shown below (Misra and Enge, 2006)

$$s(t) = AD(t)x(t)\cos(2\pi ft + \theta) \tag{1.1}$$

where A : Transmitted signal amplitude

$D(t)$: Navigation data bits at 50 Hz rate

$x(t)$: Spread spectrum code at a chipping frequency of 1.023 MHz

$\cos(2\pi ft + \theta)$: Radio frequency carrier, f is carrier frequency, and θ is transmitted carrier phase

GPS satellites use spread spectrum techniques to transmit the navigation data. Spread spectrum code will be briefly introduced in section 2.1.2 where the C/A code properties are discussed. The GPS navigation message contains information, which is necessary to perform receiver navigation computations, e.g., satellite orbit and timing information (Parkinson *et al*., 1996). The navigation data are binary phase-shift keying (BPSK) modulated onto the GPS carrier with a bit duration of 20 ms. Thus, the coherent integration duration time employed in the receiver is generally less than 20 ms for those applications where the receiver is under the open-sky conditions. In particular, 20 ms integration interval is sufficient for open-sky scenarios. However, longer integration time is required for degraded signal scenarios. In this regard, non-coherent integration has been previously applied to deal with navigation data bit transition for weak signal processing

(Borio *et al*., 2008; van Diggelen, 2009). Yet, coherent integration is of most interest in this research as the goal is to separate the LOS signal and multipath signals in the Doppler domain, which cannot be fulfilled by a non-coherent integration.

The received LOS signal can be written as:

$$s_{LOS}(t) = A_{LOS} D(t-\tau_{LOS}) x(t-\tau_{LOS}) \cos\left(2\pi(f + f_{LOS})t + \theta_{LOS}\right) + n(t) \quad (1.2)$$

where A_{LOS} : Received LOS signal amplitude

τ_{LOS} : LOS code phase delay

$\cos\left(2\pi(f + f_{LOS})t + \theta_{LOS}\right)$: Received radio frequency carrier, f is carrier frequency, f_{LOS} is LOS Doppler frequency, and θ_{LOS} is received LOS carrier phase

$n(t)$: Receiver noise

The unknown parameters of interest in the incoming signal are the code phase, Doppler frequency, and carrier phase (Ward *et al*., 2006), which can be obtained in the receiver after signal acquisition and tracking (Spilker *et al*., 1996). The Doppler frequency is of most critical parameter in this research, so the next section will introduce the theory behind the Doppler frequencies of LOS signal and multipath signals.

1.1.2 Doppler Effect and Multipath Signals

The Doppler effect - also referred to as Doppler frequency or simply Doppler - is defined as the change in frequency of a wave for an observer moving relative to its source (Ray, 2000; Misra and Enge, 2006). Given the context of this research, the Doppler frequency is the signal frequency change from satellite to receiver. The Doppler frequency is defined by

$$f = \frac{\left(\vec{V}_S - \vec{V}_R\right)\vec{H}^T + d_R}{\lambda} \tag{1.3}$$

where $\vec{V}_S$: Satellite velocity vector

$\vec{V}_R$: Receiver velocity vector

$\vec{H}$: Signal vector pointing from receiver to satellite

d_R : Receiver clock drift

λ : Signal wavelength, e.g., 0.1902 m for GPS L1 signal

For the LOS signal the signal vector is defined by

$$\vec{H}_{LOS} = \frac{\vec{P}_S - \vec{P}_R}{\left\|\vec{P}_S - \vec{P}_R\right\|} \tag{1.4}$$

where $\vec{P}_S$: Satellite position vector

$\vec{P}_R$: Receiver position vector

Alternatively, given the satellite azimuth and elevation from receiver to satellite, the signal vector can be described as

$$\vec{H}_{LOS} = \begin{bmatrix} \sin\alpha\cos\beta & \cos\alpha\cos\beta & \sin\beta \end{bmatrix} \tag{1.5}$$

where α : Satellite azimuth in the local level frame

β : Satellite elevation in the local level frame

Notice that the definitions given in Equations (1.4) and (1.5) are not necessarily the same, more specifically, the coordinate systems are different. Substituting Equation (1.4) or Equation (1.5) to Equation (1.3) yields the LOS signal Doppler frequency

$$f_{LOS} = \frac{\left(\vec{V}_S - \vec{V}_R\right)\vec{H}_{LOS}^T + d_R}{\lambda} \tag{1.6}$$

However, it is not necessarily true that the LOS signal is the only signal acquired by the receiver. The GNSS signal is affected by the surrounding objects such as high buildings, trees, etc., which will introduce multipath errors. In vehicular applications, the instantaneous frequency of multipath signals in a moving vehicle can be significantly different from the LOS signal (Misra and Enge, 2006). Figure 1.2 shows an example of multipath signal reflected by a surrounding object (e.g., a high building). The green lines are LOS signals from the satellite (effectively parallel), the red line is the reflected signal, or the multipath signal.

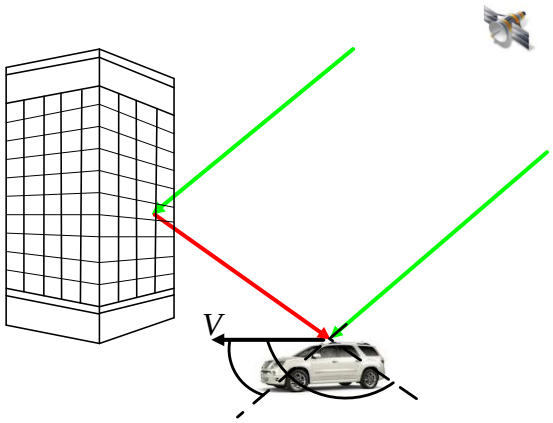

Figure 1.2: Illustration of LOS Signal and Multipath Signal in the Urban Canyon Environment

A multipath signal can be described as

$$s_{MP}(t) = A_{MP} D(t-\tau_{MP})\, x(t-\tau_{MP}) \cos\left(2\pi(f + f_{MP})t + \theta_{MP}\right) + n(t) \tag{1.7}$$

where A_{MP} : Received multipath signal amplitude

τ_{MP} : Multipath code phase delay

f_{MP} : Multipath Doppler frequency

θ_{MP} : Multipath carrier phase

The multipath Doppler frequency f_{MP} is based on the same concept as the LOS signal, however, the magnitude of the Doppler frequency is generally different compared to the LOS signal. This is due to the signal (*i.e.*, multipath signal) vector changing during the reflection or diffraction process. Notably, velocity vector will be projected differently onto the LOS vector and multipath vector for each case. The multipath Doppler frequency is defined by

$$f_{MP} = \frac{\vec{V}_S \vec{H}_{LOS}^T - \vec{V}_R \vec{H}_{MP}^T + d_R}{\lambda} \tag{1.8}$$

where $\vec{H}_{MP}$: Multipath vector (red line as shown in Figure 1.2)

A two-path signal model was proposed by Van Dierendonck (1996) under the multipath environment, which includes a LOS signal and a multipath signal

$$\begin{aligned} S = {} & A_{LOS} D(t-\tau_{LOS}) x(t-\tau_{LOS}) \cos\left(2\pi(f + f_{LOS})t + \theta_{LOS}\right) \\ & + A_{MP} D(t-\tau_{MP}) x(t-\tau_{MP}) \cos\left(2\pi(f + f_{MP})t + \theta_{MP}\right) + n(t) \end{aligned} \tag{1.9}$$

Generally, the following statements are proposed for multipath signals (Townsend and Fenton, 1994):

- The multipath signal will always arrive after the direct path signal (*i.e.*, LOS) because it travels a longer distance, *i.e.*, $\tau_{MP} > \tau_{LOS}$
- In dynamic scenarios, multipath signals generally have different Doppler frequencies compared to the LOS signal, *i.e.*, $f_{MP} \neq f_{LOS}$
- The multipath signal amplitude is generally weaker than the direct path signal, *i.e.*, $A_{MP} < A_{LOS}$

1.1.3 Urban Canyon Environment for Vehicular Applications

The main objective of this research is to improve the high sensitivity receiver performance in the urban canyon areas. Urban canyon applications are generally characterized as severe multipath environment with many tall buildings. Figure 1.3 shows an example of the urban canyon environment. Corresponding challenges are listed below (u-blox, 2010):

- At least four satellites must be identified before a position can be determined,
- Tall buildings, which can block and/or reflect GNSS signals,
- Multi-level roads, overpasses, and bridges will block GNSS signals.

Figure 1.3: Example of Urban Canyon Environment (Left: High Buildings, Right: Building Connections)

To address the detrimental effects from the multipath signals in the urban canyon area, the positioning results from a commercial high sensitivity receiver are shown first. Figure 1.4 shows the receiver performance (yellow line) where large position variations are observed; the reference trajectory (red line) is also plotted for comparison. The possible reason for the position variations is that the multipath signals are identified as LOS signals in the receiver, which introduces large pseudorange and Doppler errors. To this end, it is crucial to mitigate the multipath signals in the urban canyon applications. Section 1.1.4 will introduce several general techniques that have been proposed to mitigate multipath errors in the past decades.

Figure 1.4: Commercial High Sensitivity Receiver Performance for the Urban Canyon Applications (Red: Reference; Yellow: Commercial High Sensitivity Receiver) (plotted in Google Earth™)

1.1.4 Multipath Mitigation Techniques Overview

Code and carrier multipath is still a major challenge for high precision GNSS applications. Various multipath mitigation schemes have been proposed in the last few decades. In general, the multipath mitigation techniques operate in three areas: the antenna/hardware domain (Townsend and Fenton, 1994; Moelker, 1997; Filippov *et al.*, 1998; Bartone and Van Graas, 1998; Izadpanah, 2009), the signal processing domain (Fenton *et al.*, 1991; Townsend and Fenton, 1994; Weil 1995; McGraw and Braasch, 1999), and the navigation domain (Giremus *et al.*, 2007, Spangenberg *et al.*, 2008).

From the antenna/hardware perspective, attempts were made to eliminate the multipath signals at the pre-reception stage (*i.e.*, before signal processing). Antennas-based multipath mitigation technologies involve improving the antenna gain pattern to overcome the multipath (Ray *et al.*, 1998). The most common methods are choke ring ground planes and careful site selection (Townsend and Fenton, 1994). The main purpose of the choke ring design is to eliminate the

signals reflected from the Earth surface (Filippov *et al*., 1998). Since the GNSS signal has a right-hand circular polarization (RHCP), choke ring ground plane is very effective in this regard (Ray *et al*., 1998). The left-hand circularly polarized (LHCP) signals are removed by a specific antenna design (Bartone and Van Graas, 1998). However, it is not easy to change the antenna parameters, moreover, these methods are not always practical, especially in a kinematic environment (Jones *et al*., 2004). To this end, choke ring design is now typically only used for high accuracy static applications.

Therefore, the most important multipath mitigation approaches are correlation techniques (Irsigler and Eissfeller, 2003) implemented internally inside the receiver. One particular situation in the multipath environment is when the LOS signal is overlapping with one or several multipath components, which makes the range estimation process more difficult. Receivers try to correlate with the sum of all signals (*i.e.*, LOS signal and multipath signals), and as such, the presence of multipath signals will corrupt the correlation function. In this regard, several techniques have been proposed to mitigate the multipath errors in the correlation function domain. The internal correlation techniques can be categorized to mitigation approaches and estimation approaches (Lentmaier *et al*., 2008). The mitigation approaches take advantage of the correlation shape in the code phase domain. Some well-known examples of this category are the narrow correlator method (Fenton *et al*., 1991), multipath elimination technology (MET), strobe and edge correlator (Garin *et al*., 1996), and enhanced strobe correlator (McGraw and Braasch, 1999). Another category uses estimation techniques, which treat the multipath as something to be estimated from the correlators (Lentmaier *et al*., 2008), and using different efficient maximization strategies over the likelihood function, e.g., multipath mitigating technique (MMT)

(Weil, 1995), multipath estimating delay lock loop (MEDLL), and vision correlators (Fenton and Jones, 2005) were proposed and are less susceptible to the multipath.

The first major breakthrough in pseudorange multipath mitigation was the narrow correlator design (Fenton *et al*., 1991; Betz and Fine, 2000). For the conventional receiver design, one chip spacing (*i.e.*, wide-spacing) between the early and late correlators concept is used in most commercial C/A code receivers. The narrow correlator technique was proposed by Fenton *et al*. (1991) to minimize the multipath impact on traditional early and late discriminators by employing narrow spacing (e.g., 0.1 chips) between the early and late arms in the DLL. The improvements offered by narrow correlator arise from a wide front-end bandwidth in the receiver, which sharpens the correlation peak in the code phase domain, allowing the discriminator to still work in the linear region (Weil, 1997). The narrow correlator technique makes the hardware more complex due to a large front-end bandwidth required.

Further improvements of the narrow correlator technique are achieved by employing more than the early and late correlators; adding two more correlators, one each on the early and late sides, achieved better multipath mitigation performance (Ray, 2006). With these additional correlators, the slopes of the early and late sides can be measured, which subsequently led to the early-late-slope (ELS) correlator, also known as multipath elimination technique (MET) (Townsend and Fenton, 1994). MET method takes full advantage of the narrow correlator spacing design, but is much more resistant to multipath effects on the correlation function. The slope of the two sides of the correlation peak is estimated and the intersection point can be computed, which is used for the pseudorange correction (Irsigler and Eissfeller, 2003). Theoretically, MET method eliminates any long delay multipath, if the bandwidth is infinite (Van Dierendonck and Braasch, 1997).

However, the performance is limited due to the flatness of the correlation peak in the band-limited system.

Some other techniques that also take advantage of the additional two arms are the high resolution correlator, strobe correlator, and pulse aperture correlator. High resolution correlator can be interpreted as a narrow correlator (Irsigler and Eissfeller, 2003), which employs 0.1 chip early and late spacing and 0.2 chip very early and very late chip spacing (Bhuiyan *et al*., 2008). The Strobe Correlator employs a double delta discriminator (Ray, 2006). Double Delta discriminator employs two correlator pairs in the code phase tracking loop. The general concept was introduced in detail by McGraw and Braasch (1999). Essentially, the code discriminator can be set up by forming two pairs of correlators (*i.e.*, two early and two late).

The techniques mentioned above employ some specific discriminators to take full advantage of the correlation shape in the code phase domain. However, the multipath peak still exists in the correlation function. To this end, multipath mitigating technique, multipath estimating delay lock loop (MEDLL), and vision correlator employ another way to mitigate the multipath errors, which are based on the optimal estimation theory. The MEDLL method is addressed in the rest of this section.

The MEDLL approach proposed by Van Nee (1992) involves the decomposition of the correlation function into direct path and multipath components, which estimate the amplitude, path delay, and carrier phase of each signal by using maximum likelihood criteria, and in so doing, reduce both code and carrier multipath errors simultaneously. Basically, solving the MEDLL equations is similar to conducting a nonlinear fitting of the correlation function (Van Nee *et al*., 1994). The best combination of LOS and multipath signals is determined first, after

that, a peak removal process is conducted to remove the multipath peaks one by one. Once this peak removal process is complete, only the direct path is left. Then, a standard early and late DLL is used to estimate direct path component. However, the number of multipath signals is also unknown and has to be estimated in the MEDLL. Theoretically, an infinite number of multipath peaks can be present due to surrounding objects (Townsend *et al*., 1995). The simplest strategy is to choose a fixed value for this number in the MEDLL method (e.g. five), or a threshold is employed to stop the MEDLL process (Van Nee, 1992). However, the performance is degraded, when the assumptions were not proper. MEDLL method almost eliminates long delay multipath errors in GNSS receivers (Ray, 2006), and shows better performance than narrow and wide early and late DLLs, but it does not eliminate all multipath errors (Bhuiyan *et al.*, 2008).

1.1.5 Dead-Reckoning

Dead reckoning is the process of calculating one's current position and velocity by using a previously determined position and velocity, as well as the change of these parameters over a time interval. To overcome the drawbacks of GNSS system in the degraded signals condition, dead-reckoning (DR) was proposed in the vehicular applications to integrate with the GNSS system. Onboard vehicle sensors have been widely used, so information may be available on how to bridge gaps when the GNSS signal is not available or severely attenuated by the surrounding objects. This information may improve both the availability and accuracy of the navigation system (Li *et al*., 2010).

Varied sensor configurations can be utilized in the DR system, for cost sensitive vehicular applications, reduced Micro Electro-Mechanical Systems (MEMS) inertial measurement unit (IMU) with two accelerometers and one gyroscope, or three accelerometers and one gyroscope have been used recently. The reduced IMU algorithm and ultra-tight GNSS/DR system were

detailed by Li *et al*. (2010). To further limit the error induced from the reduced IMU configuration, a wheel speed sensor can be used to improve navigation accuracy and system redundancy (Niu *et al*., 2007), which is standard equipment in most vehicles. Those sensors are combined together to feed into the ultra-tight integration filter, and in so doing, improve the navigation performance. It is reported that the GNSS/DR ultra-tight integration system outperforms a standard GNSS receiver in terms of tracking and navigation (Li *et al*., 2010).

1.1.6 Software Receiver Introduction

The GSNRx™ software receiver is employed in this research to process the GNSS signals. GSNRx™ is a C++ based GNSS software receiver developed in the Position, Location And Navigation (PLAN) group at the University of Calgary (Petovello *et al*., 2008; O'Driscoll, 2009). GNSS software receivers replace the core components of the hardware receivers with software-based signal processing techniques. Software receivers have achieved a high level of maturity. The flexibility of software implementations allows rapid modifications of the receiver functions and parameters, which is not possible in the hardware implementations (Borre *et al*., 2006).

The high sensitivity version of the GSNRx™ software receiver was used in this research to assess the block processing strategy under the weak signal scenarios (will be detailed in section 2.2). Moreover, external navigation data bit aiding was applied in the proposed high sensitivity receiver, which could be defined as an assisted-GNSS (A-GNSS) architecture. A-GNSS improves the standard GNSS performance by providing external information that can be used to reduce the time-to-first-fix (TTFF), or improve the receiver sensitivity, etc. (van Diggelen, 2009). In this research, the A-GNSS refers to the navigation data bit aiding via wireless links, or recorded in a base station for the post processing purpose to be used in the receiver to wipe-off the navigation data bit during the coherent integration process. And in so doing, a longer than 20

ms coherent integration time is possible. As a part of the research, the tracking functions in the GSNRx™ high sensitivity receiver were modified to implement the proposed peak identification scheme.

1.2 Limitations of Previous Works

Previous multipath mitigation techniques have been proven very successful for long path delay, however, much of the work done so far is focused on the multipath mitigation in the code phase domain. In the mitigation approach aspect, the assumption for those techniques is that the correlation function is clean, yet, degraded performance is obtained when the correlation function is corrupted by noise. Specifically, in degraded signal environments, the correlation function cannot be considered as a clean shape anymore and thus cannot be easily employed in low signal to noise ratio scenarios. Moreover, existing receiver multipath mitigation algorithms are only effective in reducing error due to long path delay. The reason is that the correlation function distortion caused by the short path delay cannot be identified by the conventional methods due to the band-limited system. In the estimate approach aspect, the advantage of MEDLL is that it reduces the influence of multipath signals by estimating both LOS and multipath parameters (Bhuiyan *et al*. ,2008). The MEDLL shows better performance than narrow and wide early and late DLLs, but it does not completely eliminate all multipath errors. Generally, MEDLL is applied in the reference station case, where it is a quite open sky scenario and only one or two multipath signals exist (Fenton *et al*., 1991). Even so, this cannot be true in the multipath scenarios, such as urban canyon and under dense foliage. Usually the estimation of the number of multipath peaks is not addressed in the previous research, yet, it is crucial to correctly estimate the current number to avoid the over determination problem (Lentmaier *et al*., 2008). Degraded performance is obtained when the assumptions are not proper. Furthermore,

generally a 20 ms coherent integration time is used in the receiver design. In this regard, the correlation components for different Doppler offsets are more likely to be overlapped, which complicates removal of the multipath signals.

Existing commercial high sensitivity receivers suffer significant degradation in the multipath environments due to restricted visibility of available satellites. Even if a sufficient satellite constellation is available, the noise and multipath can lead to large position and velocity errors. The high sensitivity receiver introduced by Van Graas *et al*. (2005, 2009) is integrated with a high-cost tactical IMU, which generally is not feasible in the commercial applications. In the block processing strategy, normally the assumption is that the LOS signal is stronger than the multipath signals (O'Driscoll *et al*., 2011). To this end, commonly the correlator with largest power is selected as the LOS signal and put into the navigation filter. Nevertheless, this is not true in some scenarios. Take urban canyon scenarios for example where it is possible that the LOS signal is blocked by the high buildings and the receiver receives a strong reflected signal from a building. In this case, the initial assumption is invalid and the dominant peak is not the LOS peak (Xie and Petovello, 2011), which will introduce large positioning errors in the system. Although past studies have looked at using block processing in high sensitivity receivers, little work has been directed at exploiting block processing for identifying the LOS peak. In particular, for block processing receivers, the multipath characteristics should affect the size of the search space around the LOS parameters (ideally, it should be large enough to allow for a reliable tracking but not so large as to include multipath signals) as well as the coherent integration times used (which affect the ability to separate LOS and multipath signals in the frequency domain). What is more, the receiver anomaly (*i.e.*, position and/or velocity bias) in the block processing

strategy has not been discussed yet, leading to a degraded performance or even to divergence of the block processing receiver.

Although low-cost GNSS/DR systems perform well in some vehicular applications, they are vulnerable to the weak signal and multipath environment. Rather, if a standard GNSS receiver or high sensitivity receiver is utilized in the GNSS/DR system, the limits for the GNSS receivers shown above also limit the ultra-tight GNSS/DR system. In particular, the positioning errors will be accumulated in the GNSS/DR system when the update information is not available. Meanwhile, the quality of estimated attitude information (*i.e.*, heading angle, roll angle, and pitch angle) is degraded in the integration system, crucial for the GNSS/DR navigation filter.

1.3 Objective and Contributions

This research work aims at improving GNSS performance in the multipath scenarios for vehicular applications. The goal of the research is to develop a high sensitivity GNSS receiver for vehicular applications. The specific objectives are as follows:

1. *Signal correlation components separation in the Doppler domain*: Correlation components will be separated in this work by employing long coherent integration times. Further to this, a correlation model will be introduced to remove those correlation components in the correlation map. The peak separation ability is discussed in this work, in particular, a frequency resolution is defined as a benchmark to indicate the peak separation ability for varied coherent integration times.
2. *Multipath signal characterization in the urban canyon areas*. The objective of this task is to look at the GNSS signal characteristics under the urban canyon environments. Specifically, the distribution of Doppler offset and path delay of reflected signals, and the uncertainty of

those parameters. Proper understanding of the signal characteristics under multipath environments becomes vital for the design of GNSS receivers. As such, the primary objective of this task is to measure, and subsequently characterize multipath in vehicular applications for different conditions. Moreover, the multipath directional-dependence is evaluated and a receiver anomaly diagnosing scheme is proposed.

3. *Evaluate the performance of different search space sizes (i.e., size of the correlation map) and coherent integration times in the block processing method*. Different search space sizes and coherent integration times are compared in the block processing strategy. The key factors that affect the selection of the search space size and maximum coherent time are the frequency resolution, user dynamics, and the distribution of multipath peaks. A trade-off between the maximum coherent integration time, search space, required frequency resolution, user dynamics, and computation load will be made in this work. Multipath distribution results will be utilized in the integration time selection process, specifically, a coherent integration time should be large enough to separate peaks (both LOS peak and multipath peak) to prevent them from overlapping in the correlation domain. Nothwithstanding, the user dynamics will degrade the correlation performance. Furthermore, for longer integration time, a smaller search step is required in the frequency domain since the frequency resolution is improved, and as such, the computation load is increased.
4. *Compare different LOS signal extraction strategies in the high sensitivity receivers.* Dominant peak strategy and the assumed LOS peak strategy are introduced in this research to extract the receiver information (e.g., code phase, carrier Doppler). Generally the dominant peak is utilized in the block processing method (*i.e.*, by simply selecting the correlator with the largest amplitude), yet, it has been shown that the dominant peak is not always the best choice

in terms of the code phase and Doppler accuracies. In particular, it is uncertain if the dominant peak is the LOS peak. The performance of different LOS signal extraction strategies are compared in this thesis.

5. *Implement multipath signal directional-dependence to detect the receiver anomaly.* Multipath directional-dependence is proposed in this thesis as a means of detecting receiver anomalies. In particular, by using the estimated receiver velocity and known satellite geometry, LOS region and multipath regions can be respectively predicted within the receiver. Receiver anomalies can then be detected by checking the Doppler and code phase offsets of the observed correlator peaks and determining if they fall outside their respective regions. If so, the receiver estimates are deemed suspicious and the uncertainty of the solution is increased accordingly. The receiver anomaly detection performance will be assessed in this thesis.

The novel part of this thesis is to propose a new strategy to extract the useful signal information in the multipath weak signal environment to improve the navigation performance by separating LOS signal and multipath signals.

1.4 Thesis Outline

The structure of this thesis is summarized in the following paragraphs.

Chapter Two reviews theoretical background relative to the receiver designs. In this chapter, a brief overview of the standard receiver, vector-based receiver, and high sensitivity receiver is presented highlighting the different strategies proposed for the block processing receivers. Furthermore, the challenges of the high sensitivity receiver applications in the urban canyon areas are discussed. The impacts of search space size and coherent integration time selections are discussed. LOS region and multipath regions are proposed in this chapter to better identify the

LOS signals, moreover, the dominant peak strategy and the assumed LOS peak strategy are introduced.

Chapter Three provides a detailed analysis on the multipath distribution in urban canyon areas with respect to different conditions. A peak identification strategy is proposed in this chapter. In addition, signal availability in the urban canyon area is illustrated and the threshold used to identify the LOS signal is obtained. Peak separation performance under different receiver dynamics and for varied coherent integration times is evaluated.

Chapter Four concentrates on the multipath directional-dependence and an approach to detect the receiver anomaly is proposed. Different reflection geometry scenarios are employed to show the multipath directional-dependence phenomenon. Further to this, a case study is shown to illustrate how to implement the multipath directional-dependence to detect the receiver anomaly.

Chapter Five provides a detailed analysis on the high sensitivity receiver design highlighting the search space size and coherent integration time selection process. The performance of the standard receiver, high sensitivity receiver using the dominant peak strategy, and high sensitivity receiver using the assumed LOS peak strategy are compared. Specifically, the performance of a narrow search space size and a wide search space size are summarized and different coherent integration times are assessed. Furthermore, the advantages and drawbacks of the different strategies are illustrated. Finally, three data sets collected in the urban canyon area are employed to evaluate the performance of selected search strategy.

Chapter Six summarizes the work presented in this thesis, the conclusions are provided along with suggestions for future work.

Chatper Two: High Sensitivity Receivers Design

This chapter describes the theory behind the high sensitivity receiver proposed in this thesis. As shown in Chapter One, traditional GNSS receiver architectures usually lack the ability to maintain the signal lock under degraded signal environment; this is due to the signal being too weak or presence of multipath. In this regard, a high sensitivity receiver is proposed in this thesis to better track the GNSS signals for degraded signal applications. As mentioned in Chapter One the art of designing high sensitivity receivers is to make the correlation component big and/or clean when the signal is weak (Van Diggelen, 2009), which essentially relies on a longer integration time (Bickerstaff *et al*., 2006), or more correlators (Van Diggelen, 2009). Doing so, degraded signals are accumulated together and can then be used to generate observations.

The layout of this chapter is as follows. General receiver architectures are introduced first, where the signal properties, signal acquisition, and signal tracking theories are briefly reviewed. After that, high sensitivity receivers are discussed in detail. The concept of a vector-based receiver is introduced, and then, the LOS region and multipath region are derived with and without the uncertainties of the receiver estimates. Following is a signal correlation component model, introduced to identify different signals. Finally, the dominant peak strategy and assumed LOS peak strategy are proposed, to provide different schemes to extract the useful information from the receiver.

2.1 Generic GNSS Receiver Architecture Introduction

Before introducing the high sensitivity receiver employed in this research, the generic receiver architecture is introduced first. A general receiver scheme is shown in Figure 2.1. The GNSS radio frequency (RF) signals are received by an antenna and then pre-filtered, amplified, and

down-converted to intermediate frequency (IF) signals. Generally an RHCP antenna is utilized for the multipath mitigation consideration (Bartone and Van Graas, 1998). Following are the IF signals, sampled by an analog to digital (A/D) converter returning digital IF signals (Kaplan and Hegarty, 2006; van Dierendonck, 1996). Digital IF signals are then processed by a baseband processor that implements signal acquisition, signal tracking, and navigation processing. The main concern of a GNSS receiver is to estimate the code phase delay τ, Doppler frequency f_D, and - optionally - the carrier phase θ. This is done in two stages (Van Trees, 1968). The first stage is signal acquisition, where rough estimates of Doppler frequency and code phase delay are obtained; the second stage is local search to refine the estimates, namely, signal tracking. The basic purpose of the signal tracking is to generate a signal whose code phase, carrier frequency, and carrier phase matches the values of the received signal (Best, 2004).

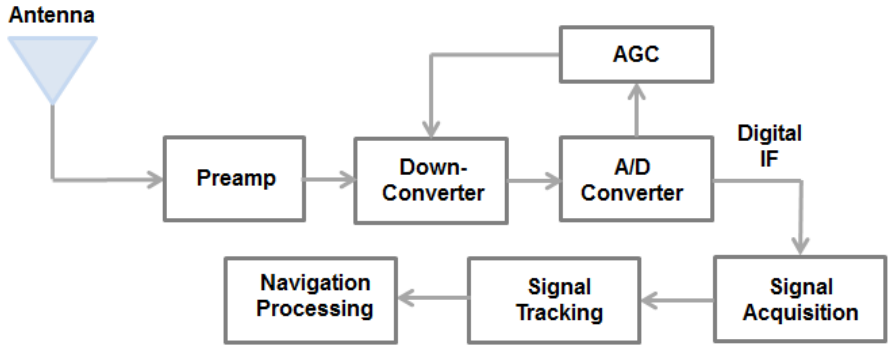

Figure 2.1: Generic Digital GNSS Receiver Diagram (Modified from Kaplan and Hegarty, 2006)

2.1.1 Signal Acquisition

The signal enters the acquisition stage after down-conversion and sampling. After down-converting, the signal is described as follows (Misra and Enge, 2006). Notice that the receiver noise is ignored in this equation.

$$s(t) = AD(t-\tau)x(t-\tau)\cos\left(2\pi\left(f_{IF} + f_D\right)t + \theta\right) \tag{2.1}$$

where f_{IF} : Intermediate frequency

The purpose of signal acquisition is to identify all satellites visible to the user (Borre *et al*., 2006), which is basically a search process (Ward *et al*., 2006). In the acquisition stage, coarse estimates of the incoming signal parameters (*i.e.*, Doppler frequency f_D and code phase delay τ) are obtained during a two-dimensional search in the Doppler domain and code phase domain. For a conventional receiver without any *a priori* knowledge of the incoming signals, the receiver would search all possible frequencies in the Doppler domain and code delays in the code phase domain. The frequency uncertainty in this case is in a range of 10 kHz to 25 kHz (Van Diggelen, 2009), which is mainly contributed by the Doppler effect, caused by the satellite motion and user dynamics, and unknown receiver oscillator frequency offset. The code delay search usually involves all possible chips, which is 1,023 chips in the code phase dimension for the GPS L1 C/A code. The search process will cover all the possible regions, still, a single correlator will be introduced first, defined as follows:

Single Correlator ("Correlator"): Value obtained after performing the Doppler wipe-off and code wipe-off, and correlation for a given Doppler frequency and code phase over a given integration interval. Doppler wipe-off and code wipe-off will be defined immediately below.

A signal correlator (*i.e.*, single correlator) block is shown in Figure 2.2, which includes three stages, namely, Doppler wipe-off (*i.e.*, stage ①), code wipe-off (*i.e.*, stage ②), and correlation (*i.e.*, stage ③). Notice that the necessary low-pass and band-pass filters are ignored in this

diagram. Also, for the purpose of the diagram, the continuous-time version of signal is shown. T_C means the coherent integration time.

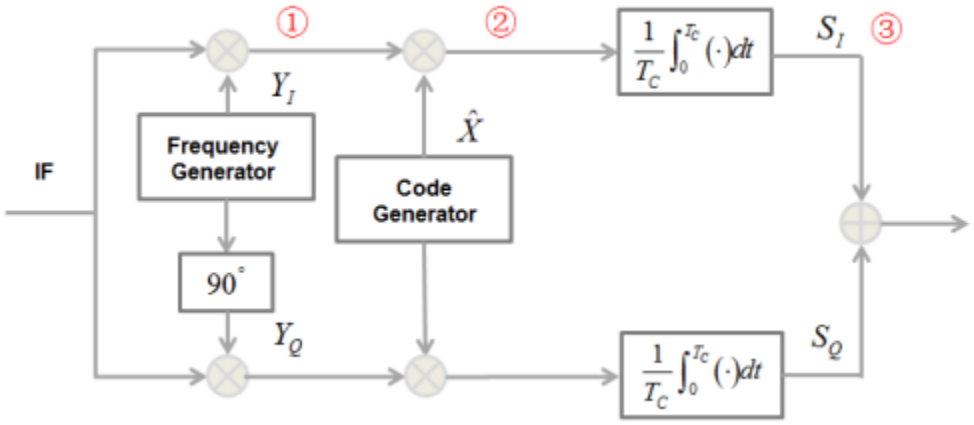

Figure 2.2: Generic GNSS Receiver Acquisition Block Diagram (Modified from Misra and Enge, 2006)

As shown in above plot, the incoming signal is then multiplied by the inphase and quadrature channels respectively. This is called Doppler wipe-off. Inphase and quadrature reference signals are respectively shown below

$$Y_I = 2\cos\left(2\pi\left(f_{IF} + \hat{f}_D\right)t + \hat{\theta}\right) \tag{2.2}$$

$$Y_Q = 2\sin\left(2\pi\left(f_{IF} + \hat{f}_D\right)t + \hat{\theta}\right) \tag{2.3}$$

where $\hat{f}_D$: Estimated carrier Doppler

$\hat{\theta}$: Estimated carrier phase

After low-pass filtering, the inphase and quadrature channels outputs are defined by (Spilker *et al*., 1996)

$$S_{I_1} = AD(t-\tau)x(t-\tau)\cos(2\pi\Delta ft + \Delta\theta) \tag{2.4}$$

$$S_{Q_1} = AD(t-\tau)x(t-\tau)\sin(2\pi\Delta ft + \Delta\theta) \tag{2.5}$$

where the subscript 1 indicates that it is the output of stage ①; Δf and $\Delta\theta$ are Doppler and carrier phase errors which are defined as

$$\Delta f = \hat{f}_D - f_D \tag{2.6}$$

and

$$\Delta\theta = \hat{\theta} - \theta \tag{2.7}$$

After Doppler wipe-off, the signals are multiplied by a local code, in a process called "code wipe-off". The local code is defined by

$$\hat{X} = x(t-\hat{\tau}) \tag{2.8}$$

where $\hat{\tau}$: Estimated code phase delay

After the code wipe-off, the signals can be described as (the same as Equations 2.4 and 2.5, here 2 indicates it is the output of stage ②)

$$S_{I_2} = AD(t-\tau)x(t-\tau)x(t-\hat{\tau})\cos(2\pi\Delta ft + \Delta\theta) \tag{2.9}$$

$$S_{Q_2} = AD(t-\tau)x(t-\tau)x(t-\hat{\tau})\sin(2\pi\Delta ft + \Delta\theta) \tag{2.10}$$

And finally, an accumulation process is conducted as a time average of Equations (2.9) and (2.10). After that, inphase and quadrature channels are obtained as follows

$$S_{I_3} = E\left(\frac{AD(t-\tau)}{T_C}\int_0^{T_C} x(t-\tau)x(t-\hat{\tau})\cos(2\pi\Delta ft + \Delta\theta)dt\right) \tag{2.11}$$

$$S_{Q_3} = E\left(\frac{AD(t-\tau)}{T_C}\int_0^{T_C} x(t-\tau)x(t-\hat{\tau})\sin(2\pi\Delta ft + \Delta\theta)dt\right) \tag{2.12}$$

where $E(\ )$ is the expectation operator. As this is the final stage of the correlation process, thus we remove the subtitle '3' from the equation and the correlation outputs can be worked out as

$$S_I = \frac{AD(t-\tau)R(\Delta\tau)}{T_C}\int_0^{T_C}\cos(2\pi\Delta ft + \Delta\theta)dt \tag{2.13}$$

$$S_Q = \frac{AD(t-\tau)R(\Delta\tau)}{T_C}\int_0^{T_C}\sin(2\pi\Delta ft + \Delta\theta)dt \tag{2.14}$$

where $R(\Delta\tau) = E\left(x(t-\tau)x(t-\hat{\tau})\right)$ is the correlation function of the C/A code (will be discussed in section 2.1.2), $\Delta\tau$ is defined as

$$\Delta\tau = \hat{\tau} - \tau \tag{2.15}$$

Finally the post-correlations of the incoming signal are defined as

$$S_I = AR(\Delta\tau)D\cdot\mathrm{sinc}(\pi T_C\Delta f)\cos(\pi T_C\Delta f + \Delta\theta) \tag{2.16}$$

$$S_Q = AR(\Delta\tau)D \cdot \mathrm{sinc}(\pi T_C \Delta f)\sin(\pi T_C \Delta f + \Delta\theta) \tag{2.17}$$

The inphase and quadrature branches are then squared and summed, removing the dependence from the input phase (Borre *et al*., 2006), and can be described as

$$S = S_I^2 + S_Q^2 = A^2 R^2(\Delta\tau) \cdot \mathrm{sinc}^2(\pi T_C \Delta f) \tag{2.18}$$

In this way, a single correlator value $S\left(\hat{f}_D, \hat{\tau}\right)$ is obtained for a given Doppler frequency $\hat{f}_D$ and code phase $\hat{\tau}$ (Borio *et al*., 2009a). The search process is then conducted in both code phase domain and Doppler domain from $\hat{f}_D \in \left[f_0 - \Re_f \quad f_0 + \Re_f \right]$ to $\hat{\tau} \in \left[\tau_0 - \Re_\tau \quad \tau_0 + \Re_\tau\right]$ as shown in Figure 2.3. The terms f_0, τ_0, $\Re_f$, and $\Re_\tau$ are defined below.

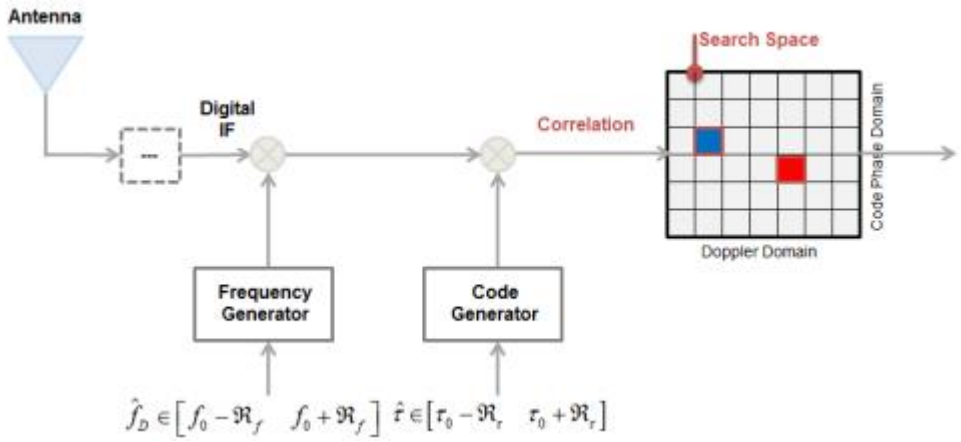

Figure 2.3: Generic Signal Correlation Diagram during the Acquisition Process

To avoid confusion, a single correlator is denoted as $S\left(\hat{f}_{D_i}, \hat{\tau}_j\right)$ (i and j indicate the indexes of the Doppler and code phase), and $S\left(\hat{f}_D, \hat{\tau}\right)$ will be used to stand for the whole correlation map.

Nominal Signal Parameters (Nominal peak): Defines the code phase and Doppler frequency values used to generate the centre of the correlation map, denoted as τ_0 and f_0, respectively. By extension, these are also referred to as the *nominal code phase* and *nominal Doppler frequency* respectively.

Search Space Size: Defines the range of correlation map in both Doppler domain (*i.e.*, $\pm\Re_f$) and code phase domain (*i.e.*, $\pm\Re_\tau$); the search space size is usually expressed with a "±" as the search process is conducted in both positive and negative planes.

A correlation map (defined in Chapter One) is obtained after the correlator values are obtained at all points in the search space. Figure 2.4 shows an example of correlation map under the open-sky condition. It is worth to address this, to be compatible with the high sensitivity receiver used in this research (which will be introduced in section 2.2), the coherent integration used is 500 ms here. Furthermore, the main-lobe width in the Doppler domain is defined by

$$f_M = \frac{2}{T_C} \tag{2.19}$$

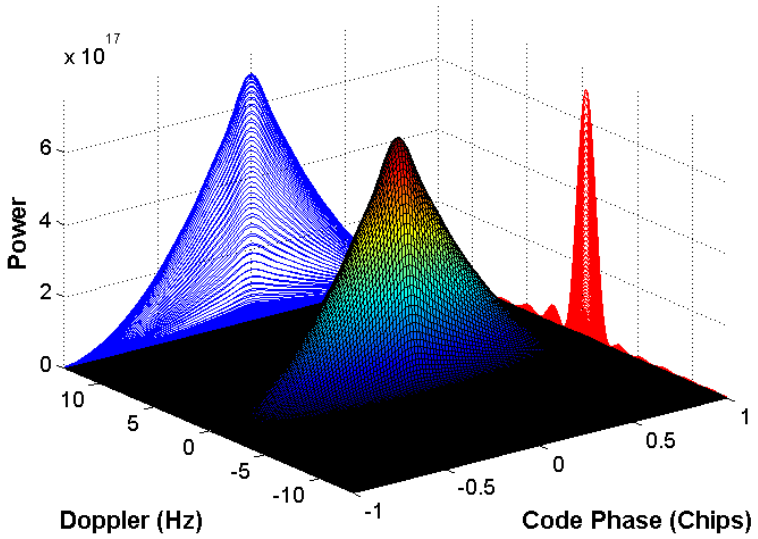

Figure 2.4: Illustration of Correlation Map under the Open-Sky Conditions

Also, some definitions can be retrieved from the correlation map:

Signal Correlation Component: The signal correlation component is the part of the correlation map that results from the presence of a single signal (be it LOS or multipath). The correlation component is also the envelope of the single signal correlation lobes. The projections of correlation component onto each domain (*i.e.*, code phase and Doppler) are illustrated in Figure 2.4. The red colour (with one main-lobe and several side-lobes in this case) is the projection on the Doppler domain. Specifically, the top red line indicates the correlation component when the code phase error is zero (*i.e.*, $S\left(\hat{f}_D, 0\right)$). The blue colour is the projection on the code phase domain. Specifically, the top blue line indicates the correlation component when the Doppler error is zero (*i.e.*, $S\left(0, \hat{\tau}\right)$).

Correlator Power: The square magnitude of a single correlator value (refer to Equation (2.18)) depends on code phase error $\Delta\tau$, Doppler error Δf, and integration time T_C. In general, this is a

unit-less quantity. Nonetheless, in this research, it is convenient to relate the correlator power to the C/N_0 of the signal used to generate it. To this end, correlator power should ideally be quoted as the "*square magnitude of the correlator obtained from a signal with a C/N_0 of xx dB-Hz*". For brevity, this will herein be shortened to "*correlator power of xx dB-Hz*".

Doppler Offset: Doppler difference between the Doppler frequency associated with a single correlator and the nominal Doppler frequency, and is denoted Δf .

Code Phase Offset: Code phase difference between the code phase associated with a single correlator and the nominal code phase, and is denoted $\Delta \tau$.

2.1.2 Correlation Properties of C/A Codes

GPS codes were selected as spreading sequences because of their auto-correlation and cross-correlation properties. The use of 1023 chips Gold codes for GPS represents a compromise between the need for rapid acquisition and the cross-correlation dynamic range. Coarse Acquisition (C/A) code is a bi-phase modulated signal with a chip rate of 1.023 MHz, thus the null-to-null bandwidth of the main lobe is 2.046 MHz (Tsui, 2005). The transmitting bandwidth in the L1 frequency is approximately 20 MHz, in this regard, many side-lobes are observed in the receiver, if a wide front-end bandwidth is employed. The correlation properties of GPS C/A code under ideal situation is shown in Figure 2.5, where the auto-correlation function of PRN 14 is plotted. The normalized auto-correlation of Gold codes can take four values as shown in Equation (2.20) (Misra and Enge, 2006)

$$R_{ii} = \left\{ 1 \quad -\frac{1}{1023} \quad \frac{63}{1023} \quad -\frac{65}{1023} \right\} \tag{2.20}$$

where i represents i th satellite.

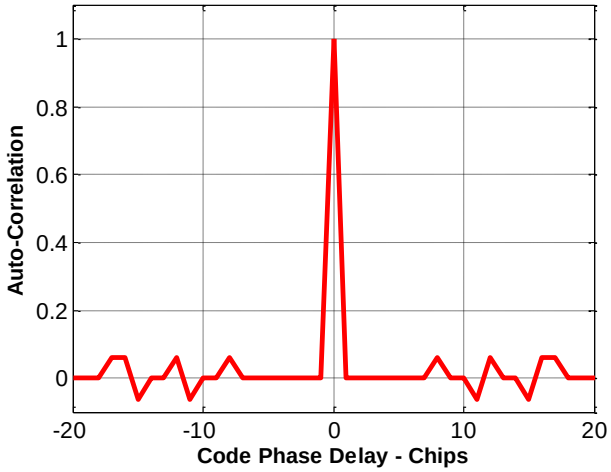

Figure 2.5: Zoom-in of Autocorrelation Function for PRN 14

The auto-correlation function within the chip duration (*i.e.*, ±1 chip) is approximated by a triangular function as shown in Equation (2.21) (Kaplan and Hegarty, 2006):

$$R(\tau)=\begin{cases} A\left(1-\dfrac{|\tau|}{T}\right), \text{ for} |\tau| \le T \\ 0 \qquad\quad , \text{ elsewhere} \end{cases} \tag{2.21}$$

where τ : Code phase offset

T : Chip duration time

However, due to a limited bandwidth in the front-end, the actual correlation function is slightly different from Figure 2.5. In particular, the peak area is smoothed by a narrow front-end bandwidth. A quadratic equation was proposed by Tsui (2005) to fit the correlation function. Still, the proposed model only performs well near the peak area.

Figure 2.6 shows the cross-correlation between two satellites (e.g., PRN 14 and PRN 17), the cross-correlation protection is defined as

$$R_{ij} = \left\{ -\frac{1}{1023} \quad \frac{63}{1023} \quad -\frac{65}{1023} \right\} \tag{2.22}$$

where i and j represent different satellites.

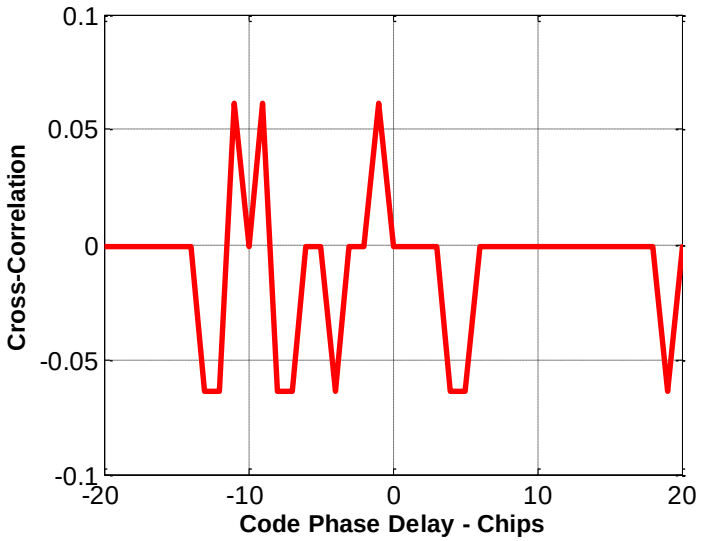

Figure 2.6: Zoom-in of Cross-Correlation Function between PRN 14 and PRN 17

In this regard, the strongest cross-correlation peak is 24 dB lower relative to the auto-correlation peak, which also suggests that the cross-correlation protection level is 24 dB.

$$P_{\text{Protection}} = 10\log_{10}\left(\frac{65}{1023}\right)^2 \approx -24\text{dB}$$

Gold codes normally work well for open-sky conditions. Furthermore, for many applications the cross-correlation peaks are negligible compared to other error sources, such as multipath errors.

On the other hand, there are certain applications where weak signal tracking is affected by presence of other strong GPS signals. A typical example would be urban canyon positioning, where weak signals may coexist with stronger signals. A typical GPS receiver in the open-sky scenario can receive a signal with a C/N_0 in the range of 45 dB-Hz to 52 dB-Hz. By extension, the maximum cross-correlation peak can reach 21 dB-Hz to 28 dB-Hz (*i.e.*, 24 dB lower) exceeding the receiver detection threshold in this context (*i.e.*, below 20 dB-Hz). In this case, the cross-correlation peak may be falsely identified as LOS or multipath peak, limiting ability to identify LOS peaks in this research. In this respect, 24 dB-Hz cross-correlation protection may not be sufficiently large.

According to Balaei and Akos (2011) cross-correlation peaks from strong signal are observed at every 1000 Hz (*i.e.*, for GPS applications) in the correlation map during weak signal correlation process. A closed formula was presented there and candidate Doppler offset of cross-correlation peaks can be defined as follows:

$$f = \Delta f + 1000 \cdot k \tag{2.23}$$

where Δf is the Doppler difference between strong signal and weak signal, and k is any integer number. A simulated case is applied here to demonstrate this phenomenon. Xie and Petovello discuss this in more detail (2012). Two satellite signals were simulated in the absence of noise with the parameters shown in Table 2.1. A coherent integration time of 10 ms is utilized in the acquisition process, yielding a Doppler resolution of 100 Hz.

Table 2.1: Signal Specifications for Strong Signal and Weak Signal for Cross-Correlation Illustration

Satellites	Power	Doppler
PRN 14	45 dB-Hz	1500 Hz
PRN 17	20 dB-Hz	200 Hz

The correlation outputs of PRN 17 are shown in Figure 2.7 over a search space in the Doppler domain of 10 kHz, and 1023 chips in the code phase domain. Note that the correlation map is centred at 200 Hz frequency (*i.e.*, PRN 17). It is clearly observed that the cross-correlation peaks appear at every 1000 Hz, that is, at -700 Hz, 300 Hz, 1300 Hz, etc. It is worth noting that there is a set of correlation peaks observed in the code phase domain associated with each Doppler candidate, different from the auto-correlation performance where the correlation peak in the code phase domain is unique.

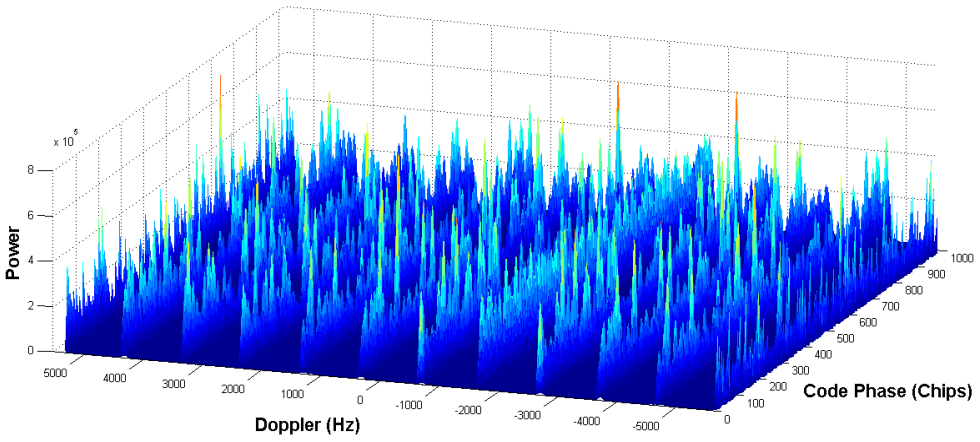

Figure 2.7: Cross-Correlation Peaks from PRN 14

The goal of this section is to identify the cross-correlation peaks among LOS and multipath peaks. Since a vector-based strategy (this will be introduced in the next section) is utilized in the

software receiver and the Doppler for satellites with weak signal can be predicted, the Doppler frequency for all satellites can be determined. By extension, the possible cross-correlation peaks can be removed or ignored. However, if the satellite Doppler cannot be accurately predicted, the cross-correlation peaks removal performance will be degraded.

2.1.3 Peak Separation Ability

According to Equations (2.18) the width of the correlation component (main lobe) in the Doppler domain is a function of coherent integration time, and this, affects the LOS peak identification performance. To this end, signal components overlapping and peak separation are identified in this research.

Signal Components Overlapping: LOS signal component and multipath signal component are overlapped in the correlation map, particularly, the main lobes are overlapped. An example is shown in Figure 2.9.

Peak Separation: Even LOS signal component and multipath signal component are overlapped in the correlation map, LOS peak and multipath peak are separable that the LOS signal parameters (associated with the LOS peak) can be extracted without losing information. The key factor that affects the peak separation ability is the LOS signal Doppler and multipath signal Doppler difference.

A two-path signal model introduced in section 1.1.2 is employed here to show the signal component overlapping phenomenon and peak separation ability. The inphase and quadrature correlator outputs of the signal expressed as that of Equation (1.9) can be described as:

$$S_I = A_{LOS} R(\Delta\tau_{LOS}) \operatorname{sinc}(\pi T_C \Delta f_{LOS}) \cos(\Delta\theta_{LOS}) + A_{MP} R(\Delta\tau_{MP}) \operatorname{sinc}(\pi T_C \Delta f_{MP}) \cos(\Delta\theta_{MP}) \quad (2.24)$$

$$S_Q = A_{LOS} R(\Delta\tau_{LOS}) \mathrm{sinc}(\pi T_C \Delta f_{LOS}) \sin(\Delta\theta_{LOS}) + A_{MP} R(\Delta\tau_{MP}) \mathrm{sinc}(\pi T_C \Delta f_{MP}) \sin(\Delta\theta_{MP}) \quad (2.25)$$

where $\Delta\theta_{LOS}$: LOS signal phase error

$\Delta\theta_{MP}$: Multipath signal phase error

The correlator power is described by Equation (2.18). Generally $\Delta\theta_{LOS}$ and $\Delta\theta_{MP}$ are different and unknown; a multipath signal may have constructive or destructive effect with respect to the LOS signal. Obviously, if the Doppler difference between the LOS signal and multipath signal is larger than the width of the main lobe in the Doppler domain (*i.e.*, f_M defined in Equation (2.19)), two signal components will not be overlapped. To this end, LOS signal parameters can be extracted without losing information. An example is shown in Figure 2.8, where the signal parameters are specified in Table 2.2. The Doppler difference between LOS and multipath signals is 10 Hz, the coherent integration time used is 200 ms (*i.e.*, $f_M = 10\,\mathrm{Hz}$), and the correlation map is centred at the 100 Hz and 0 chip. It is observed that the main-lobes associated with LOS and multipath signals are not overlapped.

Table 2.2: Signal Specifications for LOS and Multipath Signals without Overlapping

	Normalized Signal Power	Doppler Frequency	Code Phase	Carrier Phase
LOS	1	100 Hz	0 chip	0 degree
Multipath	1	110 Hz	0.2 chips	90 degrees

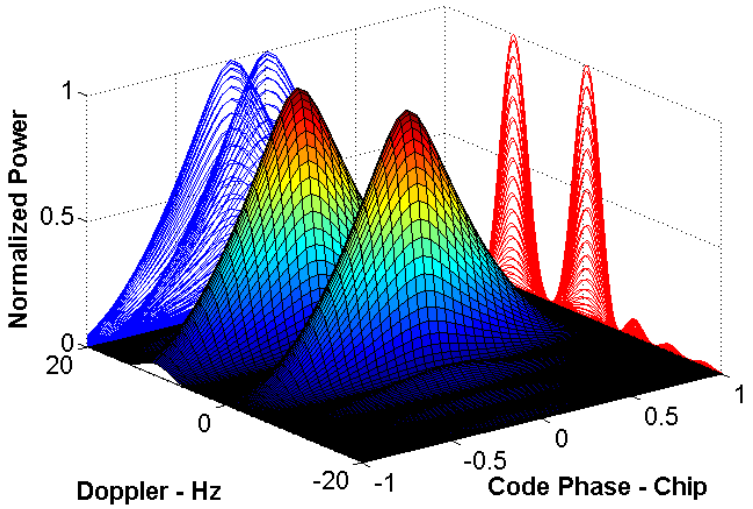

Figure 2.8: Correlation Map when the LOS signal and Multipath Signal Doppler Difference is Equivalent as the Main-Lobe Width in the Doppler Domain

Note that even the LOS signal component and the multipath signal component are overlapped in the correlation map, it is still possible to identify the LOS peak correctly without losing information. Further to this, the frequency resolution is defined in this work as a benchmark to show the peak separation ability. The frequency resolution is given by

$$f_R = \frac{1}{T_C} \tag{2.26}$$

It is observed that the frequency resolution is the width of half of the main-lobe in the Doppler domain. To illustrate, the Doppler difference is equivalent to the frequency resolution, the signal parameters are specified in Table 2.3. The coherent integration time is 200 ms, and the Doppler difference between the LOS signal and multipath signal is 5 Hz. The correlation map is shown in Figure 2.9. Three peaks are observed in the correlation map. These are listed in Table 2.4. The first two peaks are signal main lobe peaks and the third peak is a side lobe peak. It is observed

that although two signal components are overlapped, the LOS correlation peak is isolated from the multipath correlation peak. Notice that the correlation map is centred at the 100 Hz and 0 chip.

Table 2.3: Signal Specifications for LOS and Multipath Signals with Overlapping

	Normalized Signal Power	Doppler Frequency	Code Phase	Carrier Phase
LOS	1	100 Hz	0 chip	0 degree
Multipath	1	105 Hz	0.2 chips	90 degrees

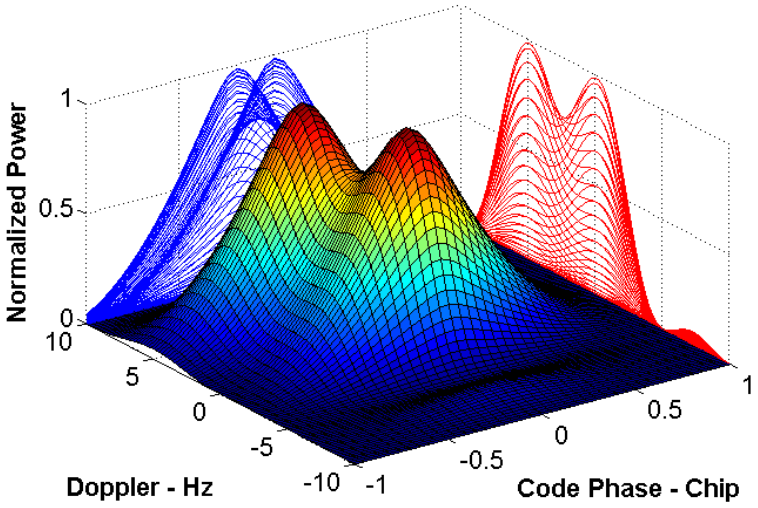

Figure 2.9: Correlation Map when the LOS signal and Multipath Signal Doppler Difference is Equivalent as the Frequency Resolution

Table 2.4: Correlation Peaks observed from the Correlation Map when the LOS signal and Multipath Signal Doppler Difference is Equivalent as the Frequency Resolution

	Doppler Offset	Code Phase Offset
1	0 Hz	0 chip
2	5 Hz	0.2 chips
3	-7.2 Hz	-0.05 chips

It is known that different signal parameters (e.g., signal power, code phase offset, carrier phase) may have different peak separation performance. For example, if the LOS signal power is much lower than the multipath signals, the LOS signal peak may not be separated from the multipath peaks when the Doppler difference is f_R. Nevertheless, frequency resolution gives a rough indication of the peak separation performance, which will be used in Chapter Three.

2.1.4 Signal Tracking

In this section, a generic GNSS tracking strategy is briefly described. Since the coarse frequency and code phase from the acquisition stage cannot meet most positioning requirements, signal tracking loops are used to refine the parameters from the acquisition. A tracking loop is a feedback system that tracks the code phase, carrier frequency or carrier frequency and phase of a received signal. The tracking loop contains three essential elements: a discriminator, a loop filter, and a numerically controlled oscillator (NCO) (Gardner, 2005).

Similar to the signal acquisition block shown in Figure 2.1, signal enters tracking loop after down-conversion and sampling. After the carrier and code wipe-off (over a pre-defined integration interval), inphase and quadrature correlator outputs are passed to the discriminators (Borre *et al*., 2006). In the standard receiver architecture, a delay lock loop (DLL) is utilized to track the code phase, while a frequency lock loop (FLL) or a phase lock loop (PLL) are utilized to track the carrier Doppler or carrier Doppler and carrier phase. The purpose of a DLL or FLL (PLL) is to generate a signal whose code phase or frequency (frequency and phase) match the code phase or frequency (frequency and phase) of the received signal (Best, 2004). A discriminator defines the type of tracking loop: for a DLL, the discriminator is used to obtain the code phase error between the received signal and the local replica; for an FLL (PLL), the

discriminator is used to obtain the frequency (phase) difference between the received signal and the local replica (Ward *et al*., 2006). Several types of frequency detector and phase detector are introduced by Ward *et al*. (2006). The errors from the discriminators are then fed to the loop filter, that then delivers a suitable control signal to the NCO to generate a local replica. Generally a first-order loop filter is utilized to track the code phase, if aided by a carrier loop, meanwhile, a second-order or third-order loop filter is utilized to track the carrier Doppler and/or carrier phase (O'Driscoll, 2009).

A DLL tracking loop is used here to briefly introduce the general tracking concept. In a conventional receiver a wide-spacing early-prompt-late (*i.e.*, one chip between the early and late correlators) DLL is employed to track the code delay. DLL measures the code phase of incoming signal and hence is used to compute the pseudorange measurements (Misra and Enge, 2006).

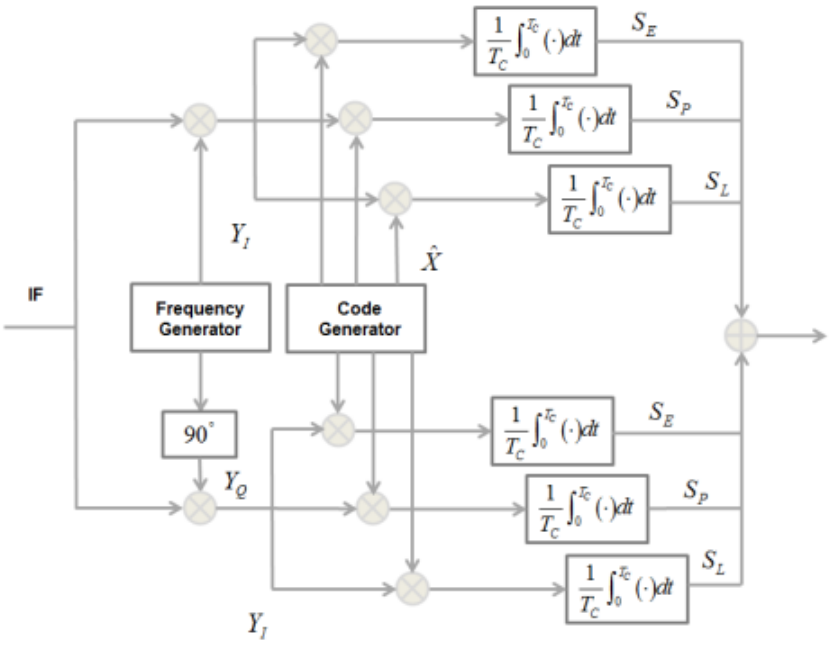

Figure 2.10: Delay-Lock-Loop Block Diagram with Early-Prompt-Late Correlators (Modified from Borre *et al*., 2006)

Figure 2.11 shows the DLL tracking performance under open-sky scenario, where a clean correlation function is observed. After employing early and late correlators the peak can be tracked properly (assume the correlator power is used in the receiver to track the signal, thus the correlation function in the code phase domain, *i.e.*, $S(0,\Delta\tau)$, is no longer a triangle).

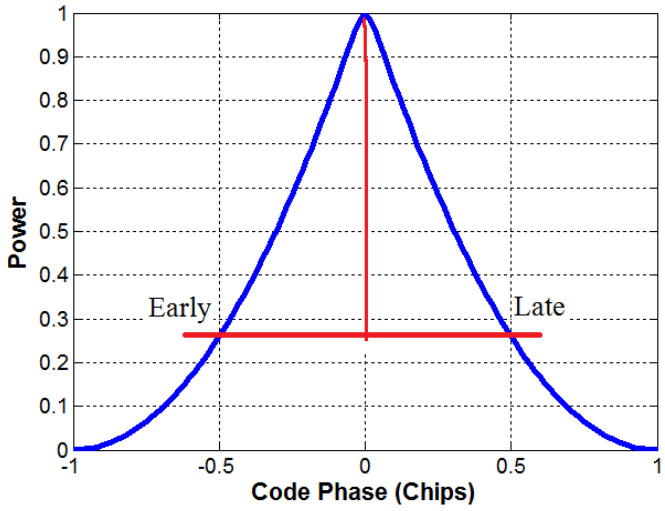

Figure 2.11: Ideal Code Phase Tracking Scenario

Yet, in the multipath environment the correlation function will be distorted by the multipath signals: an example is shown in Figure 2.12, where the LOS signal and a multipath signal are both present. The multipath signal path delay is -0.5 chips, the amplitude of the multipath signal is 80 percent of the LOS signal, and the Doppler frequency difference is 20 Hz as shown in Table 2.5.

Table 2.5: LOS and Multipath Signals Summarization for 20 ms Coherent Integration Case

	Code Phase Delay	Doppler Frequency	Normalized Signal Power
LOS Signal	0	1000 Hz	1
MP Signal	-0.2 chips	1020 Hz	0.8

If a 20 ms coherent integration time is employed (which is relatively short for weak signals, yielding a frequency resolution of 50 Hz), LOS signal correlation component and multipath signal correlation component will be overlapped together as shown in Figure 2.12. Note that correlation centered at the LOS signal parameters (*i.e.*, the correlation map centre stands for 1000 Hz Doppler frequency and 0 code phase offset). So, the receiver cannot separate these two correlation functions, thus the LOS peak will not be correctly tracked. In particular, a distorted shape (in the code phase domain) is tracked by the DLL as shown in Figure 2.13. Thus a biased pseudorange measurement is obtained.

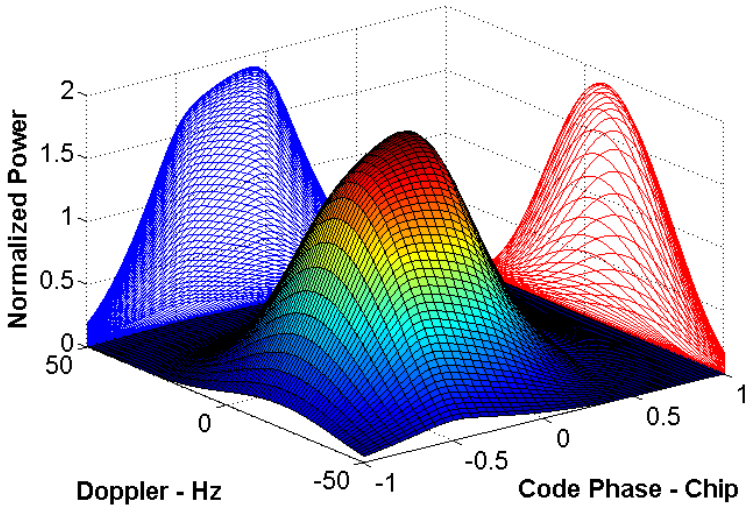

Figure 2.12: Correlation Map under the Multipath Environment for a 20 ms Coherent Integration Time

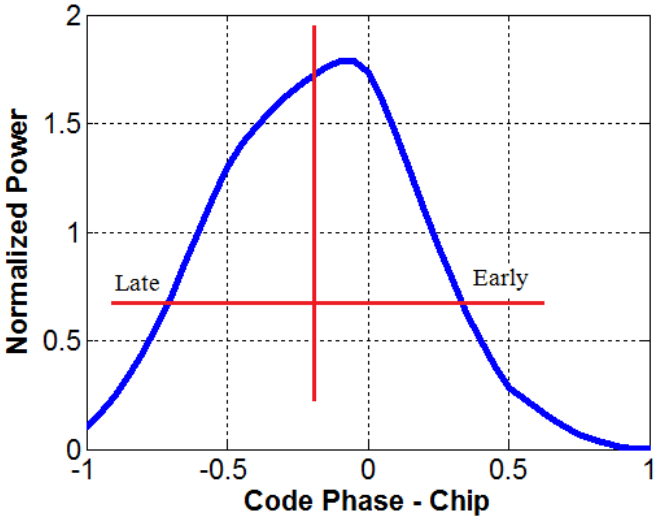

Figure 2.13: Code Phase Tracking under Multipath Environment for a 20 ms Coherent Integration Time

If LOS and multipath signals can be separated in the first place, a better code phase tracking performance is expected. This is discussed in section 2.2, where a completely new scheme is utilized to track (or refine) the code phase and carrier Doppler. More specifically, a set of correlators will be employed other than just several correlators used in the typical tracking loop.

2.2 High Sensitivity Receiver

Because of the signal degradation in the adverse environments, high sensitivity receivers were proposed to track the GNSS signals in weak signal scenarios. As mentioned before the high sensitivity receiver design relies on a longer integration time, or more correlators. Block processing employs a large number of correlators categorized as a high sensitivity strategy. The concept of block processing is presented in various publications (Van Graas *et al*., 2005, Soloviev *et al*., 2011, O'Driscoll *et al*., 2011), and will be discussed in this section compared to the standard tracking strategy with DLL and FLL (or PLL), where only a few correlators are

employed in the tracking stage. A grid of correlators is utilized in the block processing strategy, and all of the values are employed to track the signal. The signal parameters (*i.e.*, code phase and carrier Doppler) are estimated directly from the correlator outputs (although a DLL or FLL can be used to track the identified 'LOS' correlation component).

To this end, block processing strategy has attracted a lot of attention over the past few years due to its capability of tracking weak signals. It is important to mention that closed-loop signal processing method is well recognized, while block processing method remains underutilized (Van Graas *et al*., 2009). In contrast to closed-loop approaches, block processing techniques do not separate acquisition and tracking stages. A specific version will be introduced first, *i.e.*, GSNRx-ss™ receiver. And then, a more generic case will be introduced, *i.e.*, GSNRx-hs™ version, including the coherent integration time and search space size considerations. As a vector-based receiver concept is applied in both receivers, it is introduced first.

2.2.1 Vector-Based Receiver

The vector-based receiver concept was initially introduced by Spilker (1994). In a standard receiver, signal tracking is done on a satellite-by-satellite basis, with all satellites being tracked separately and no information being shared between channels. This kind of architecture is more robust and one satellite does not corrupt another. A vector-based receiver combines tracking of all visible satellites through a navigation filter that is introduced in Appendix B. It operates on a simple principle that the code phase and carrier Doppler of the received signal are based on the position and velocity of the receiver and satellite, as well as the receiver clock bias and clock drift. This way, the navigation solution is used to drive the code and frequency of numerically controlled oscillators (NCOs) in the receiver (also called nominal values). There are several vector-based schemes, such as the vector delay lock loop (VDLL) (Van Dierendonck, 1996), the

vector frequency lock loop (VFLL) (Kiesel *et al*., 2008), and the vector delay/frequency lock loop (VDFLL) (Petovello and Lachapelle, 2006). VDLL employs the receiver position, receiver clock bias, and satellite position to predict the code phases of the received satellites. VFLL employs the receiver velocity, receiver clock drift, and satellite velocity to predict the carrier Doppler of the received satellites. VDFLL is used to control both code NCO and carrier NCO. The NCO code phase (*i.e.*, nominal code phase) is determined by

$$\tau_0 = \frac{\left(\vec{P}_S - \hat{\vec{P}}_R\right)\hat{\vec{H}}_{LOS}^T + \hat{b}_R}{L} \tag{2.27}$$

where $\vec{P}_S$: Satellite position vector

$\hat{\vec{P}}_R$: Estimated receiver position vector

$\hat{\vec{H}}_{LOS}$: Estimated LOS signal vector

$\hat{b}_R$: Estimated receiver clock bias

L : Code chip length

The NCO carrier frequency (*i.e.*, nominal carrier frequency) is described by

$$f_0 = \frac{\left(\vec{V}_S - \hat{\vec{V}}_R\right)\hat{\vec{H}}_{LOS}^T + \hat{d}_R}{\lambda} \tag{2.28}$$

where $\hat{\vec{V}}_R$: Estimated receiver velocity vector

$\hat{d}_R$: Estimated receiver clock drift

The primary advantage of vector-based architectures is that noise is reduced in all channels, and the receiver is less likely to enter the non-linear tracking regions, which in turn, should improve the signal tracking ability under weak signal scenarios (Petovello and Lachapelle, 2006). Still, it is worth mentioning that the navigation solution errors will drive the NCO values away from the true parameters.

The vector-based strategy employed in this research is demonstrated in Figure 2.14. The red color in the search space means the LOS peak, and blue color means the multipath peak. Notice that for case ① the NCOs are driven by a reference trajectory, and for case ② the NCOs are driven by a navigation filter (*i.e.*, Kalman filter or Least-squares solution). Kalman filter theory is well documented by Gelb (1974), Brown and Hwang (1996), and Zarchan (2005), and will not be repeated here. Yet, it is worth to address that the receiver estimated of uncertainty (*i.e.*, variance-covariance matrix, denoted as P) is available in the Kalman filter.

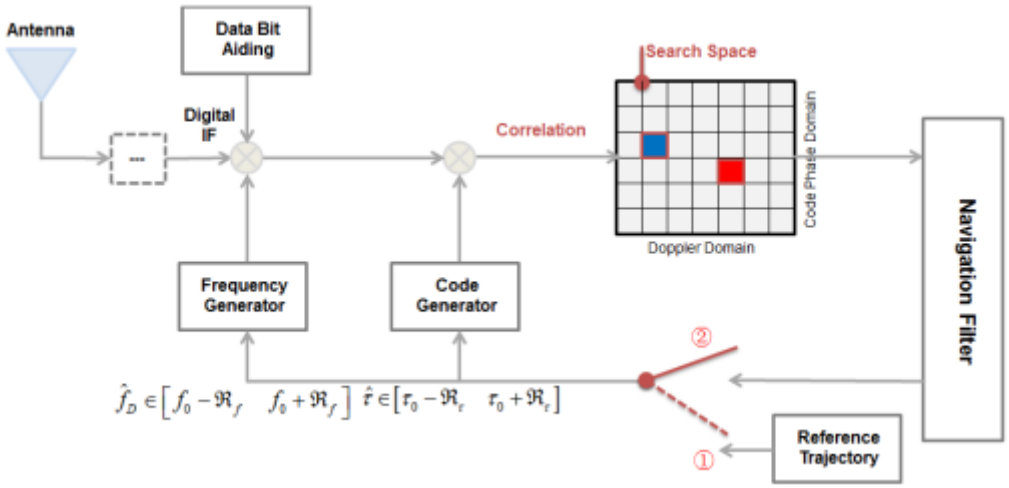

Figure 2.14: Illustration of Vector-Based Strategy employed in the High Sensitivity Receiver

2.2.2 GSNRx-ss™ Receiver

GSNRx-ss™ receiver is utilized in this research to characterize the signals from the correlation map, in particular, to identify the LOS signal and multipath signals at each epoch. This can be done by using block processing techniques and identifying the various peaks. Still, this is insufficient, since the characterization should also be able to determine the power, code phase and Doppler offsets relative to the LOS signal. Finally, it is desirable to know whether the LOS signal is present. None of these latter parameters are available from straightforward block processing approach. Instead, it is necessary to know the LOS signal parameters a priori. If these parameters are used to define the nominal signal parameters (i.e., the centre of the corrosion map), then the LOS signals should only appear near the centre of the map and the multipath signals should be displaced from the centre in the code phase and/or Doppler dimensions.

To approximate the ideal situation described above, a special test setup was used. Reference position and velocity solutions were obtained in post-mission using a differential GPS solution integrated with an inertial navigation system (introduced in section 3.1.1). These solutions were then used with the satellite position and velocity to determine the LOS signal parameters (called "reference parameters in the GSNRx-ss™ receiver") for each satellite over time. These values were then passed into a block processing software receiver and were used to define the centre of the correlation map. GSNRx-ss™ receiver strategy is shown in Figure 2.14 as case ①, and the multipath identification strategy will be discussed in section 2.3.

2.2.3 GSNRx-hs™ Receiver

A high quality reference trajectory is not available in the GSNRx-hs™ receiver, and predicted values of position, velocity, clock bias, and clock drift from the navigation filter are fed to the

receiver and considered as a "nominal" reference trajectory. The GSNRx-hs™ receiver is illustrated in Figure 2.14 as case ②. At each epoch, a "nominal" trajectory from the navigation filter is used to generate the nominal code phase and carrier Doppler which is then passed to signal processing channels. Data bits are wiped off using the known data bit information thus making long coherent integration possible.

Note that in Figure 2.14 the red bin shown in the correlation map represents the location of the LOS signal peak, and blue bin is the location of a multipath signal peak. That said, more than one signal peak can be observed on the correlation map. In the blocking processing method, generally the correlator with the strongest power is assumed to be the LOS peak (O'Driscoll *et al*., 2011). The associated code phase offset and Doppler offset are extracted to generate the pseudorange and Doppler measurements that are pass into the navigation filter to estimate the receiver position and velocity. Recall that the code phase offset (Doppler offset) is defined as the relative code phase difference (Doppler frequency difference) as compared to the nominal code phase (Doppler frequency).

Several important characteristics of the block processing strategy are summarized below:

- A bank of correlators is used in the block processing strategy. The correlation is conducted in both Doppler domain and code phase domain.
- Raw data bit from the external aiding are utilized to wipe off the navigation data bit enabling longer coherent integration time without loss of information.
- A "nominal trajectory" is used to obtain nominal LOS parameters and is also a starting point of block processing. However, the nominal trajectory may contain errors.

- The receiver will start from standard tracking strategy, and transfer to block processing strategy after obtaining navigation estimates. After that, the signal will be tracked until it is out of view. Block processing process will be applied during the whole receiver process suggesting that the number of tracked satellites represents the number of successfully initialized tracking channels.
- Carrier phase is not available from the proposed high sensitivity receiver strategy.

Different from the signal acquisition stage, where a search process is also applied in both code phase domain and Doppler domain, block processing strategy search space size and search step are significantly smaller. Also, the coherent integration time is different, *i.e.,* generally 1 ms integration time is applied during the acquisition process. Different from the acquisition process, LOS parameters are always assumed to be at (or close to) the centre of the correlation map in the block processing strategy.

The dominant peak is utilized in general block processing strategy as shown above. A completely different scheme is applied in this research and is summarized in Figure 2.15. Several peaks are observed on the correlation map after the coherent integration. LOS peak and multipath peaks are identified during the peak characterization stage, introduced in section 2.3. After that, LOS peak region is predicted to better identify the LOS peak; this is introduced in the section 2.4. And finally, observations are extracted from the identified LOS peak. Note that a receiver anomaly diagnosis is applied between the peak characterization process and peak region prediction process, introduced in section 4.3.

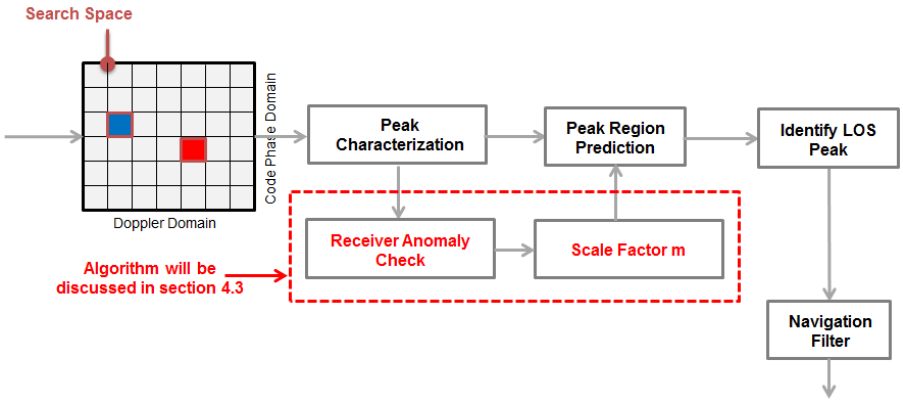

Figure 2.15: Proposed LOS Information Extraction Scheme for the High Sensitivity Receiver

The main task of this research is the search space size and coherent integration time applied in the high sensitivity receiver - collectively named "search strategy" - discussed in detail in the following sections. The search space size should be optimized in the block processing strategy. The key factors that affect the selection of the search space size and maximum coherent time are the distribution of multipath peaks and nominal signal parameter uncertainty. The coherent integration time and search space need to be carefully selected in high sensitivity receiver. Multipath distribution results should ideally be utilized for selecting integration time. The coherent integration time should be large enough to separate peaks (both LOS and multipath peaks) to avoid them overlapping in the correlation domain. A trade-off between the maximum coherent integration time, search space size, and computation load is made in this thesis.

2.2.3.1 Coherent Integration Time

The ability of the block processing method to separate multipath and LOS signals in the Doppler domain is discussed by Van Graas *et al.* (2005), Soloviev *et al.* (2008), Xie *et al.* (2011), motivating this research to mitigate multipath signals in high sensitivity receivers. In the section 2.1.1 it was shown that different integration times having different frequency resolution. In

particular, for integration times longer than 200 ms, the frequency resolution is smaller than 5 Hz. As shown in Equation (2.18) the correlator outputs are a function of coherent integration time T_C. Correlator outputs for 200 ms, 500 ms, and 1 s integration time are shown in Figure 2.16 in the Doppler domain. In this figure, the frequency resolution is 5 Hz for 200 ms integration time (Ward *et al*., 2006), and 1 Hz for 1 s integration time. Different integration times have different peak separation abilities, with longer integration times improving the separation of multipath peaks.

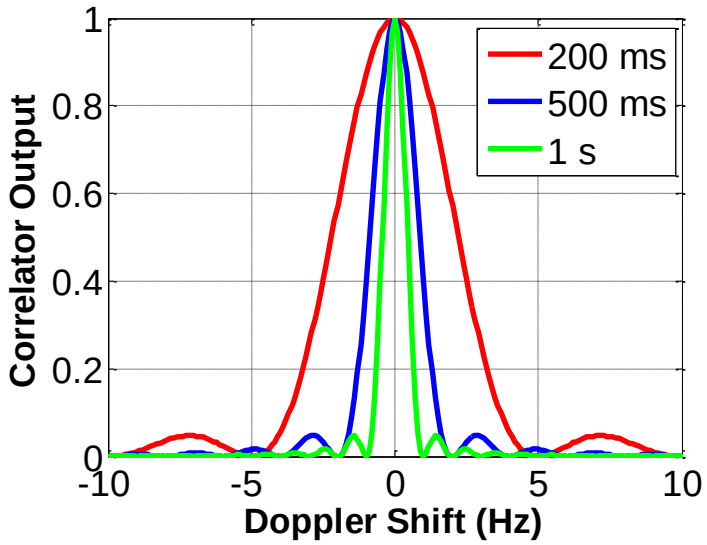

Figure 2.16: Normalized Correlations for Different Coherent Integration Times

Figure 2.17 shows a peak separation example, where the LOS signal and multipath signal shown in Table 2.1 are simulated. It is observed that two peaks are separated in the Doppler domain after employing 200 ms coherent integration time. This is due to the fact that Doppler difference (*i.e.*, 20 Hz) between LOS signal and multipath signal is larger than the frequency resolution (*i.e.*, 5 Hz). Further to this, if the LOS signal component can be identified/isolated from the multipath signal component, better Doppler and code phase information can be extracted, and receiver

performance would be improved. However, it is also acknowledged that if the LOS signal and multipath signals cannot be separated in the Doppler domain (e.g., overlapped in the code phase domain), receiver performance will be degraded as peaks in the code phase domain have not been separated in this research (although the performance may potentially be improved using the methods introduced in section 1.1.4).

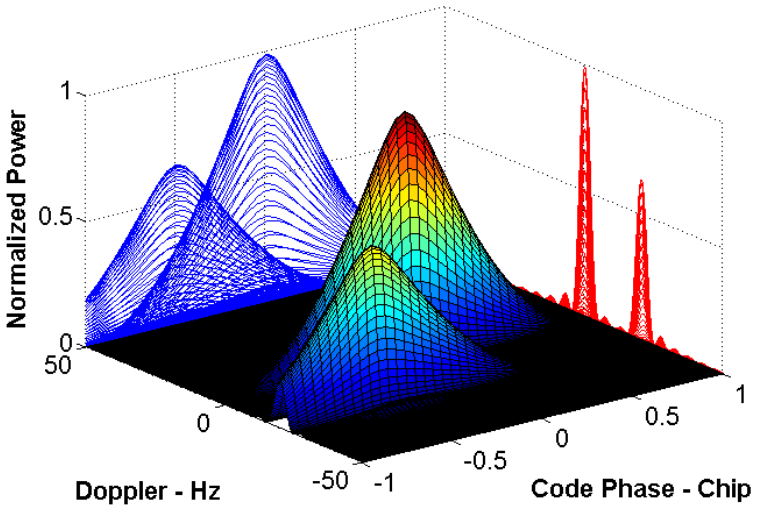

Figure 2.17: Multipath Separation in the Multipath Environment

A shorter coherent integration time is employed and illustrated in Figure 2.12 (20 ms coherent integration time), where the LOS peak and multipath peak are overlapped. Thus, the receiver cannot separate these two peaks and the LOS peak is not correctly tracked. So, a proper coherent integration time should be selected in the receiver. This coherent integration time should be long enough to separate peaks (both LOS peak and multipath peak) to prevent them from overlapping in the correlation domain. From the peak separation perspective, longer integration time is preferred since it improves the receiver sensitivity (Van Diggelen, 2009) and allows to separate two close peaks, e.g., 1 s integration time allows to avoid the overlap phenomenon between the two peaks whose Doppler difference is as little as 1 Hz.

A trade-off should also be made between the computation load and frequency resolution. The longer integration time is not always superior to shorter integration time. First or all, a smaller frequency step in block processing is required for longer integration time periods since the frequency resolution is increased, thus increasing the computational load. Second, the oscillator stability and user dynamics degrade the correlation performance. Third, fewer observations are made available to the navigation filter (*i.e.*, lower data rate).

2.2.3.2 Search Space Size

The search space size plays an important role in this research as it is crucial for practical implementations. Ideally, the search space size (both in code phase and Doppler domains) should be large enough to include the LOS peak, if present, meanwhile, being small enough to avoid the multipath signals in the search region (as generally LOS signal and multipath signal have different Doppler frequency). If a relatively accurate trajectory is available, for example, the receiver's solution integrated with the DR system, it is not necessary to employ a large search space in both code phase domain and Doppler domain, as the LOS signal should be very close to the "nominal" signal parameters. Yet, imperfect nominal parameters (*i.e.*, NCO parameters) may cause the true LOS signal to fall outside the estimated search space. To this end, it is necessary to expand the search space to include the LOS signal. Still, it is inevitable that some multipath peaks will be included as well, so when this happens, a peak separation and identification process is required to identify the LOS peak.

Before moving to the next section, signal correlations under real multipath conditions (*i.e.*, live data collected in the urban canyon area (see section 3.1.1 for details) are discussed, addressing the main challenge of the urban canyon positioning. To do this, the GSNRx-ss™ receiver is applied here to generate correlation map in different scenarios. Figure 2.18 shows a weak

multipath condition (*i.e.*, multipath signal is weaker than the LOS signal), where a strong LOS peak is shown at the centre of the correlation map. A weak (compared to the LOS peak) multipath is observed with 19.5 Hz Doppler offset. From the receiver perspective, if a 20 ms coherent integration time is utilized, the LOS peak and multipath peak will be overlapped. Thus, the correlation peak will be distorted and a traditional receiver architecture (*i.e.*, early-prompt-late DLL) cannot track the undisturbed LOS peak. Narrow correlator technique may work in this condition for a large path delay; even so, it cannot identify the LOS peak if the path delay is shorter than 0.1 chips (Irsigler and Eissfeller, 2003). In contrast, for a longer coherent integration time (e.g., 500 ms shown in this case), the multipath peak is separated from the LOS peak.

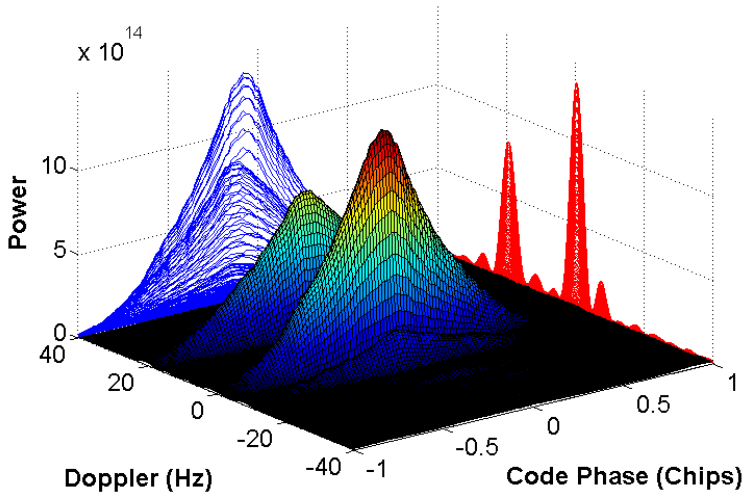

Figure 2.18: Correlation Peak under Weak Multipath Conditions

In contrast to the above situation, Figure 2.19 shows a strong multipath condition (*i.e.*, multipath signal is stronger than the LOS peak), where the LOS peak is also observed at the centre of correlation map. However, a strong multipath correlation component is observed not far away from the LOS peak. Again, the multipath peak will be tracked by a traditional DLL architecture and thus pseudorange will be biased. Even if the block processing strategy is employed, it still

needs identify the LOS peak from multipath peaks (remember that in the real applications, a very accurate “reference” trajectory is not feasible, thus the LOS peak may not be observed at the centre of the correlation map, as it is observed here). The goal of this research is to identify the LOS peak on the correlator map, which is the main objective of Chapter Four.

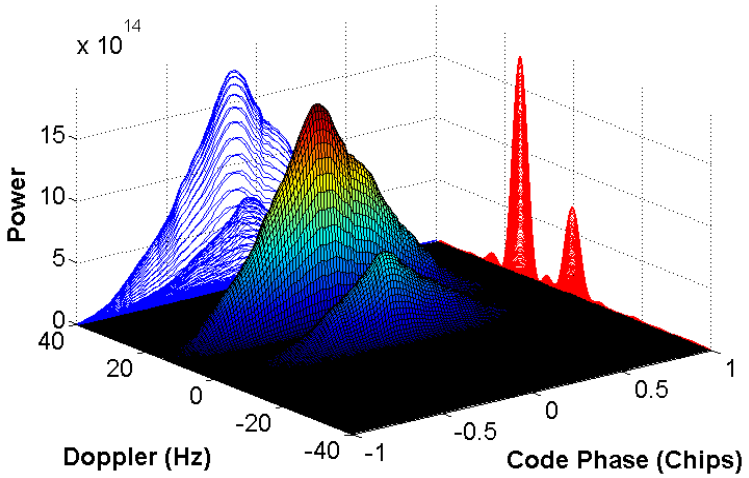

Figure 2.19: Correlation Peak under Strong Multipath Conditions

Figure 2.20 shows a severe multipath condition where more than one multipath peak is observed. The LOS signal is absent (or is very weak, to the point of being unidentifiable) at this epoch. In this case, the receiver must reject all of the peaks.

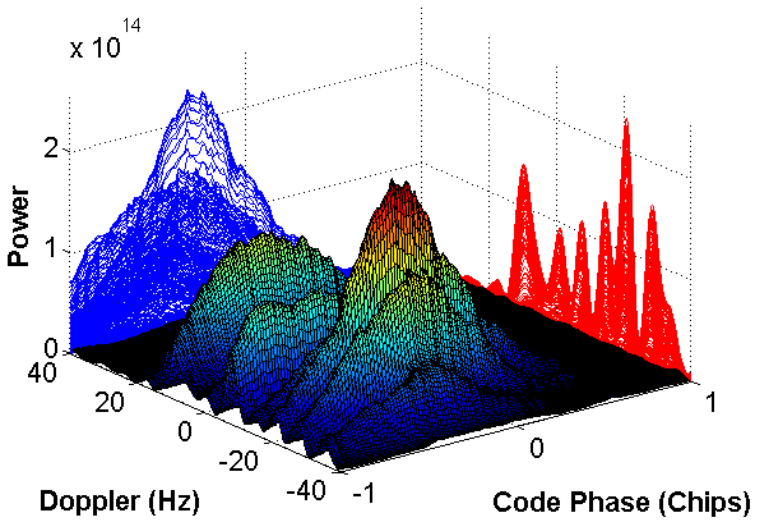

Figure 2.20: Correlation Peak under Severe Multipath Conditions

2.3 Peak Identification Method

The correlation outputs in the urban canyon area were shown in the previous section. Several correlation components were found on the correlation map. So, this section discusses how to identify the various peaks by first fitting an ideal correlation component to the strongest correlation component in the correlator map, and then by subtracting this ideal component from the actual data. The output is then revisited once again in search for another peak, and so on. This is a way to identify the peaks one by one. To identify the peaks on the correlation map, a hyperbolic model introduced by Sharp (2008, 2009) is presented in this section to fit the correlation component. The equation in the code phase domain follows

$$R(\tau)=\left(A\cdot\left[1-\sqrt{\left(\tau-\tau_p\right)^2+\delta^2}\right]\right)^2 \tag{2.29}$$

where A : Peak amplitude

τ_p : Code phase offset of the correlation peak

δ : Signal power loss (unit-less)

Then, the simulated correlation component model is given by

$$S(\tau, f) = \left(A \cdot \left[1 - \sqrt{(\tau - \tau_p)^2 + \delta^2} \right] \cdot \text{sinc}(f - f_p) \right)^2 \tag{2.30}$$

where f_p : Doppler offset of the correlation peak

Assuming the low-pass filtering effects in the front-end can be represented as an ideal rectangular filter, the power loss can be obtained as (Sharp, 2009)

$$\delta = 1 - 2\int_0^B sinc^2 x dx \tag{2.31}$$

where B is the front-end bandwidth normalized to the chip rate. For a bandwidth of 10 MHz, the power loss is 0.02 (*i.e.*, two percent) and for a bandwidth of 2 MHz, the power loss is 0.1 (*i.e.*, ten percent). After obtaining the power loss from the above, it is held fixed for all subsequent processing (*i.e.*, front-end bandwidth selected in this work is 10 MHz). The equation in the code phase domain thus becomes

$$R(\tau) = \left(A \cdot \left[1 - \sqrt{(\tau - \tau_p)^2 + 0.02^2} \right] \right)^2 \tag{2.32}$$

Figure 2.21 and Figure 2.22 respectively show the peak fitting performance in the code phase domain under a high C/N_0 case (48 dB-Hz) and a low C/N_0 case (22 dB-Hz). It is observed that for high C/N_0, the hyperbolic model fits the real peak very well.

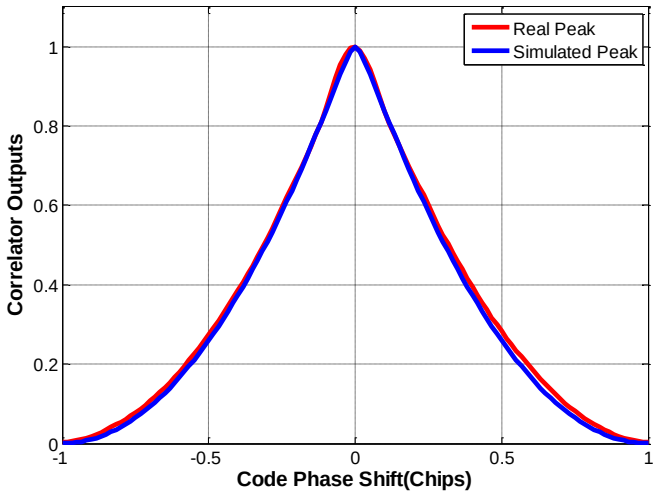

Figure 2.21: Comparison between Hyperbolic Model and Real Peak under 48 dB-Hz Scenario

For a low C/N_0 case, the differences between the real peak and simulated peak increase. This is due to the increased noise present at this epoch and possibly the presence of multipath signals.

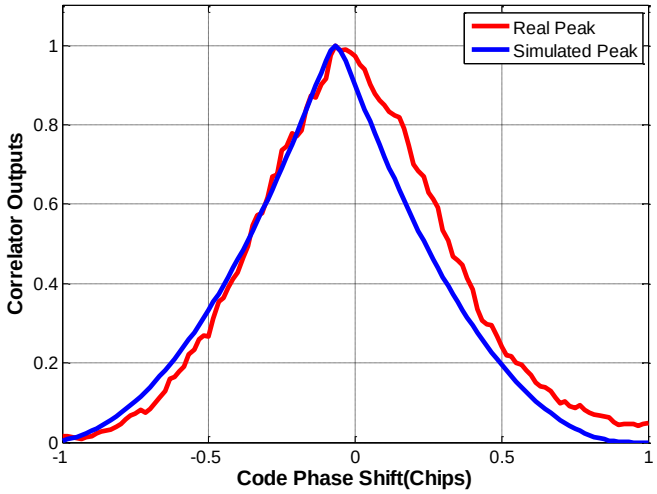

Figure 2.22: Comparison between Hyperbolic Model and Real Peak under 22 dB-Hz Scenario

A peak removal example is shown through Figure 2.23 to Figure 2.25. Figure 2.23 shows the original correlation map from GSNRx-ss™ receiver, three signal components are observed at this epoch.

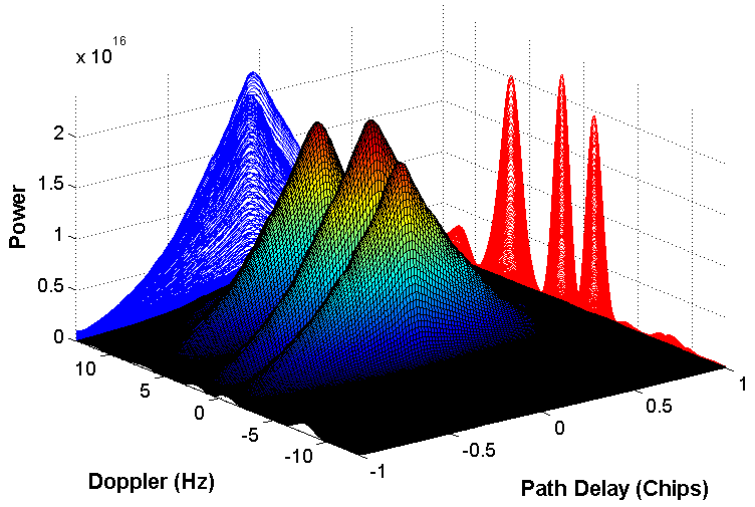

Figure 2.23: Original Correlation Map from GSNRx-ss™ Receiver under Multipath Environment

The code phase offset and Doppler offset of the strongest correlation peak is then identified in the receiver, as well as its signal power. After that, an ideal correlation component based on the identified code phase offset, Doppler offset, and signal power is generated in the receiver as shown in Figure 2.24.

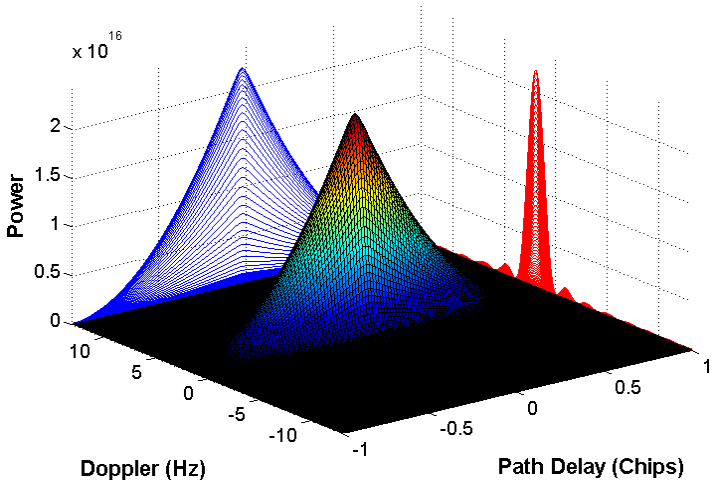

Figure 2.24: Simulated Correlation Component based on the Given Code phase offset, Doppler offset, and Power

Figure 2.25 shows the remaining correlation map after subtracting the simulated signal component from the original correlator outputs. It is clearly shown that only two signal components remain after the signal removal process. At the same time, the code phase offset and Doppler offset associated with the strongest peak are recorded. This signal removal process continues until all peaks are identified/removed (i.e., signal power is below the threshold).

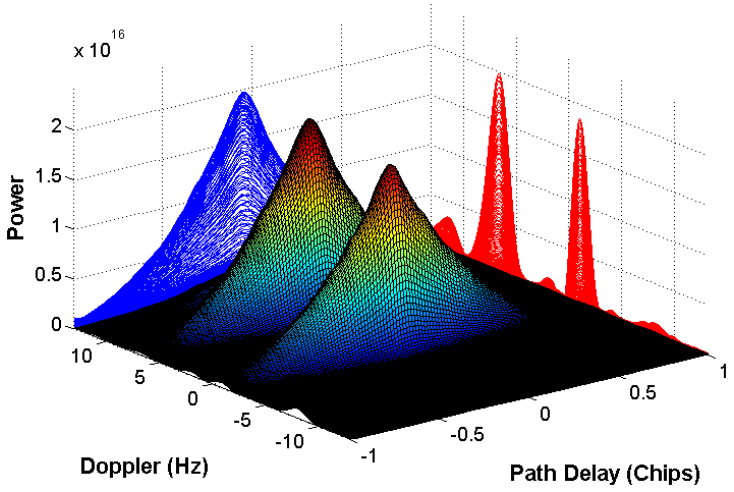

Figure 2.25: Correlation Map after Subtracting the Simulated Correlation Component from the Original Correlation Map

2.4 LOS Peak and Multipath Peak Regions

As mentioned in the previous sections, nominal or reference signal parameters are employed in the block processing receiver. Nominal parameters are predicted in the receiver or refined using a reference trajectory. Note that the LOS signal and multipath signal(s) generally have different Doppler frequency and code phase delay, thus a LOS region and a multipath region are defined in this work.

LOS Region: The region within the search space where LOS signal is expected to be found is denoted as $LOS_{\Re}$. The LOS region reflects the NCO uncertainties in the receiver. If no errors associated with the nominal signal parameters (e.g., GSNRx-ss™ receiver) are found, the LOS region is renamed as "the LOS place", since the LOS signal should lie at this single correlator.

Multipath Region: The region within the search space, where multipath signals are expected to be found, is denoted as $MP_{\Re}$.

The LOS and multipath regions are derived in this section with focus on the Doppler domain. Two terms are introduced, namely, LOS Doppler, multipath Doppler. LOS Doppler refers to the Doppler associated with the LOS signal; hence, multipath Doppler refers to the Doppler associated with the multipath signal. GSNRx-ss™ receiver is considered to be the first receiver where a sufficiently high quality reference trajectory is available such that its uncertainty can be ignored. Then, the nominal parameter uncertainties are taken into consideration in the GSNRx-hs™ receiver.

2.4.1 Without Uncertainty Case

In this section, the multipath distribution region is derived theoretically based on a given receiver velocity and satellite geometry for the GSNRx-ss™ receiver (*i.e.*, without the uncertainties of the receiver estimates). First, the Doppler of the LOS peak, multipath peak, and nominal signal (*i.e.*, the starting point of the high sensitivity receiver) is defined. Then, the Doppler offset of a multipath peak and LOS peak with respect to the nominal signal parameters is derived, thus yielding the multipath and LOS regions, respectively. The nominal Doppler is determined by

$$f_0 = \frac{\left(\vec{V}_S - \hat{\vec{V}}_R\right)\vec{H}_{REF}^{T} + \hat{d}_R}{\lambda} \tag{2.33}$$

where $\hat{\vec{V}}_R$: Reference velocity

$\vec{H}_{REF}$: Reference vector

$\hat{d}_R$: Reference clock drift

For the GSNRx-ss™ receiver architecture, which assumes a high quality reference trajectory (also a very stable oscillator) is available, $\hat{\vec{V}}_R$ and $\hat{d}_R$ are denoted as $\vec{V}_R$ and d_R (*i.e.*, true values), assuming no uncertainty corresponding to the reference trajectory exists. Thus, the nominal (also called "reference") Doppler can be described as follows

$$f_0 = \frac{\left(\vec{V}_S - \vec{V}_R\right)\vec{H}_{LOS}^T + d_R}{\lambda} \tag{2.34}$$

Note that the Doppler frequency of the LOS signal was defined in Chapter One (*i.e.*, Equation (1.6)), which is repeated as

$$f_{LOS} = \frac{\left(\vec{V}_S - \vec{V}_R\right)\vec{H}_{LOS}^T + d_R}{\lambda} \tag{2.35}$$

And for the multipath signal it is represented by

$$f_{MP} = \frac{\vec{V}_S\vec{H}_{LOS}^T - \vec{V}_R\vec{H}_{MP}^T + d_R}{\lambda} \tag{2.36}$$

So, the Doppler difference between the LOS peak and the nominal signal is defined as

$$\Delta D_{LOS} = f_{LOS} - f_0 \tag{2.37}$$

Again, the Doppler difference between the signal peak and nominal peak is defined as the observed Doppler offset. The multipath Doppler offset is described as

$$\Delta D_{MP} = f_{MP} - f_0 \tag{2.38}$$

Substituting Equations (2.34), (2.35) and (2.36) to Equation (2.37) yields the observed LOS and multipath Doppler offsets with respect to the nominal signal

$$\Delta D_{LOS} = 0 \tag{2.39}$$

and

$$\Delta D_{MP} = \frac{\vec{V}_R \vec{H}_{LOS}^T - \vec{V}_R \vec{H}_{MP}^T}{\lambda} \tag{2.40}$$

The multipath Doppler offset is generally not zero. This is caused by the fact that projections of the velocity vector to the LOS vector (*i.e.*, $\vec{H}_{LOS}$) and multipath vector (*i.e.*, $\vec{H}_{MP}$) are usually different. Obviously, the magnitude of the observed multipath Doppler offset is determined by the projection of vehicle velocity to the multipath vector. It can be easily concluded that the maximum multipath Doppler offset is obtained when the multipath vector coincides with the velocity vector. In particular, if the multipath vector coincides with the receiver velocity vector, either maximum Doppler offset or minimum Doppler offset is obtained. The maximum Doppler offset is determined by

$$\Delta D_{MP_{\max}} = \frac{\vec{V}_R \vec{H}_{LOS}^T + \left|\vec{V}_R\right|}{\lambda} \tag{2.41}$$

and the minimum Doppler offset is determined by

$$\Delta D_{MP_{\min}} = \frac{\vec{V}_R \vec{H}_{LOS}^T - \left|\vec{V}_R\right|}{\lambda} \tag{2.42}$$

Note that $\left|\vec{V}_R\right| \geq \vec{V}_R \vec{H}_{LOS}^T$ is valid for any LOS directions and no assumptions are used in the derivations, so $\Delta D_{MP_{\max}} \geq 0$ and $\Delta D_{MP_{\min}} \leq 0$ are valid for any circumstance. It is also observed that the magnitude of the Doppler offset can be zero, and this happens when the vehicle velocity is zero, or the included angles between the direction of travel and multipath signal, and direction of travel and LOS signal are the same. In this case, the projections of vehicle velocity to the multipath signal vector and LOS signal vector are the same, thus Doppler offset is zero. Moreover, a relatively small Doppler offset will be observed, if these two angles included are nearly equivalent, which happens very often in the urban canyon areas (will be shown in Chapter Three). Following is a multipath region definition to illustrate the possible multipath peak falls area. The multipath region is defined as

$$MP_{\mathbb{R}_f} = \left[\Delta D_{MP_{\min}} \quad \Delta D_{MP_{\max}} \right] \tag{2.43}$$

Multipath region suggests possible frequencies at which multipath peaks are observed. Furthermore, given the vehicle velocity (*i.e.*, $\vec{V}_R$) and satellite geometry (*i.e.*, $\vec{H}_{LOS}$), the multipath peak can be only observed in the region predicted by Equations (2.41) and (2.42). Note that $\Delta D_{MP_{\max}}$ and $\Delta D_{MP_{\min}}$ are generally not the same in terms of the absolute value, suggesting that the multipath distribution is directional-dependent in the Doppler domain.

An illustration of multipath region is shown in Figure 2.26, where a two-dimensional space is presented in the code phase domain and Doppler domain. The multipath region is only located at negative code phase domain because, by definition, multipath signal has longer path than the LOS signal (*i.e.*, negative code phase in this research). Multipath region is bounded in this figure (*i.e.*, at the right side), however, it does not necessarily only lie within the search space. The

possible multipath Doppler offset is ±150 Hz (Xie et al. 2011) in the downtown area assuming 50 km/h speed limit. Notwithstanding, those multipath signals cannot be observed in the receiver for a narrow search space (*i.e.*, outside of the search space), so they are not plotted in this figure. LOS region is also illustrated in this figure, but only a single correlator is shown in this figure as the nominal parameters are considered error free and the LOS region is shrunk to a single correlator.

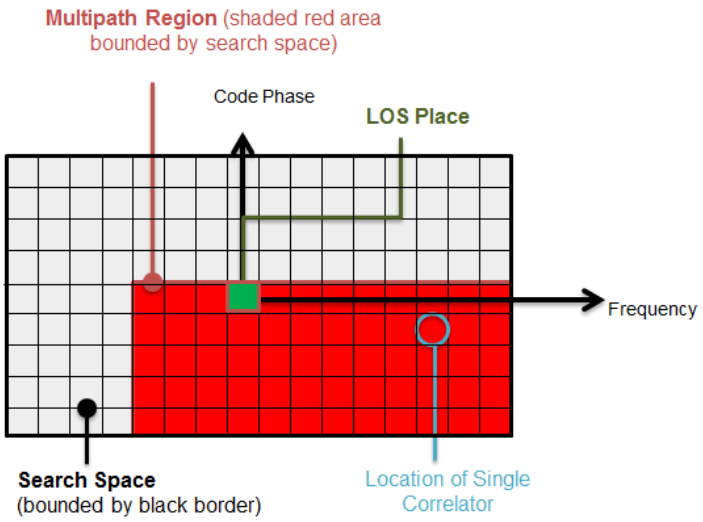

Figure 2.26: Illustration of LOS Region, Multipath Region, and Search Space without Considering the Nominal Signal Uncertainty

2.4.2 With Uncertainty Case

As discussed in section 2.2.3 no reference trajectory is available in the GSNRx-hs™ receiver, thus an uncertainty will be introduced in the receiver estimates of the nominal signal parameters. As Kalman filtering is utilized in the high sensitivity receiver, the estimation uncertainty is indicated by the estimates variance-covariance matrix (Brown and Hwang, 1996). In this section, the LOS region and multipath region are derived by assuming that the estimates uncertainty is

available in the receiver. The remaining work is based on the Kalman filter estimation. The analysis is also valid for any un-biased estimation techniques.

2.4.2.1 DOPPLER DOMAIN

The nominal Doppler offset was derived in section 2.4.1 (*i.e.*, Equation (2.33)), where a reference trajectory is available. In particular, in the GSNRx-ss™ receiver architecture $\hat{\vec{V}}_R$ and $\hat{d}_R$ are denoted as $\vec{V}_R$ and d_R (*i.e.*, true values), assuming no uncertainty corresponding to the reference trajectory. However, for the GSNRx-hs™ receiver architecture a high quality reference trajectory is not available, and thus, $\hat{\vec{V}}_R$ and $\hat{d}_R$ are denoted as $\hat{\vec{V}}_{HS}$ and $\hat{d}_{HS}$. Assuming that the estimated position from the high sensitivity receiver is better than 1 km, thus there is no (or minor) difference between $\vec{H}_{REF}$ and $\vec{H}_{LOS}$. Equation (2.33) can be rewritten as

$$f_0 = \frac{\left(\vec{V}_S - \hat{\vec{V}}_{HS}\right)\vec{H}_{LOS}^T + \hat{d}_{HS}}{\lambda} \tag{2.44}$$

Remember that ideally the Kalman filter is an unbiased estimator, and so

$$E\left(\hat{\vec{V}}_{HS}\right) = \vec{V}_R,\ E\left(\hat{d}_{HS}\right) = d_R$$

and

$$\mathrm{var}\left(\begin{bmatrix}\hat{\vec{V}}_{HS} & \hat{d}_{HS}\end{bmatrix}\right) = P_{vd}$$

where P_{vd} can be obtained from the navigation Kalman filter directly.

The expectation of the Equations (2.37) and (2.40) can be respectively given as

$$E\left(\Delta D_{LOS}\right)=0 \tag{2.45}$$

and

$$E\left(\Delta D_{MP}\right)=\frac{-\vec{V}_R\vec{H}_{MP}^{T}+\vec{V}_R\vec{H}_{LOS}^{T}}{\lambda} \tag{2.46}$$

Yet, $\vec{V}_R$ is generally unknown and the best approximation is $\vec{V}_R \approx \hat{\vec{V}}_{HS}$, thus Equation (2.46) can be rewritten as

$$E\left(\Delta D_{MP}\right)\approx\frac{-\hat{\vec{V}}_{HS}\vec{H}_{MP}^{T}+\hat{\vec{V}}_{HS}\vec{H}_{LOS}^{T}}{\lambda} \tag{2.47}$$

The uncertainty of the LOS Doppler offset and multipath Doppler offset are determined by the following equations respectively

$$\sigma_{LOS_f}^{2}=\mathrm{var}\left(\Delta D_{LOS}\right)=\frac{\left[\vec{H}_{LOS}\quad 1\right]P_{vd}\left[\vec{H}_{LOS}\quad 1\right]^{T}}{\lambda^{2}} \tag{2.48}$$

and

$$\sigma_{MP_f}^{2}=\mathrm{var}\left(\Delta D_{MP}\right)=\frac{\left[\vec{H}_{LOS}\quad 1\right]P_{vd}\left[\vec{H}_{LOS}\quad 1\right]^{T}}{\lambda^{2}} \tag{2.49}$$

It is observed that the uncertainties for the LOS Doppler offset and multipath Doppler offset are the same. This can be explained by the fact that the uncertainty is introduced by the nominal

parameters, not the LOS signal or multipath signal. In this regard, the LOS peak region can be presented as

$$LOS_{\mathbb{R}_f} = \left[-m\sigma_{LOS_f} \quad m\sigma_{LOS_f} \right] \tag{2.50}$$

where m is scale factor which indicates the confidence level, e.g., $m = 1$ for 68.3% and $m = 2$ for 95.4%.

Consequently, the multipath peak observed in the high sensitivity receiver should fall within the region shown below

$$MP_{\mathbb{R}_f} = \left[\Delta D_{MP_{\min}} - m\sigma_{MP_f} \quad \Delta D_{MP_{\max}} + m\sigma_{MP_f} \right] \tag{2.51}$$

2.4.2.2 CODE PHASE DOMAIN

Similar to the Doppler domain analysis, the LOS code phase is determined by

$$\tau_{LOS} = \frac{\left(\vec{P}_S - \vec{P}_R \right) \vec{H}_{LOS}^T + b_R}{L} \tag{2.52}$$

where $\vec{P}_S$: Satellite position vector

$\vec{P}_R$: Receiver position vector

b_R : Receiver clock bias

L : Code chip length

The nominal code phase is given by

$$\tau_0 = \frac{\left(\vec{P}_S - \hat{\vec{P}}_R\right)\vec{H}^T_{LOS} + \hat{b}_R}{L} \tag{2.53}$$

where $\hat{\vec{P}}_R$: Nominal receiver position vector

$\hat{b}_R$: Nominal receiver clock bias

For the GSNRx-hs™ receiver architecture, the nominal code phase can be written as follows

$$\tau_0 = \frac{\left(\vec{P}_S - \hat{\vec{P}}_{HS}\right)\vec{H}^T_{LOS} + \hat{b}_{HS}}{L} \tag{2.54}$$

where $\hat{\vec{P}}_{HS}$: Estimated receiver position vector

$\hat{b}_{HS}$: Estimated receiver clock bias

The code phase offset is then defined as

$$\Delta\tau_{LOS} = \tau_{LOS} - \tau_0 \tag{2.55}$$

Substituting Equations (2.52) and (2.54) to Equation (2.55) yields the observed code phase offset with respect to the nominal peak

$$\Delta\tau_{LOS} = \frac{\left(\hat{\vec{P}}_{HS} - \vec{P}_R\right)\vec{H}^T_{LOS} + \left(b - \hat{b}_{HS}\right)}{L} \tag{2.56}$$

Also in the Kalman filter

$$E\left(\hat{\vec{P}}_{HS}\right)=\vec{P}_R,\ E\left(\hat{b}_{HS}\right)=b_R$$

Thus the expectation of the LOS peak code phase offset is determined by

$$E\left(\Delta\tau_{LOS}\right)=0 \tag{2.57}$$

Correspondingly, the variance is given by

$$\sigma^2_{LOS_\tau}=\frac{\left[\vec{H}_{LOS}\quad 1\right]P_{pb}\left[\vec{H}_{LOS}\quad 1\right]^T}{L^2} \tag{2.58}$$

And finally the LOS peak code phase region can be described as

$$LOS_{\mathbb{R}_\tau}=\left[-m\sigma_{LOS_\tau}\quad m\sigma_{LOS_\tau}\right] \tag{2.59}$$

Also, as the uncertainty is introduced by the nominal signal parameters uncertainty, the multipath code phase offset should have the same uncertainty as shown in Equation (2.59). To this end, the LOS region and multipath region shown in Figure 2.26 should be modified accordingly. In particular, the LOS region and multipath region are expanded as shown in Figure 2.27.

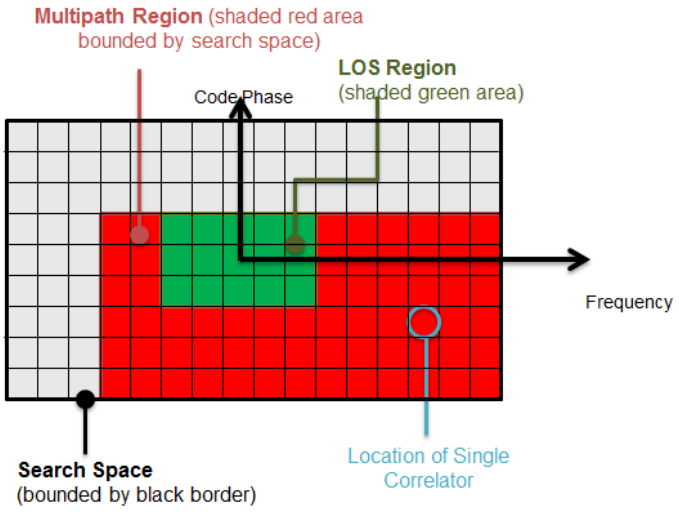

Figure 2.27: Illustration of LOS Region and Multipath Region after Considering the Nominal Signal Uncertainty

Compared to Figure 2.26, some important differences are listed below:

- Multipath region is increased, because of the nominal signal parameters uncertainty.
- LOS region is also expanded due to the nominal signal uncertainty, as a result, the LOS region is no longer a single correlator.

2.5 Dominant Peak Strategy and Assumed LOS Peak Strategy

Signal peak and noise peak were defined in section 2.1.1 to distinguish correlation peaks observed in the correlation map. Signal peak means the correlation peak is from a signal, in contrast, noise peak means the correlation peak is from noise. Notice that a threshold is utilized in the receiver to correctly detect a signal for different receiver strategies (Misra and Enge, 2006, Borio *et al*., 2008). In this research, the signal peaks are roughly defined as having a C/N_0 larger than 16 dB-Hz (van Diggelen, 2009). By extension, noise peaks are defined as peaks with C/N_0 below 16 dB-Hz. Still, this is not enough to identify the LOS signal, as the antenna ultimately

receives both LOS and multipath signals. If this is the case, a LOS peak identification strategy should be applied in the high sensitivity receivers. In ideally cases, the power of LOS peak is much stronger than the multipath peaks and the signal parameters can be extracted from the dominant peak directly (*i.e.*, assumed as the LOS peak). In multipath environments several multipath peaks can be observed and at the same time, the LOS peak may be corrupted by noise or attenuated by surrounding objects. The LOS peak is not necessarily the dominant peak. So, the concepts of the "dominant peak" and the "assumed LOS peak" are introduced in this section:

- Dominant Peak: The peak having the strongest power among all available peaks.
- Assumed LOS Peak: The peak that is assumed to be the LOS peak based on a LOS peak identification scheme.

Subsequently, the dominant peak strategy and the assumed LOS peak strategy are proposed in this thesis.

2.5.1 Dominant Peak Strategy

It was noted that the dominant peak was generally utilized in the block processing method. This is herein called "the dominant peak strategy". For the dominant peak strategy, the receiver only needs identify the correlator with the maximum power from the correlation map, which is very easy to implement. An example is shown in Figure 2.28, where the receiver is surrounded by buildings, and LOS and multipath peaks are both observed at this epoch. Obviously, the Doppler error of the dominant peak (*i.e.*, 18.9 Hz) is larger than the assumed LOS peak (*i.e.*, 0.2 Hz), suggesting that it is not always wise to select the dominant peak in the navigation filter to estimate the vehicle velocity. Xie *et al*. (2011) state that in the urban canyon area generally the dominant peak is not the LOS peak over 20 percent of the time. By extension, those dominant

peaks (*i.e.*, multipath peaks) are considered the LOS peaks and large positioning errors will be introduced in the receiver.

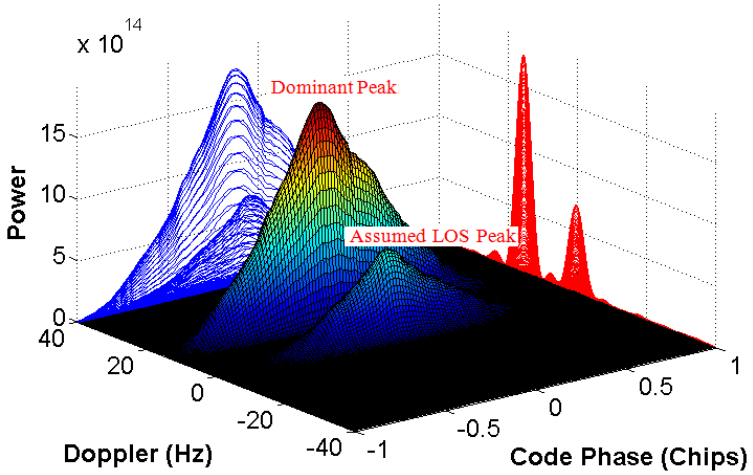

Figure 2.28: Illustration of the Dominant Peak and Assumed LOS Peak

2.5.2 Assumed LOS Peak Strategy

It has been shown that the dominant peak is not always a wise choice in terms of the code phase and Doppler accuracies. If this is the case, it makes it difficult to extract the LOS signal parameters from the correlation map. Especially in this case, a LOS peak search strategy is proposed to identify the LOS peak; this is called “the assumed LOS peak strategy”. The assumed LOS peak strategy is illustrated in Figure 2.29, where several signal peaks are presented (*i.e.*, red colour indicates the LOS peak, and blue colour indicates the multipath peak).

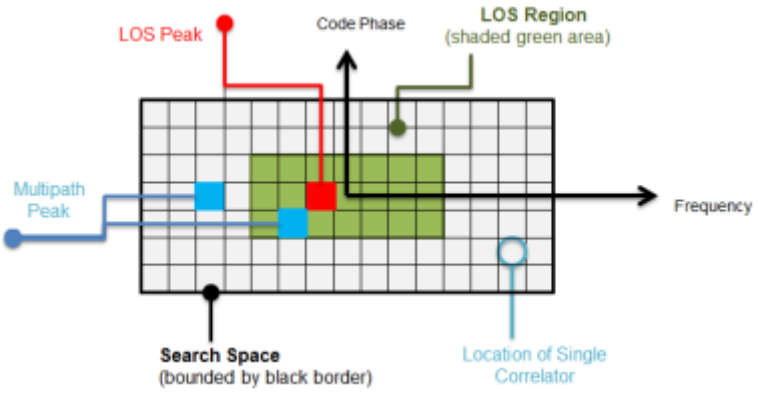

Figure 2.29: Illustration of Search Space, LOS Region, LOS peak, and Multipath Peaks

The LOS peak identification strategy is summarized in Table 2.6 where $\Re_f$ stands for the Doppler LOS region size, and $\Re_\tau$ stands for the code phase LOS region size. The LOS peak is declared under the following three conditions:

- The power is larger than 42 dB-Hz regardless of whether or not the peak is in the predefined LOS region. The 42 dB-Hz threshold is selected from the multipath characterization stage, discussed in Chapter Three.
- The power is larger than 16 dB-Hz, but smaller than 42 dB-Hz, and the peak is in the predefined LOS region.
- If several peaks are observed in the LOS region, the one that has the smallest code phase offset relative to the nominal signal will be considered as the LOS peak.

Prior to this, however, the cross-correlation peak should be removed from the correlation map. Recall section 2.1.2 that the Doppler offset of the possible cross-correlation peaks can be predicted in the vector-based receiver mode. Thus any peak whose Doppler offset coincides with

the predicted cross-correlation will be removed. Further to this, any peak that is outside the predefined LOS region will be considered as a multipath peak.

Table 2.6: Assumed LOS Peak Identification Strategy for the Proposed High Sensitivity Receiver

Classification		C/N_0 (dB-Hz)	Doppler Shift (Hz)	Code Shift (chips)
Signal Peak	Assumed LOS	≥ 42	N/A	N/A
		≥ 16	$\leq \Re_f$	$\leq \Re_\tau$
	Multipath	≥ 16	$> \Re_f$	$> \Re_\tau$
	Cross-Correlation	≥ 16	N/A	N/A
Noise Peak		< 16	N/A	N/A

Still, a vital challenge for the assumed LOS peak strategy is to correctly identify the receiver anomaly, which is defined below.

Receiver anomaly: LOS signal peak is outside the predefined LOS region, effectively, it also means that the nominal signal parameters have a bias in the Doppler domain or/and in the code phase domain. More specifically, imperfect nominal parameters will degrade the peak selection performance. When this happens, the NCO values may be outside of the assumed LOS region. Thus the LOS peak will be outside of the assumed LOS region and a mis-detection may occur. Furthermore, if a multipath peak is observed in the LOS region, a false-identification may occur.

Figure 2.30 shows an example of receiver anomaly, where the NCO frequency error is larger than the predicted LOS region $\Re_f$ in the Doppler domain.

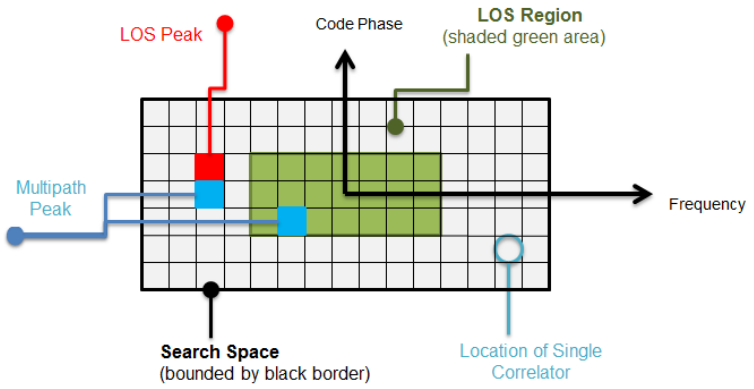

Figure 2.30: Illustration of Receiver Anomaly in the Assumed LOS Peak Strategy

In this case, the LOS region should be expanded to observe the LOS peak in the correlation outputs. The receiver anomaly check is discussed in section 4.3 to evaluate the predefined LOS region quality. Further to this, after a receiver anomaly is declared, the LOS region will be refined. Compared to the dominant peak approach, the advantages of the assumed LOS peak approach are three-fold: first, most of the multipath peaks are ignored (or effectively removed) on the correlation map; second, the assumed LOS peak is identified on the correlation map (may or may not the dominant peak); third, pseudorange and Doppler accuracies are improved, so is the measurement reliability. That said, it is possible that the multipath peak will be rejected in the navigation filter for the dominant peak strategy, however, the LOS peak is also ignored as it is weaker than the dominant peak. In contrast, for the assumed LOS peak approach, the multipath peak is ignored in the correlation map via the predefined LOS region, and meanwhile, the LOS peak is identified on the correlation map. This is crucially important especially in the urban canyon area, where only few satellites can be correctly tracked. It will be shown in Chapter Five that most of the multipath peaks are removed in the receiver.

Chatper Three: Multipath Distribution in the Urban Canyon Environment

In an open sky environment the GNSS signal is represented by the line-of-sight (LOS) transmission of the signal. However, in the urban canyon area this LOS signal is often blocked and/or reflected by the surrounding objects. The presence of multipath signals generally results in range errors and carrier phase errors. Generally, the standard receiver architectures cannot provide an accuracy level sufficient for use in vehicular applications in all environments. This is especially true for urban canyon environments, where the presence of large buildings leads to frequent shadowing of signals, several multipath peaks can potentially exist in the correlator outputs.

High sensitivity receivers are utilized in this research to better track the GNSS signals in the urban canyon areas. The motivation of this work is to separate the LOS signal with the multipath signals in the Doppler domain. It is important to understand the multipath distributions in the urban canyon area, in particular, the Doppler frequency and code phase delay under different conditions, *i.e.*, vehicle speed, signal power. By doing so, these results can be explicitly applied in the receiver to better mitigate the multipath signals. More specifically, the multipath distribution will eventually affect the search strategy (*i.e.*, search space size, coherent integration time) utilized in the high sensitivity receiver. This chapter provides an intensive characterization of the LOS signal availability and multipath distributions in the urban canyon environment. The layout of this chapter is given as follows. First, the data collection setup is summarized and the method to identify multipath peaks is proposed. Then, the signal distribution in the urban canyon is determined, which essentially provides the availability of LOS signals in the urban canyon area. And finally, multipath distributions for different conditions are described.

3.1 Data Collection and Proposed Assessment Method

3.1.1 Data Collection

To assess the multipath distributions in vehicular applications, three live data sets were collected in downtown Calgary, AB, Canada. The tests were performed on March 3, 2011, August 19, 2011, and August 16, 2012, respectively. Totally more than two hours worth of data were collected. The environment is an example of an urban canyon with buildings ranging in height from a few stories to over 50 stories. Each data collection session started with a static open-sky period of approximately three minutes used to initialize the high sensitivity receiver (e.g., initialize the receiver position and velocity). Figure 3.1 shows the test trajectories in Google Earth™, the majority of the routes covered almost the whole downtown area, with significant signal blocking most of the time.

Figure 3.1: Downtown Data Collection Trajectories, Green: March 3, 2011, Blue: August 19, 2011, Red: August 16, 2012 (from Google Earth™)

Table 3.1 summaries the equipment setup for data collection. A NovAtel SPAN system with a tactical grade UIMU-LCI inertial sensor (*i.e.*, SPAN LCI system) was used to generate the reference trajectory using NovAtel Inertial Explorer. The gyro bias for the LCI inertial

measurement unit (IMU) is specified to be less than 1 degree per hour. A National Instrument (NI) RF front-end was used to collect the IF data from the antenna. Also, a very stable Oven Controlled Crystal Oscillator (OCXO) was used. For the GPS L1 signal the IF frequency is 1575 MHz, the bandwidth is 10 MHz, and the sampling rate was 12.5 MHz (complex data). A base station was also applied to collect raw navigation data bit used for the proposed high sensitivity receiver to enable long coherent integration.

Table 3.1: Data Collection Equipment Summary

Item	Details
IMU	Northrop-Grumman UIMU-LCI
GPS Receiver	NovAtel OEMV3 SPAN System
Front-End	National Instruments
Base Station	NovAtel OEMV3 Receiver

August 16, 2012 data (about 20 minutes) is selected in this section to show the signal characterization in the urban canyon environment (March 3, 2011 data set (about one hour) is shown in Appendix A). The sky plot is shown in Figure 3.2, and Figure 3.3 shows reference velocity during data collection. Both static and moving sections are observed.

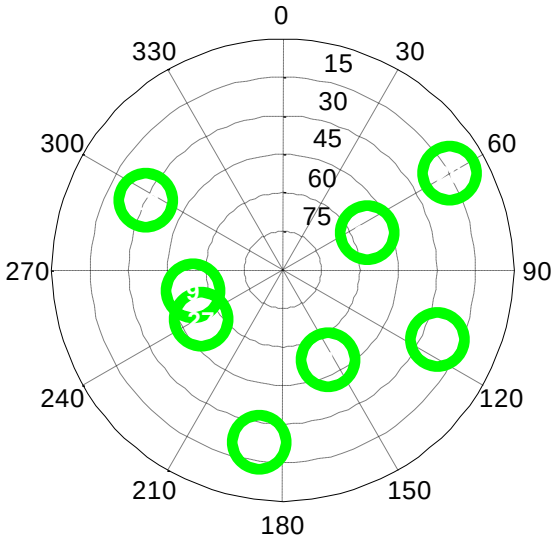

Figure 3.2: Sky-Plot of August 16, 2012 Data Set at the Start of Test

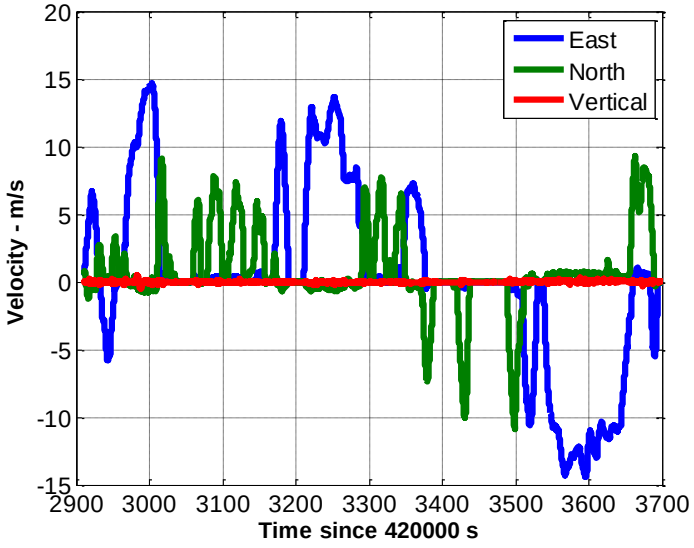

Figure 3.3: Reference Velocity of August 16, 2012 Data Set

Figure 3.4 shows the estimated accuracy (1σ, from NovAtel Inertial Explorer Outputs) of the SPAN LCI solution during the data collection. The position errors are estimated to be less than 0.5 m (0.002 chips), and the velocity errors are less than 1 cm/s (0.05 Hz).

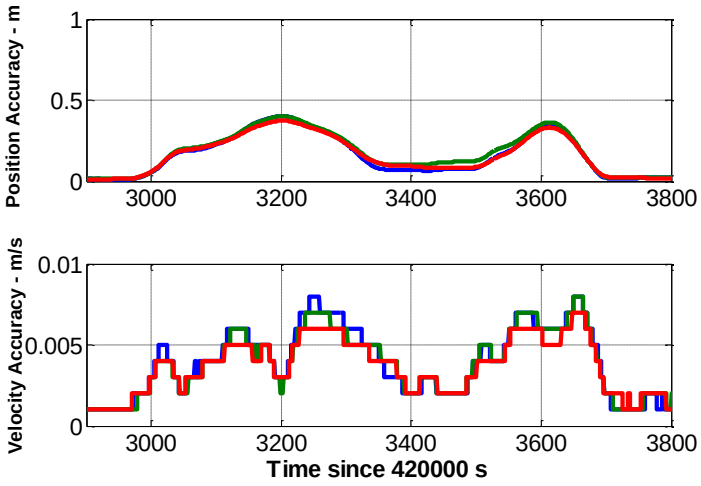

Figure 3.4: Position and Velocity Accuracies (1σ) from the SPAN LCI System during the Test Performed

3.1.2 Proposed Peak Separation and Identification Method

The key challenge for the multipath characterization is to separate correlation peaks in the correlation map, and identify the LOS peak and multipath peaks. To this end, GSNRx-ss™ receiver introduced in section 2.2.2 was applied to separate LOS peak and multipath peaks during post-processing. The reference trajectory from SPAN LCI can be utilized to generate the nominal signal parameters. The reasons for this are:

- SPAN LCI position accuracy is better than 0.5 meter and the velocity accuracy is better than 0.01 m/s, which means that the nominal parameter errors in the GSNRx-ss™ receiver introduced by the reference trajectory have an accuracy of 0.002 chips in code phase dimension and 0.05 Hz in Doppler dimension, respectively.
- The oscillator in the national instrument (NI) front-end is a very stable (OCXO, the short term frequency stability is better than 1e-11 (Gaggero, 2008)), thus the frequency uncertainty

introduced by the oscillator can be ignored (Gaggero and Borio, 2008). In this regard, the clock drift can be fixed in the analysis when predicting the nominal Doppler frequency. Also, clock bias can be predicted by using a fixed clock drift.

Table 3.2 shows the receiver strategy applied in the GSNRx-ss™ receiver. To identify the correlation peaks from the receiver, the peak identification method introduced in section 2.3 is applied to identify and remove peaks one by one, and at the same time, the code phase offset, Doppler offset, and signal power associated with each peak are saved. The search space size applied is ±40 Hz in the Doppler domain, and ±300 m in the code phase domain, respectively. The coherent integration time utilized is 1 s and the frequency resolution is 1 Hz respectively, which means that the peaks could be separated, if the Doppler difference between any of two peaks is larger than 1 Hz. Receiver dynamics are compensated by the input reference trajectory (*i.e.*, position and velocity), in so doing, 1 s coherent integration time is possible. Although the coherent integration time used in the GSNRx-hs™ receiver is generally less than 1 s in this research, nevertheless, 1 s coherent integration time gives an overall understanding of the collected signals. The search step in the code phase domain and Doppler domain is 5 m and 0.2 Hz, respectively.

Table 3.2: Block Processing Strategy for GSNRx-ss™ Receiver used to Characterize Correlation Peaks

Integration Time	1 s	
Search Space	Doppler Domain	±40 Hz
	Code Phase Domain	±300 m
Search Step	Doppler Domain	0.2 Hz
	Code Phase Domain	5 m

3.2 Signal Peaks Characterization

During the test the LOS signal availability is assessed, specifically, rough thresholds can be made to identify the LOS peak and multipath peaks from the correlation map. That said, if the code phase offset is less than 10 m, and at the same time, the Doppler offset is less than 2 Hz, the conclusion can be made that the identified peak is the LOS peak, otherwise it is a multipath peak. Note that the thresholds selected here are conservative, especially in the Doppler domain (*i.e.*, 2 Hz). However, the accuracies of the identified signal parameters (*i.e.*, code phase offset and Doppler offset) are affected by the frequency resolution (1 Hz for 1 s coherent integration time) and signal power (refer to Figure 2.20 where large variations on the correlation component can be observed when the signal power is low). In this regard, the threshold cannot be set too small.

The correlation map for each single satellite is categorized into three types: LOS signal only epoch, multipath present epoch, and no signal epoch, as defined below.

LOS Signal Only Epoch: means only LOS signal presents at this epoch for this satellite, specifically, no multipath peak exists. In this circumstance, the LOS peak can be easily (relatively, as only one signal component observed) identified in the receiver.

Multipath Present Epoch: means multipath peak(s) is observed at this epoch for this satellite, however, the LOS peak may or may not be present at this epoch. Consequently, misdetection or false identification may occur. Misdetection means the LOS peak is present at this epoch, however, it is identified as a multipath peak and ignored by the receiver. False identification means the multipath peak is falsely identified as a LOS peak.

No Signal Epoch: means no signals present at this epoch and as a result, no measurements can be obtained from this satellite. Note that for the standard receiver architecture it may lose signal

lock during the no signal epochs. However, the block processing architecture still ‘tracks’ this satellite (as vector-based concept is employed), thus the correlation map is available from this satellite.

Further to this, the LOS signal only epoch or multipath present epoch is also called a “signal epoch”. Although already introduced in previous sections, it is worth to address the goal of this research again. The objective of this thesis is to remove (or ignore) the multipath peaks from the observations. Particularly, based on the categorization above, the main goal is to identify the LOS peaks from the LOS only epochs, and meanwhile, remove the multipath peaks during the multipath present epochs. Figure 3.5 shows the satellite C/N_0 estimations from the GSNRx-ss™ receiver, and Figure 3.6 shows the cumulative histogram of C/N_0 for each satellite. It is observed that the C/N_0 is generally more than 35 dB-Hz, and may drop to 20 to 30 dB-Hz in the deep urban canyon area. For the high elevation satellite (e.g., PRN 4) 70 percent of the time the signal power is stronger than 40 dB-Hz. Still, for low elevation satellites (e.g., PRN 28) only 20 percent of time the signal power is stronger than 40 dB-Hz.

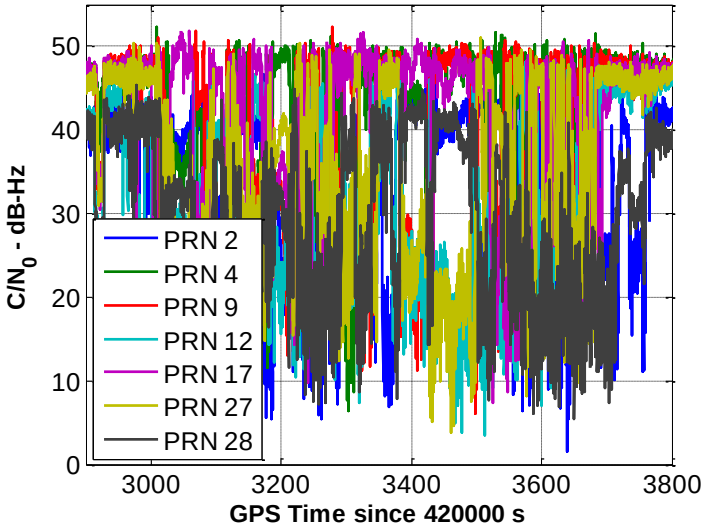

Figure 3.5: Signal to Noise Ratio (C/N_0) Estimates during the Urban Canyon Environment from the GSNRx-ss™ Receiver

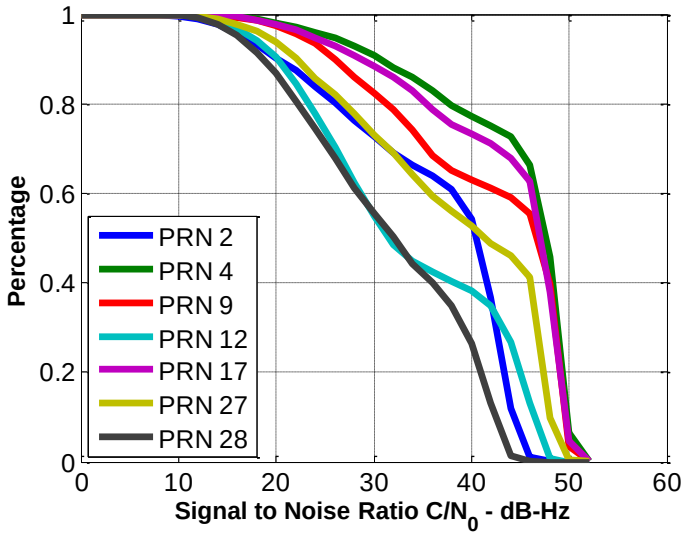

Figure 3.6: Cumulated Signal to Noise Ratio (C/N_0) during the Urban Canyon Environment from the GSNRx-ss™ Receiver

Figure 3.7 shows the signal distribution during the test performed, where the percentages of LOS only epoch, multipath present epoch, and noise only epoch are shown. For high elevation satellites, e.g., PRN 4, more than 60 percent of epochs are LOS only epochs, suggesting that high quality measurements can be extracted from the correlation map. In contrast, for low elevation satellites, e.g., PRN 28, only 15 percent of epochs are LOS only epochs, while the multipath present epochs are close to 42%. This is straightforward as most of the LOS signals are blocked by the surrounding objects (e.g., high buildings). In this regard, the receiver should be very careful to select the LOS peak from the correlation map. Large pseudorange and/or Doppler errors are expected, if a multipath peak is falsely identified as the LOS peak.

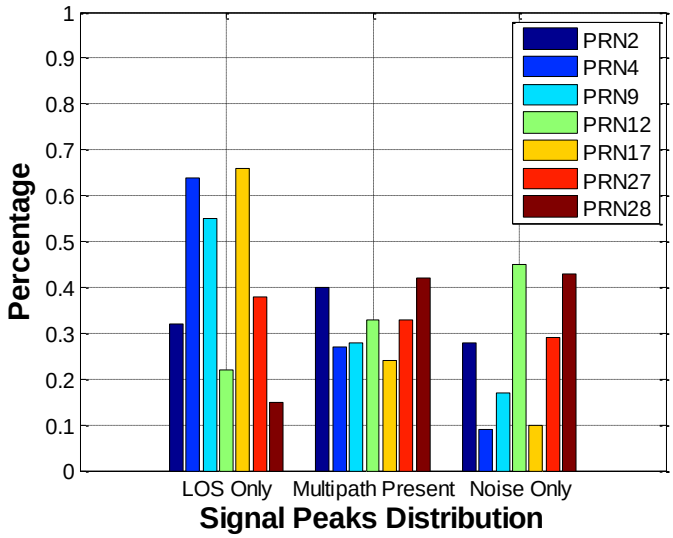

Figure 3.7: Signal Peak Characterization for the August 16, 2012 Data Set

Obviously, for the dominant peak strategy the measurements are available for each signal epoch (*i.e.*, LOS only and multipath present epochs). By extension, the receiver will not separate LOS peak and multipath peaks. Yet, for the assumed LOS peak strategy proposed in this thesis the

measurements may not be available for every signal epoch as a LOS region is applied to only select peaks in the LOS region.

Another critical statistic of the signal characterization is the percentage of time that the dominant peak is the LOS peak (also called "LOS percentage"). As introduced in section 2.5.1 for the dominant peak strategy the dominant peak is not necessarily the LOS peak. Figure 3.8 shows the percentage of time that the dominant peak is the LOS peak for different search space size for six different satellites. It is observed that the percentage of time is decreased after increasing the search space size in the Doppler domain. Take PRN 4 for example, for 5 Hz search space size the percentage of time that the dominant peak is the LOS peak is 81%, however, it drops to 72% for 15 Hz search space size, and finally drops to 62% for 40 Hz search space size. This can be explained by the fact that after expanding the search space size in the Doppler domain, it is more likely that a stronger peak is observed which is not a LOS peak. In this regard, the percentage of time that the dominant peak is the LOS peak is decreased. It also suggests that a smaller search space size returns better LOS peak identification performance. From a navigation perspective, a small search space size is therefore preferred to avoid multipath peaks. Nevertheless, remember that the small search space size only happens for the ideal case, where a high accuracy reference trajectory is provided (*i.e.*, GSNRx-ss™ version). Given the GNSS only circumstance in this research (*i.e.*, GSNRx-hs™ version), a high accuracy reference trajectory is impossible and as a result, may shift the LOS peak outside of the search space for some instances. Therefore the smallest search space size may not actually the best.

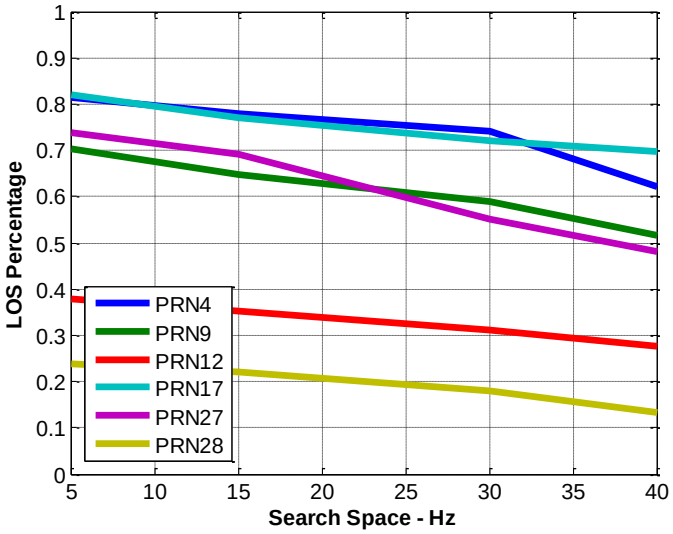

Figure 3.8: LOS Peak Percentage for Different Search Space Sizes

3.3 Multipath Distributions for Different Conditions

After the signal peak characterization from the previous section, multipath peak distributions under different conditions are then assessed in this section for the same data set (August 16, 2012 data set), the data set collected on March 3, 2011 will be assessed in Appendix A. Specifically, different vehicle speeds and signal powers are considered. To start with, the multipath peaks obtained from all satellites are plotted together in Figure 3.9. It is observed that the multipath peaks are scattered all over search space, with more density between the -0.4 chips to 0 chip region in the code phase domain, and -20 Hz to 20 Hz region in the Doppler domain. Note that the LOS peaks are removed from this plot (*i.e.*, the blank area shown in the region of -0.03 chips to 0 in the code phase domain, and -2 Hz to 2 Hz in the Doppler domain, refer to section 3.1.2).

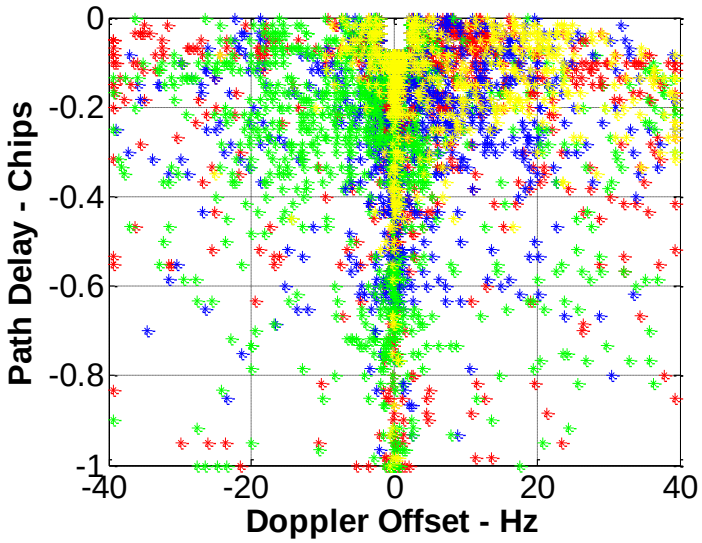

Figure 3.9: Multipath Distribution for All Satellites

Figure 3.10 and Figure 3.11 show the multipath peak distributions in the Doppler domain and code phase domain, respectively. The figure in the left shows the multipath distribution and the figure in the right shows the cumulative histogram. Recall that the main goal of this work is to separate the peaks in the Doppler domain. In this regard, we are more concerned about the multipath distribution in the Doppler domain, not code phase domain, as no efforts have been made in this research with respect to the correlation components overlapping in the code phase domain. It is observed that more than 50 percent of the multipath Doppler offsets are less than 2 Hz, and more than 60 percent of them are less than 5 Hz. It is also observed that more than 40 percent of the code phase offsets are longer than 0.2 chips.

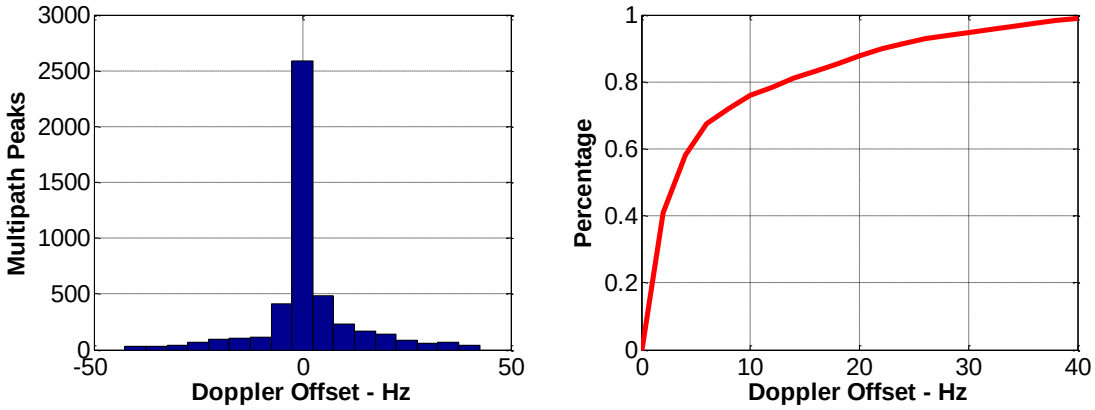

Figure 3.10: Multipath Distribution in the Doppler Domain for All Satellites

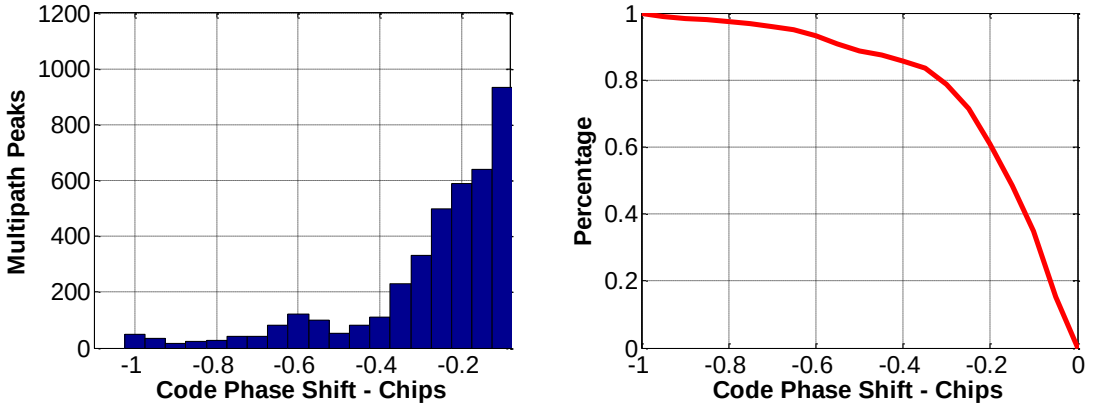

Figure 3.11: Multipath Distribution in the Code Phase Domain for All Satellites

3.3.1 Multipath Distributions of Different Speeds

As observed in Equation (2.41) and Equation (2.42) the Doppler offset associated with the multipath peak is a function of vehicle velocity. Furthermore, higher speed introduces larger Doppler offset. To this end, multipath distribution of different vehicle dynamics is assessed in this section. In particular, for a given multipath direction (*i.e.*, multipath vector) and vehicle direction of travel (*i.e.*, velocity vector), higher vehicle speed returns a larger multipath Doppler offset. From a block processing perspective (*i.e.*, block processing), a relatively large multipath

Doppler offset is preferred. In this case, multipath signal can potentially be isolated from the LOS peak (*i.e.*, the Doppler offset is larger than the frequency resolution). This makes extracting the LOS information from the correlation map more reliable.

The frequency resolution for a given coherent integration time is defined in Chapter Two. To recall, frequency resolution means any signal component whose Doppler offset is larger than the frequency resolution, the signal component overlapping effect is minor. To begin with, a low velocity is considered. Figure 3.12 shows the multipath distribution when the vehicle speed is less than 2 m/s. In this circumstance, the maximum multipath Doppler offset is 20 Hz (refer to Equation (2.41)). Six satellites are shown in this figure (each color refers to a different satellite), it is observed that most of the multipath peaks are within a small Doppler offset region, *i.e.*, from -5 Hz to 5 Hz.

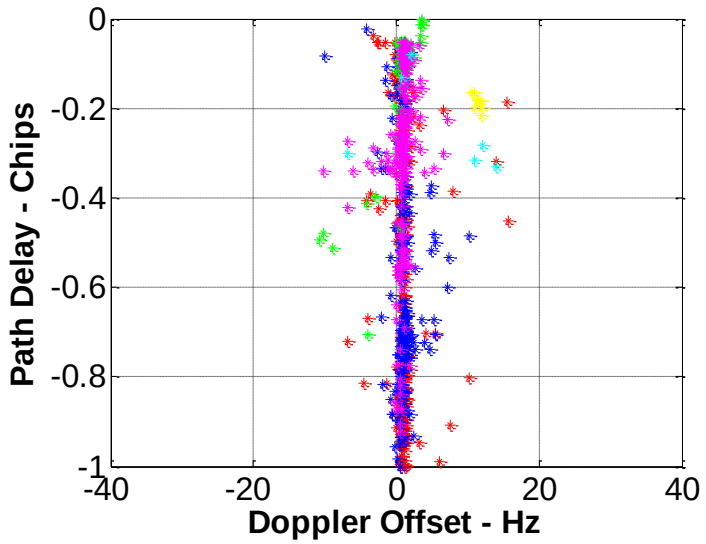

Figure 3.12: Multipath Distribution for Vehicle Speed lower than 2 m/s, August 16, 2012 Data Set

Figure 3.13 shows the histogram of multipath peaks in the Doppler domain when the vehicle speed is less than 2 m/s. Totally 685 multipath peaks are observed during the test performed. It is shown that in the Doppler domain 603 out of 685 (88%) peaks the Doppler offsets are less than 5 Hz, indicating that 88% of the multipath peaks cannot be reliably separated from the LOS peak if the coherent integration time is less than 200 ms (*i.e.*, the frequency resolution is larger than 5 Hz).

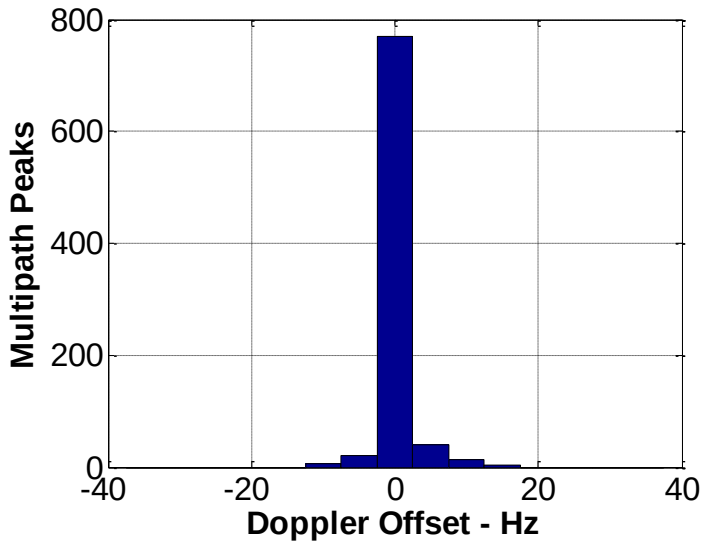

Figure 3.13: Histogram for a Vehicle Speed that is lower than 2 m/s, August 12, 2012 Data Set

Even so, for a higher speed it is more likely that the multipath peaks and LOS peak could be separated in the Doppler domain. Figure 3.14 shows the multipath distribution when the vehicle speed is larger than 5 m/s, it is observed that the multipath peaks are scattered across the whole search space (both code phase and Doppler domain).

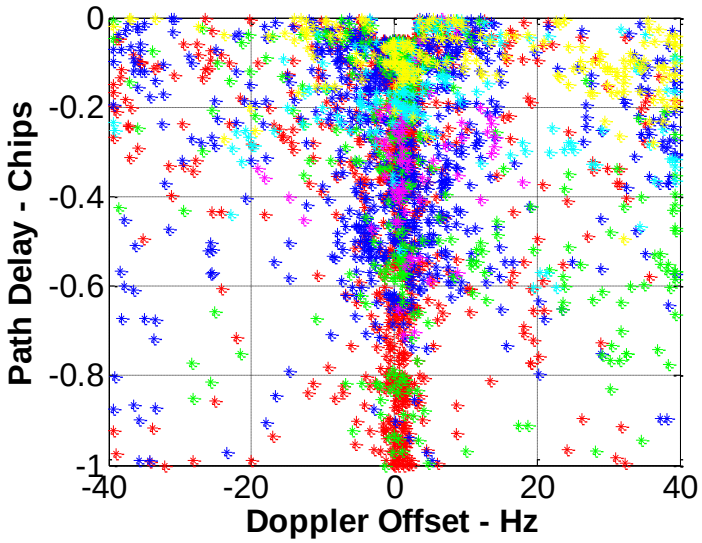

Figure 3.14: Histogram for a Vehicle Speed that is Higher than 5 m/s, August 12, 2012 Data Set

Figure 3.15 shows the histogram of multipath peaks when the vehicle speed is higher than 5 m/s. Only 37 percent of the multipath peaks are in the region of -5 Hz to 5 Hz, suggesting that 63 percent of the multipath peaks will be separated from the LOS peak if the coherent integration time is longer than 200 ms. Recall that only 12 percent of multipath peaks are separated from LOS peak when the speed is less than 2 m/s. It follows therefore that a higher speed is preferred from the receiver perspective because it is more reliable to separate the LOS peak and multipath peaks for a higher speed. Furthermore, if a longer coherent integration time is used (e.g., 500 ms), the peak separation percentage is further increased (*i.e.*, 81 percent of multipath Doppler offsets are larger than 2 Hz). It is also observed that even for a higher vehicle speed, it is still very common that a multipath peak has a small Doppler offset (*i.e.*, the Doppler offsets associated with 37 percent of multipath peaks are less than 5 Hz). This can be explained by the fact that most of the high buildings and their surfaces in the urban canyon area are parallel to the

direction of travel, thus the included angle between the direction of travel and multipath signal and the included angle between the direction of travel and LOS signal are almost the same.

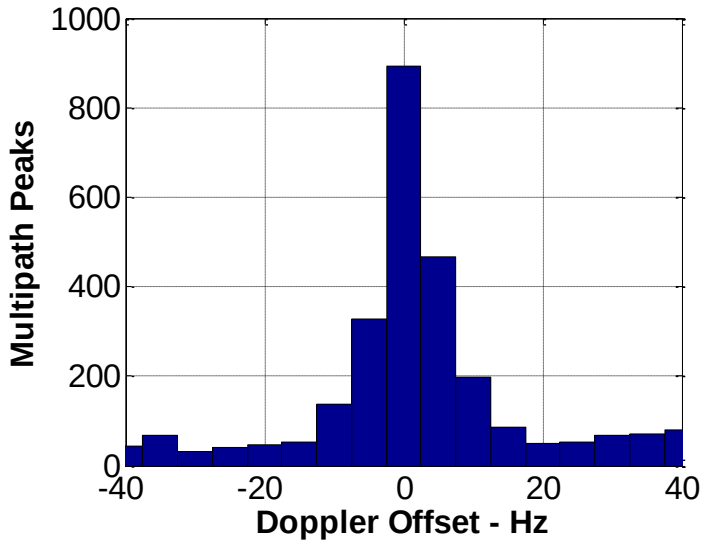

Figure 3.15: Multipath Peak Histogram when the Vehicle Speed is Larger than 5 m/s

The peak separation performance for different vehicle speed and for different coherent integration times are summarized in Figure 3.16. Velocity is increased by 1 m/s for each step, for example, 1 m/s shown in this figure means the velocity region is from 0 m/s to 1 m/s. Accordingly, 2 m/s means the velocity region is from 1 m/s to 2 m/s. As expected, higher vehicle speed returns better peak separation performance, which in turn improves navigation performance. Take 200 ms coherent integration time for example. If the vehicle speed is less than 1 m/s, more than 90% of the multipath peaks cannot be reliably separated from the LOS peak. However, if the vehicle speed is higher than 10 m/s, more than 50% of the multipath peaks could be separated from the LOS peak. These results suggest that higher vehicle dynamics can potentially improve navigation performance. It is also observed that after increasing the speed to 10 m/s, improvement in terms of the peak separation performance is minor.

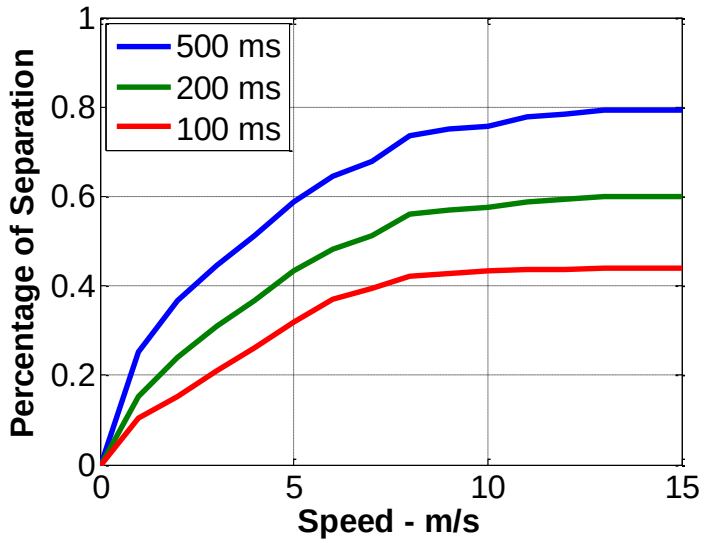

Figure 3.16: Peak Separation Performance of Different Vehicle Speed for 100 ms, 200 ms, and 500 ms Coherent Integration Times

For a short coherent integration time (e.g., 100 ms shown in Figure 3.16), a degraded peak separation performance is observed where only 40% of the multipath peaks were separated from the LOS peak even the speed is higher than 10 m/s. In contrast, after employing a longer coherent integration time (e.g., 500 ms shown in Figure 3.16), the peak separation performance is improved to 80% (*i.e.*, the speed is higher than 10 m/s) compared to the 100 ms integration time. This result suggests that the LOS peak identification performance can be improved by a longer coherent integration time.

3.3.2 Multipath Distributions of Different C/N_0

Multipath distributions of different speeds were assessed in the previous section, where the main focus is multipath peaks, *i.e.*, LOS peaks were ignored. However, it is impossible to remove multipath peaks completely in the receiver, thus the measurement accuracy is degraded when false identification of LOS peak happens. This section aims at developing a measurement

weighting model in the multipath environment when it is not assured of the signal being tracked (e.g., LOS signal or multipath signal). For the LOS environment (*i.e.*, no multipath signal), the pseudorange and Doppler measurements can be weighted by the signal power, loop filter bandwidth, and coherent integration time (Borio *et al*., 2009b; Langley, 1997). By extension, if the receiver is not assured of the signal being tracked, *i.e.*, LOS signal or multipath signal, the receiver can either remove this satellite from the navigation filter, or adjust the weighting scheme accordingly to keep this satellite in the filter. LOS peak and multipath peaks are assessed together in this section, instead of removing LOS peak and only assessing multipath peaks.

After including all LOS peaks and multipath peaks from the test performed, Figure 3.17 shows the multipath distribution for different signal power conditions. It is observed that the code phase accuracy is highly correlated with the signal power. More specifically, higher C/N_0 returns more accurate measurements in terms of code phase offset. For the signal power lower than 30 dB-Hz, it is very common that the code phase offset is larger than 0.5 chips (*i.e.*, 150 m). In contrast, most of the code phase offsets are less than 0.2 chips if the signal power is stronger than 35 dB-Hz. These results indicate that signal attenuation is a function of path delay, and longer path delay introduces more signal attenuation (Ashman and Garrison 2013). Moreover, it is very rare that the multipath peak power is stronger than 42 dB-Hz. In other words, the power of the multipath peaks is lower than 42 dB-Hz most of the time. Therefore an assumption is made in this thesis, that if the peak power is stronger than 42 dB-Hz, it corresponds to a LOS peak (recall the assumed LOS peak identification strategy in section 2.5.2). This is also used to detect the receiver anomaly discussed in Chapter Four.

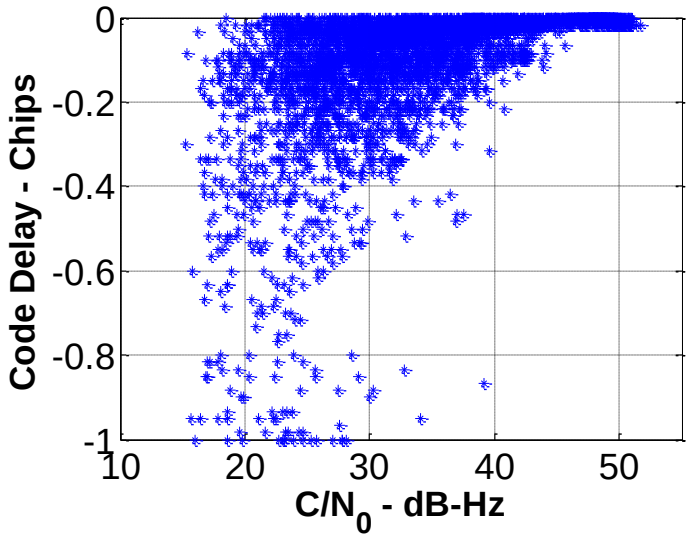

Figure 3.17: Signal Peak Code Phase Delay for Different Signal Powers, August 16, 2012 Data Set

Figure 3.18 shows the code phase delay standard deviation for different signal powers, fitting results are outlined in red. The fitting equation is shown below

$$\sigma_\tau^2 = \sigma^2 10^{(\alpha - C/N_0)/\eta} \tag{3.1}$$

where $\sigma^2 = 100\ m^2$ is the LOS signal code delay variance, $\alpha = 48$ dB-Hz is the nominal LOS signal power, and $\eta = 15$ is an empirical constant factor.

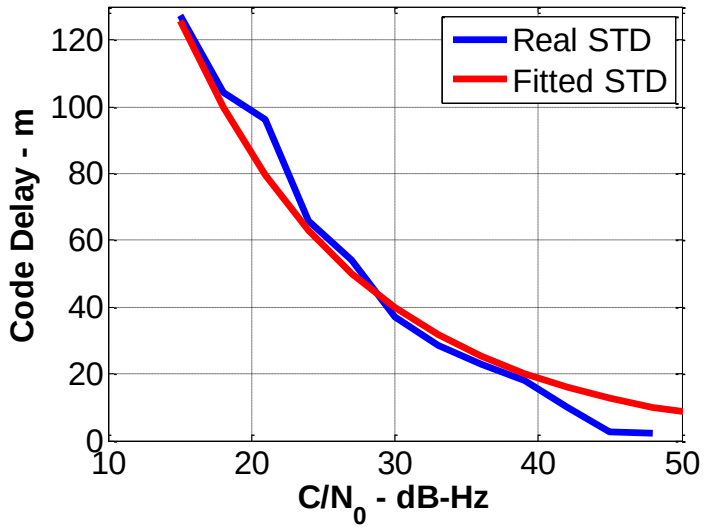

Figure 3.18: Peak Code Phase offset Standard Deviation Fitting Performance, August 16, 2012 Data Set

If the receiver is not assured of the signal being tracked, the pseudorange accuracy can be approximated as 116 m for 16 dB-Hz signal power. However, if the observed peak power is larger than 30 dB-Hz, the pseudorange accuracy is improved to less than 40 m.

Figure 3.19 shows the Doppler offsets for different signal powers, a clear trend is also observed in this figure that the Doppler offset variation is a function of signal power. In particular, the Doppler variation is decreased after increasing the signal power. For the C/N_0 larger than 35 dB-Hz, the Doppler offset is generally less than 10 Hz. Nevertheless, it is observed that it is very common that the Doppler offset is larger than 20 Hz if C/N_0 is smaller than 30 dB-Hz.

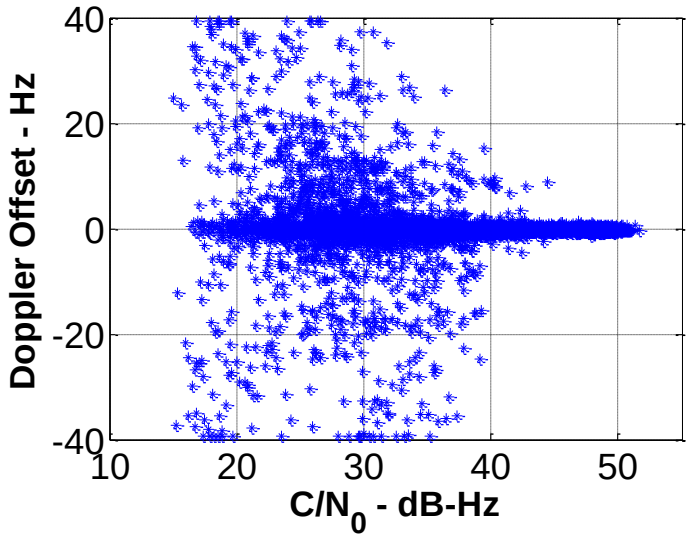

Figure 3.19: Signal Peak Doppler offset for Different Signal Powers, August 16, 2012 Data Set

Figure 3.20 shows the Doppler offset standard deviation for different signal powers, also, the fitted standard deviation from Equation (3.2) is plotted for comparison.

$$\sigma_\rho^2 = \sigma^2 10^{(\alpha - C/N_0)/\eta} \tag{3.2}$$

where $\sigma^2 = 3\ \text{Hz}^2$ is the LOS signal Doppler standard deviation, $\alpha = 48$ dB-Hz is the nominal signal power, and $\eta = 15$ is an empirical constant factor.

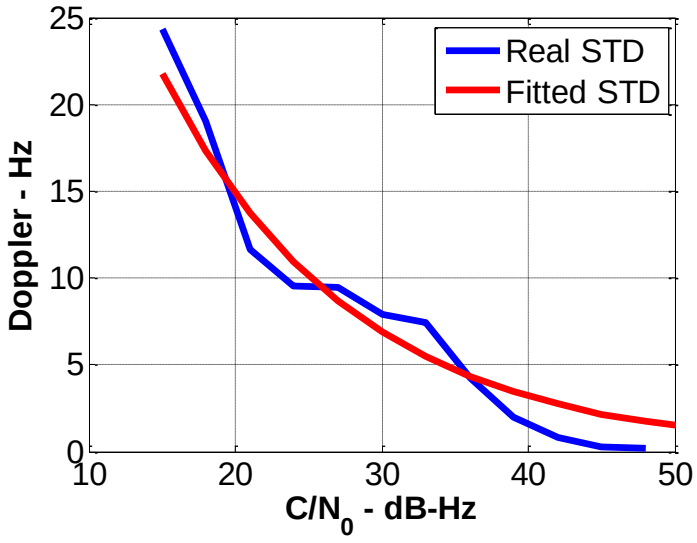

Figure 3.20: Peak Doppler offset Standard Deviation Fitting Performance, August 16, 2012 Data Set

If the receiver is not assured of the signal being tracked, the Doppler accuracy can be approximated as 22 Hz for 16 dB-Hz signal power. However, if the observed peak power is larger than 35 dB-Hz, the Doppler accuracy is improved to less than 5 Hz. These results can be employed in the navigation filter to weight the measurements (*i.e.*, measurement variance).

Chatper Four: Multipath Directional-dependence and Receiver Anomaly Check

After looking at the multipath distributions for different conditions in Chapter Three, this chapter concentrates on the directional-dependence of multipath peaks in high sensitivity receivers. The maximum and minimum Doppler offsets were theoretically derived in Chapter Two (Equation (2.43)) and were generally found not to be equal in trends of absolute value. To this end, an interesting result was shown by Xie *et al*. (2011), that the multipath Doppler offset distributions are varied with respect to the vehicle's direction of travel. This Chapter starts with an ideal case assuming a reference trajectory is available (recall the GSNRx-ss™ receiver concept). Furthermore, two special cases are used to show the directional-dependence of multipath signals in the urban canyon environment.

Note that the GSNRx-ss™ receiver was applied to calibrate the multipath distributions, where a high quality receiver trajectory was utilized. Yet, position and/or velocity estimates could be biased in the receiver (thus NCO errors are present). This is especially true in the urban canyon areas, where the velocity error can reach as much as 10 m/s, thus the receiver estimates need be validated first. As discussed in Chapter Two, a vital challenge for the assumed LOS peak strategy is to correctly identify the receiver anomaly. Again, receiver anomaly means the LOS signal peak is outside the predicted LOS region (predicted from nominal signal parameters). Imperfect nominal signal parameters degrade the peak selection performance. This chapter looks at how to implement the multipath directional-dependence as well as the LOS signal parameters to detect receiver anomaly, and a case study will be shown afterwards.

4.1 Parallel Case

Directional-dependent multipath was proposed in the Chapter Two. In this section, a special case is analyzed to describe this phenomenon. An extreme case where the LOS signal vector is parallel to the velocity vector is utilized. In this regard, the projection of vehicle velocity to the LOS signal vector will satisfy

$$\vec{V}_R \vec{H}_{LOS}^T = \left|\vec{V}_R\right|$$

Substituting the above result to Equations (2.41) and (2.42), the multipath region is defined as

$$MP_{\mathbb{R}_f} = \begin{bmatrix} 0 & \dfrac{2\left|\vec{V}_R\right|}{\lambda} \end{bmatrix}$$

These results suggest that the multipath peak can only be observed in the positive Doppler plane of the correlator map. Considering the speed limit in downtown of most Canadian cities is 50 km/h, the maximum multipath Doppler offset is 150 Hz. An example is shown below where the live data collected in the downtown Calgary is utilized (the same data set was used in Chapter Three), in particular, only the period where the vehicle traveled in West-East direction is used. There is no satellite whose azimuth is completely parallel to the vehicle velocity, so, a LOS vector close to parallel to the vehicle velocity is used. PRN 9 is selected due to its azimuth being 108 degrees (angle between direction of travel and LOS vector is less than 20 degrees), and the elevation being 14 degrees. The maximum vehicle speed being 14.7 m/s during the test performed. Substituting the above velocity and geometry to Equations (1.5), (2.41), and (2.42), the multipath region is calculated as

$$MP_{\mathbb{R}_f} = \left[-5.1 \text{ Hz} \quad 127.4 \text{ Hz}\right]$$

The above multipath region is verified in Figure 4.1 (the same strategy used in Chapter Three to identify the multipath peaks is employed here), where it is observed that most of the multipath peaks fall in the positive Doppler plane (*i.e.*, multipath Doppler offset is positive). Note that the search space size applied in the receiver is ±40 Hz, as a search space as large as the one given above is not practically feasible (i.e., computation load is high). Also the minimum Doppler offset is only -3.1 Hz, larger than the predicted minimum Doppler offset (*i.e.*, -5.1 Hz). This can be explained by the fact that the multipath signal is not coming from all directions during the test performed (although theoretically it may), thus $\vec{V}_R \vec{H}_{MP}^T$ cannot be simplified as $\left|\vec{V}_R\right|$ in Equation (2.42). This also indicates that the assumption that multipath signals could be from any direction made in Equations (2.41) and (2.42) is conservative.

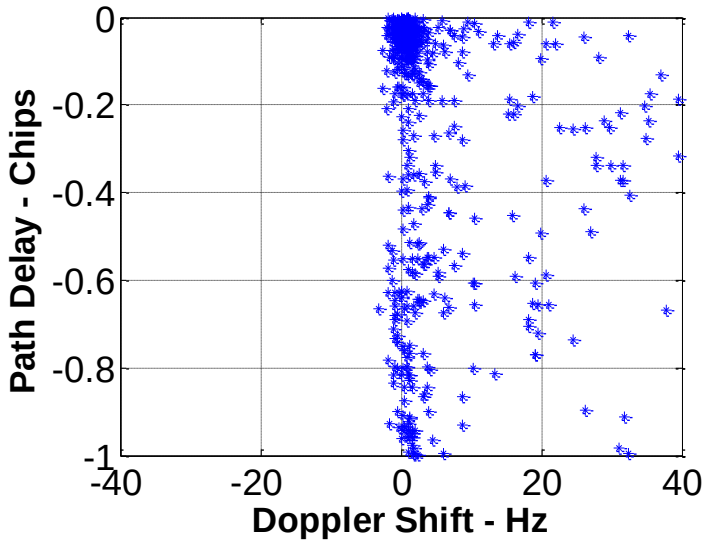

Figure 4.1: Multipath Peak Distribution for the LOS Signal close to Parallel to the Vehicle Velocity

4.2 Orthogonal Case

Having looked at the case where the signal vector and velocity vector are nearly parallel, the analysis now shifts to another extreme, case where the LOS signal vector is orthogonal to the velocity vector. The Equations (2.41) and (2.42) show that if the LOS vector is orthogonal to the velocity vector, the projection of vehicle velocity to the LOS signal vector will satisfy

$$\vec{V}_R \vec{H}_{LOS}^T = 0$$

Substitute the above result to Equations (2.41) and (2.42), the multipath region can be described as

$$MP_{\mathbb{R}_f} = \left[-\frac{\left|\vec{V}_R\right|}{\lambda} \quad \frac{\left|\vec{V}_R\right|}{\lambda} \right]$$

This result suggests that the multipath peak can be observed in both positive and negative planes. An example is shown below, again, there is no satellite whose azimuth is completely orthogonal to the vehicle velocity, so a satellite close to orthogonal to the velocity vector is utilized. PRN 2 is selected as its azimuth is 192 degrees during the test performed. The multipath distribution is shown in Figure 4.2 and Figure 4.3, where the multipath peaks fall approximately equally in the positive and negative planes for both West-to-East direction and East-to-West direction.

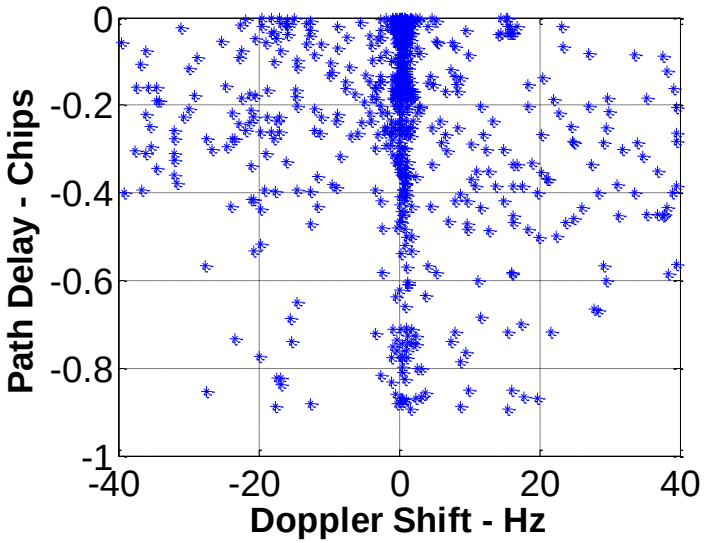

Figure 4.2: Multipath Peak Distribution for the LOS Signal close to Orthogonal to the Vehicle Velocity, West-East Direction

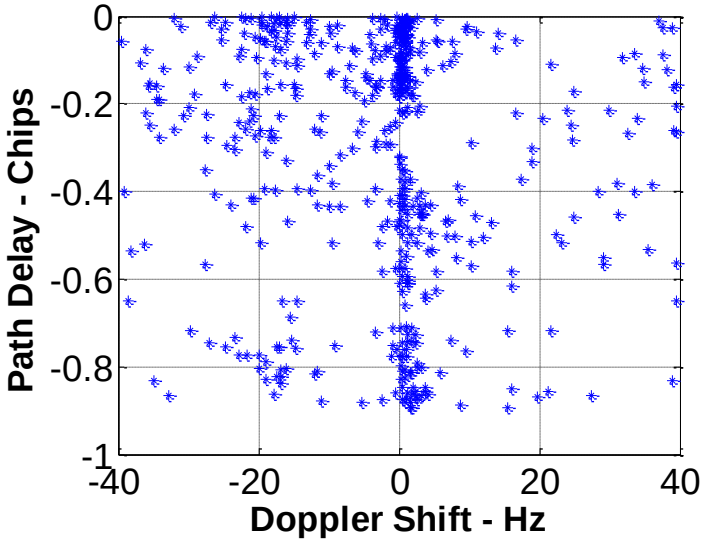

Figure 4.3: Multipath Peak Distribution for the LOS Signal close to Orthogonal to the Vehicle Velocity, East-West Direction

4.3 Receiver Anomaly Check

This section analyzes how to apply the multipath directional-dependence and LOS signal parameters to detect anomalies in the receiver's navigation solution (primarily in velocity), specifically, for the GSNRx-hs™ receiver (i.e., no reference trajectory is available) although its performance will be assessed in Chapter Five. Recall that receiver anomaly is defined as the NCO error is larger than the predicted regions (*i.e.*, LOS region). Moreover, NCO errors indicate the predicted LOS region veracity. The receiver correlation process centred at the NCO values (*i.e.*, the start point of the correlation map), however, due to the NCO errors the LOS peak may not be found at the starting point. In this regard, the LOS region is utilized to select the LOS peak.

As discussed in the section 2.4 the Kalman filter variance-covariance is an effective way of determining the LOS region. Specifically, the variance-covariance matrix obtained from Kalman filter indicates the accuracy of the receiver estimates, which can be used to predict the LOS peak region in the high sensitivity receiver. To ensure the LOS region is large enough to include LOS peaks, the three-sigma uncertainties are employed in this work (*i.e.*, 99.5% confidence level).

4.3.1 Receiver Anomaly Detection Scheme

A receiver anomaly detection scheme proposed in this thesis is based on the shifts (both code phase offset and Doppler offset) of the observed LOS peak and/or multipath peaks. LOS region and multipath region were introduced in Chapter Two, containing all possible LOS and multipath shifts that can be expected. By extension, if an observed correlator peak is outside of the predicted region, the estimates in the receiver are considered suspicious and the LOS region and multipath region should be refined respectively.

As biases in the nominal signal are generally unknown, an effective way to refine the LOS and multipath regions is to use a scaled version of the Kalman filter variance-covariance matrix (thus increasing the predicted peak region) until all peaks are in the refined regions. More specifically, if the observed multipath peak is outside the predicted multipath region, the scale factor m defined in Equation (2.51) is increased so that the predicted region contains all the peaks. Still, the scale factor m is reset to the original value (three in this work) at every epoch after LOS peak identification. In other words, the variance-covariance matrix used by the filter is not affected by this process. An example will be shown in the next section to detect the velocity anomaly. If the velocity anomaly is reported based on the LOS peak, *i.e.,* the LOS peak is outside the predicted region. The same method is applied to the LOS peak region until the LOS peak is in the predicted region.

The receiver anomaly detection process is broken down into two parts; one for position anomalies and another for velocity anomalies. The position anomaly detection scheme is summarized in Figure 4.4. LOS peak code phase offset can be utilized to diagnose the position anomaly in the receiver. If the LOS peak falls in the predicted code phase region, no position anomaly is reported. Alternatively, if the LOS peak falls outside of the predicted region as shown in Equation (2.59), a position anomaly will be reported and correspondingly, the LOS region in the code phase domain should be refined. Note that the position anomaly is difficult to be identified as only LOS signal can be used.

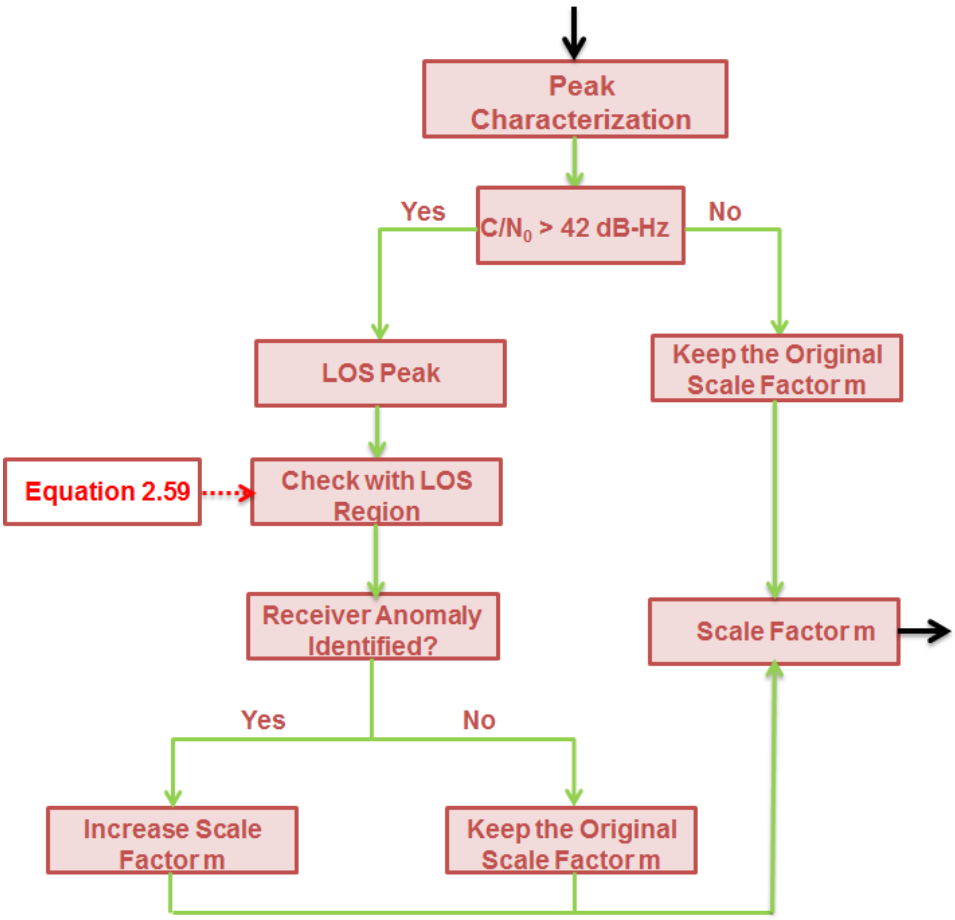

Figure 4.4: Proposed Receiver Position Anomaly Check Strategy in the High Sensitivity Receiver

The velocity anomaly is identified more effective to be in comparison with the position anomaly due to the fact that both LOS and multipath peaks can be used. In this section, the main goal is to identify the velocity anomaly. If the identified peak is the LOS peak (*i.e.*, C/N_0 is larger than 42 dB-Hz, refer to Table 2.6), the Doppler offset associated with this peak is compared to the predicted LOS region. In contrast, if the identified peak is a multipath peak, the Doppler offset associated with this peak is compared to the predicted multipath region. Finally, if any peak is

outside of its predicted region, velocity anomaly is reported and as a result, the peak regions will be refined. Receiver anomaly check scheme is summarized in Figure 4.5.

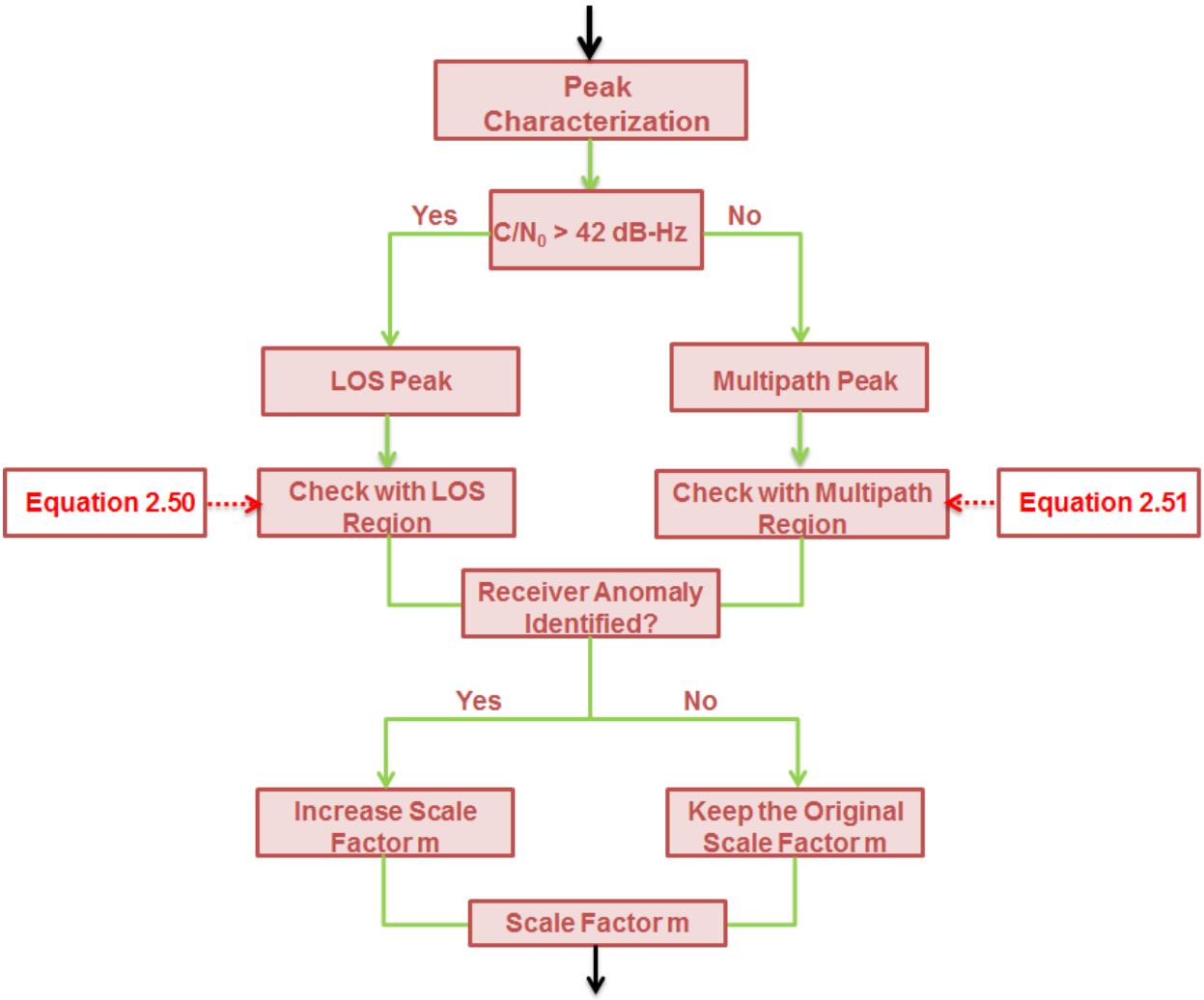

Figure 4.5: Proposed Receiver Velocity Anomaly Check Strategy in the High Sensitivity Receiver

4.3.2 Case Study

An example is shown here to illustrate how the directional-dependence of multipath is used to detect velocity anomaly in the GSNRx-hs™ receiver. An example of velocity anomaly is shown

in Table 4.1, where the velocity error is larger than 2 m/s, and as a result, the NCO frequency errors for PRN 12 and PRN 28 are 11.2 Hz and 9.7 Hz, respectively. The estimated velocity and associated uncertainty from the receiver are also shown. Remember that the multipath region can be predicted by the given velocity vector (*i.e.*, estimated velocity), satellite geometry, and receiver estimates uncertainty.

Table 4.1: Velocity and Clock Drift Errors when the Velocity Anomaly Occurs

Velocity	North	East	Up	Clock
Real	3.4 m/s	1.7 m/s	0.0 m/s	-4.1 m/s
Estimated	1.5 m/s	1.5 m/s	-0.4 m/s	-3.8 m/s
Error	-1.9 m/s	-0.2 m/s	-0.4 m/s	0.3 m/s
Uncertainty	0.3 m/s	0.3 m/s	0.4 m/s	0.3 m/s

The satellites geometries are shown in Table 4.2. Note that only the estimated velocity is applied to predict the multipath region.

Table 4.2: Multipath Region Prediction when the Velocity Anomaly Occurs

Satellite	Elevation	Azimuth
PRN12	30 degrees	297 degrees
PRN28	23 degrees	114 degrees

PRN 28 is used first to show the velocity anomaly check performance, and PRN 12 will be applied later to illustrate the dependence of the proposed algorithm on satellite geometry. The LOS vector of PRN 28 is described by

$$\bar{H}_{LOS} = \begin{bmatrix} -0.84 & 0.37 & -0.39 \end{bmatrix}$$

Receiver velocity output (*i.e.*, estimated velocity) is

$$\vec{V}_R = \begin{bmatrix} 1.5 & 1.5 & -0.4 \end{bmatrix}$$

After submitting $\vec{H}_{LOS}$ and $\vec{V}_R$ to Equations (2.41) and (2.42) return

$$MP_{\mathbb{R}_f} = \begin{bmatrix} -12.8 \text{ Hz} & 7.3 \text{ Hz} \end{bmatrix}$$

The variance-covariance matrix from Kalman filter is determined by (for convenience, only the diagonal units are shown, but the full matrix is used to predict the uncertainty in the receiver)

$$P_{vd} = diag\begin{pmatrix} 0.11 & 0.11 & 0.17 & 0.07 \end{pmatrix}$$

And the multipath uncertainty can be predicted as

$$\sigma_{MP}^2 = \frac{\begin{bmatrix} \vec{H}_{LOS} & 1 \end{bmatrix} P_{vd} \begin{bmatrix} \vec{H}_{LOS} & 1 \end{bmatrix}^T}{\lambda^2} = 5.2\text{Hz}^2$$

If $m = 2$, based on Equations (2.50) and (2.51) the LOS region and multipath region are respectively predicted as

$$LOS_{\text{Region}} = \begin{bmatrix} -4.6\text{Hz} & 4.6\text{Hz} \end{bmatrix} \text{ and } MP_{\text{Region}} = \begin{bmatrix} -17.3\text{Hz} & 11.7\text{Hz} \end{bmatrix}$$

Two peaks are observed in this epoch and are listed in Table 4.3, obviously, none of them are LOS peaks. By extension, they are considered as multipath peaks and are compared to the predicted multipath region.

Table 4.3: Multipath Peaks Observed from PRN 28 when the Velocity Anomaly Occurs

Peaks	Doppler offset	Code phase offset	C/N_0
Dominant peak	12.6 Hz	-0.10	34.7 dB-Hz
Second peak	18.9 Hz	-0.14	28.4 dB-Hz

The LOS and Multipath regions are illustrated in Figure 4.6, along with the observed multipath peaks. The multipath peaks are outside the predicted multipath region, so a velocity anomaly is reported and a scaled version of the variance-covariance matrix is used to (effectively) push the multipath peaks inside the multipath region.

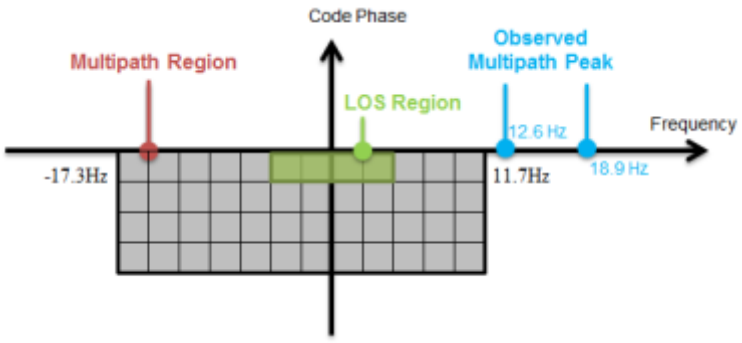

Figure 4.6: Illustration of the Predicted LOS and Multipath Regions

After increasing m to 6 the multipath region is expanded to

$$MP_{\text{Region}} = \left[-26.5\text{Hz} \quad 20.9\text{Hz}\right]$$

The observed multipath peaks are in the multipath region as shown in Figure 4.7. Consequently, the LOS region is expanded to

$$LOS_{\text{Region}} = \left[-13.7\text{Hz} \quad 13.7\text{Hz}\right]$$

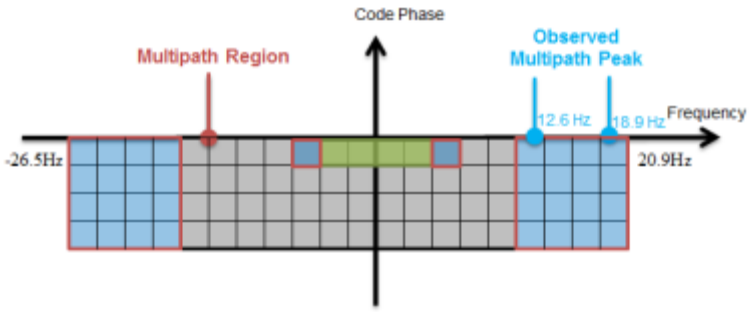

Figure 4.7: Illustration of the Refined Multipath Region

Note that the NCO frequency error at this epoch is -11.2 Hz, so the LOS peak can potentially be identified if present after expanding the LOS region from 7.3 Hz to 13.7 Hz. After checking the receiver anomaly, the LOS peak is eventually included in the predicted LOS region improving availability. However, the LOS peak cannot always be pushed back to the LOS region using this method.

Note that the receiver anomaly detection is highly reliant on the satellite geometry as shown below using PRN12. The LOS vector of PRN 12 is defined by

$$\vec{H}_{LOS} = \begin{bmatrix} 0.77 & -0.39 & -0.50 \end{bmatrix}$$

Substituting $\vec{H}_{LOS}$ and $\vec{V}_R$ to Equations (2.41) and (2.42) results in

$$\Delta D_{MP_{\max}} = 14.0\,\text{Hz} \text{ and } \Delta D_{MP_{\min}} = -6.0\,\text{Hz}$$

The predicted LOS and multipath regions are described by

$$LOS_{\text{Region}} = \begin{bmatrix} -4.6\,\text{Hz} & 4.6\,\text{Hz} \end{bmatrix} \text{ and } MP_{\text{Region}} = \begin{bmatrix} -10.5\,\text{Hz} & 18.5\,\text{Hz} \end{bmatrix}$$

Only one peak is observed from PRN 12 at this epoch. The details are presented in Table 4.4. This peak is in the predicted multipath region and no velocity anomaly is reported from this satellite.

Table 4.4: Correlation Peaks Observed from PRN 12 when the Velocity Anomaly Occurs

Peaks	Doppler offset	Code phase offset	C/N_0
Dominant peak	-7.2 Hz	-0.23	34.7 dB-Hz

Note that the receiver anomalies are not reported on a satellite-by-satellite basis. Rather, all of the satellites in view are used to check the receiver anomaly as the receiver anomaly detection is highly reliant on the satellite geometry. Also note that once a receiver anomaly is reported, the LOS region expansion will be applied for all the satellites (although the amount of expansion may vary between satellites).

Chatper Five: High Sensitivity Receiver Performance

Recall that the GSNRx-ss™ receiver was used in the previous two chapters to characterize the multipath signals, where a high quality reference trajectory was used. However, this is not a practical scenario. Rather, the best that a receiver can do is to use its predicted navigation solution as the "reference trajectory" to generate the signal parameters for each satellite. This is what is done with the GSNRx-hs™ version of the software used for this thesis, and is the focus of this chapter.

LOS peak identification strategies, specifically, the dominant peak strategy and the assumed LOS peak strategy, were proposed in Chapter Two and are evaluated and compared in this chapter. Most of the multipath peaks are removed in the receiver after using assumed LOS peak strategy, consequently, pseudorange and Doppler accuracies are improved substantially.

The multipath distribution was obtained in Chapter Three. In particular, the Doppler offsets of most of the multipath peaks are larger than 2 Hz (*i.e.*, 80 %), and 60 percent of the multipath peaks are larger than 5 Hz during the dynamic period (refer to Figure 3.16), thus different coherent integration times have different ability to separate multipath peaks. Different search strategies are therefore implemented in this chapter. Also, the standard receiver and the high sensitivity receiver are respectively utilized.

The chapter is organized as follows. First, the performance of the standard receiver is presented, and limited position results are shown. Second, the method used to evaluate the measurement quality (and thus the ability of the receiver to identify the LOS signal) is presented. Third, the performance of high sensitivity receiver using the dominant peak strategy is presented by using different coherent integration times. Finally, the assumed LOS peak scheme is utilized and

compared with the dominant peak strategy. Better position performance is obtained using the assumed LOS peak strategy. As mentioned in Chapter Three that three data sets were collected in the downtown Calgary. The August 16, 2012 data set (the same data set as used in Chapter Three) is used first to evaluate the receiver performance (*i.e.*, sections 5.1, 5.3, and 5.4). Another two data sets will be assessed in section 5.5. Moreover, dense foliage and suburban data sets are utilized to confirm the receiver strategy proposed in this work

5.1 Standard Receiver

The performance of the standard receiver is shown briefly first, where the maximum coherent integration time is 20 ms. Figure 5.1 shows the performance of the standard receiver. The red curve shows the reference trajectory and the blue dots show the positions obtained from the standard receiver. Figure 5.2 shows the reference trajectory on Google Earth™. As expected, the standard receiver has limited capabilities for urban canyon navigation as the position availability is less than 10 percent. Only in those areas with partial open-sky can the signal be tracked by the standard receiver. This can be explained by the fact that the standard tracking loop is unable to maintain lock of the LOS signal, either due to the absence of the LOS peak or because the LOS signal is too weak (refer to Figure 3.5 where the signal power is shown), or due to the presence of multipath.

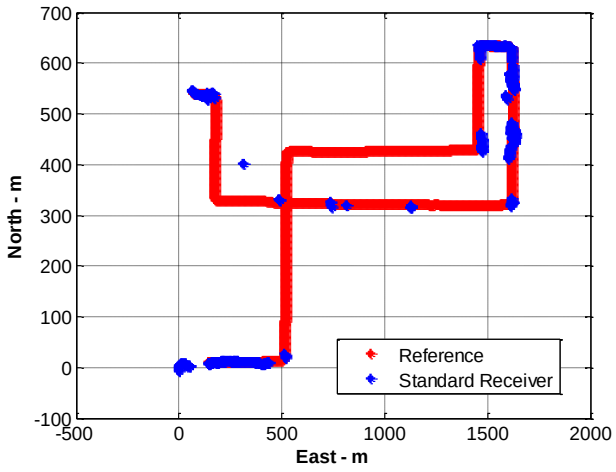

Figure 5.1: Position Performance of the Standard Receiver by Employing Least-Squares

Figure 5.2: Reference Trajectory of the August 16, 2012 Data Set shown in Google Earth™

5.2 Measurement Quality Evaluation for the High Sensitivity Receivers

As standard receivers have limited capabilities for urban canyon navigation, high sensitivity receivers are used for the remainder of this chapter. Before looking at the results in detail, this section describes how the ability of a high-sensitivity receiver to correctly identify LOS signals is quantified. Figure 5.3 shows the data processing approach used to assess the identified LOS peak quality, where the estimated observations (*i.e.*, pseudorange and Doppler) are obtained from the GSNRx-hs™ receiver. Meanwhile, the reference observations (or true observations) are

obtained in the GSNRx-ss™ receiver, where a reference trajectory is utilized (recall section 3.1.2). Thus, the observation errors can be obtained by comparing the estimated observations and the true observations. The same thresholds used in section 3.1.2 are applied here to evaluate the identified LOS peak quality. Specifically, if the pseudorange error is less than 10 m, and at the same time, the Doppler error is less than 2 Hz, the conclusion can be made that the identified LOS peak is a real LOS peak.

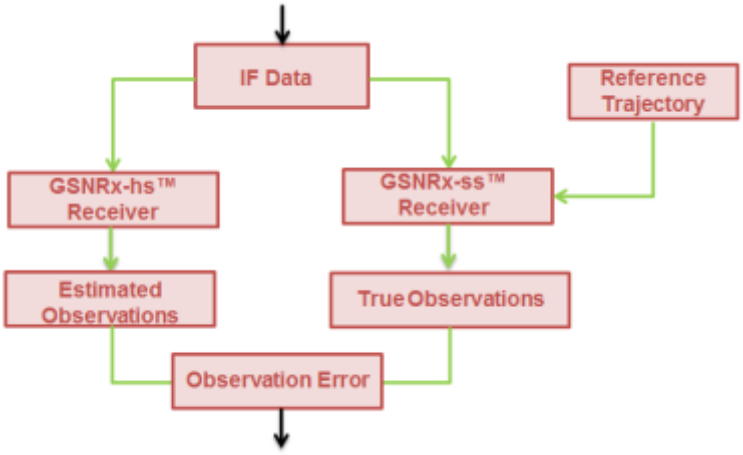

Figure 5.3: GSNRx-hs™ receiver Observation Quality Assessment Strategy

Furthermore, availability and reliability are defined in this research to evaluate the peak identification performance. In this work, availability refers to the percentage of time an observation to a satellite can be generated, be it from an LOS or multipath signal. Reliability is the percentage of time an available measurement corresponds to an LOS signal. In other words, a satellite may have 50% availability, but if all measurements are from LOS signals, the reliability would be 100%.

5.3 Dominant Peak Strategy

A high-sensitivity receiver based using the dominant peak strategy is evaluated in this section. Specifically, longer coherent integration times compared to the standard receiver are applied (*i.e.*, longer than 20 ms). Then, as described in Chapter Two, the peak with the strongest power is selected within the receiver. The corresponding code phase offset and Doppler offset are then extracted to generate the measurements. A narrow search space size and a wide search space size are also compared and contrasted.

5.3.1 Narrow Search Space Size

As shown in the multipath distribution chapter, during dynamic periods, only 40 percent of multipath peaks are in the region of ±5 Hz in the Doppler domain (refer to Figure 3.16). Thus, a narrow search space size can theoretically "automatically" exclude more than half of the multipath peaks. Also, Figure 3.8 shows that a narrow search space size can improve the probability of the dominant peak being the LOS peak. The benefit of a narrow search space is two-fold: first, the possibility to exclude multipath peaks from the correlation map is increased; second, it reduces the computation load as fewer correlators are required (compared to a wide search space size). However, a narrow search space size may not be suitable for this research since position and/or velocity may be biased by multipath signals which results on the LOS peak falling outside the search space (let alone the LOS region). As a result, no LOS measurements are available from this satellite thus degrading the receiver performance, which will be shown later.

In this research, the narrow search space size is defined as ±5 Hz in the Doppler domain and ±90 m in the code phase domain. The coherent integration times applied are 40 ms and 200 ms. Most of the LOS peak and multipath peaks will be overlapped for the 40 ms case (*i.e.*, resolution is 25

Hz), nonetheless, they will be separated for the 200 ms case (*i.e.*, resolution is 5 Hz). The block processing strategy used is summarized in Table 5.1.

Table 5.1: Block Processing Strategy for the Dominant Peak Strategy using a Narrow Search Space Size

Integration Time	40 ms (200 ms)	
Search Space	Doppler Domain	±5 Hz
	Code Phase Domain	±90 m
Search Step	Doppler Domain	2 Hz
	Code Phase Domain	10 m

Figure 5.4 shows the position performance of 40 ms and 200 ms coherent integration times. It is observed that the receiver diverges for both cases after travelling into the urban canyon (refer to Figure 5.2). This can be explained by the fact that for the block processing receiver, the search space size should be sufficiently wide to tolerate large navigation errors in order to maintain reliable tracking. A ±5 Hz and ±90 m search space size is not wide enough to include the LOS signal in the search space, when large navigation errors occur.

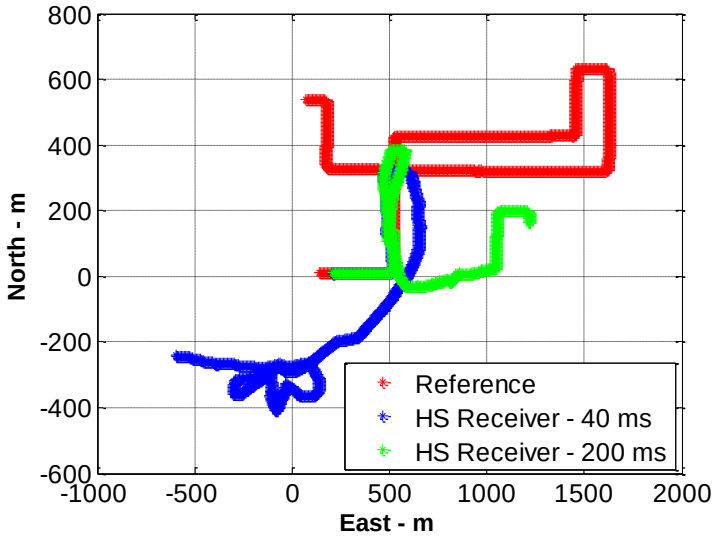

Figure 5.4: Position Performance of the 40 ms and 200 ms Coherent Integration Times using Narrow Search Space Size Strategy (Dominant Peak Strategy)

5.3.2 Wide Search Space Size

The focus then moves to avoid the divergence phenomenon observed in the previous section when a narrow search space size was used. Specifically, a wider search space size (±30 Hz in the Doppler domain, and ±150 m in the code phase domain) is applied to tolerate larger navigation errors. After expanding the search space size the probability of the dominant peak being the LOS peak is decreased for the dominant peak strategy. More multipath peaks with strong signal power may be identified as LOS peaks (refer to Figure 3.8). Still, the benefit of a wider search space size is that the LOS peak can possibly be observed in the search space even if the position and/or velocity are biased by the multipath measurements (*i.e.*, receiver anomaly).

Note that the signal peak power is not attenuated by the receiver anomaly if the search space is large enough (Van Diggelen, 2009). Although a 500 ms coherent integration time has better peak separation performance (*i.e.*, frequency resolution is 2 Hz), the correlation performance is

degraded by the receiver dynamics (shown later in this section). Thus a 200 ms coherent integration time is applied first (yielding the best results), and then the performance of different coherent integration times are summarized. The block processing strategy applied for 200 ms coherent integration time is shown in Table 5.2.

Table 5.2: Block Processing Strategy for the Dominant Peak Strategy using Wide Search Space Size

Integration Time	200 ms	
Search Space	Doppler Domain	±30 Hz
	Code Phase Domain	±150 m
Search Step	Doppler Domain	2 Hz
	Code Phase Domain	10 m

Figure 5.5 to Figure 5.7 show the position and velocity performance for a 200 ms coherent integration time. A relatively large position error variation is observed during the period of 423100 s to 423300 s, and again, during the period of 423550 s to 423600 s. This is due to multipath signals with large pseudorange errors being considered as the LOS peaks in the receiver. The velocity errors are less than 1 m/s most of the time and reach a maximum of 6 m/s. In such cases, since vector-tracking is used, the receiver NCO frequency can be shifted by a few Hz to tens of Hz relative to the actual value.

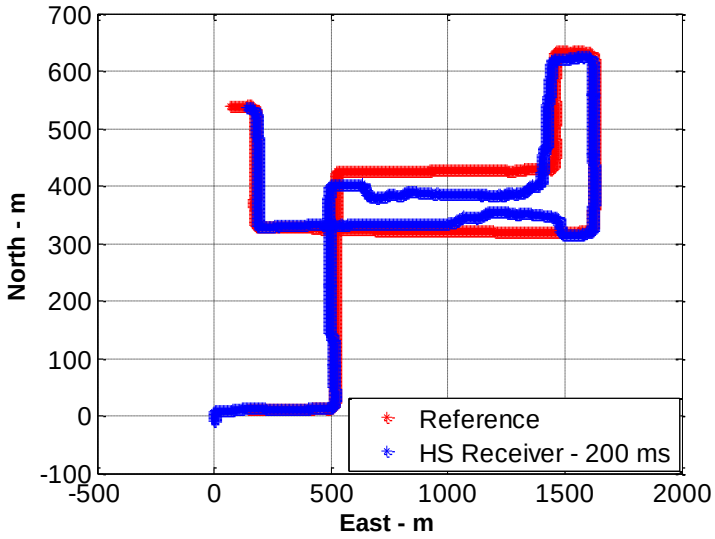

Figure 5.5: Estimated Trajectory for 200 ms Coherent Integration of the Dominant Peak Strategy using a Kalman Filter

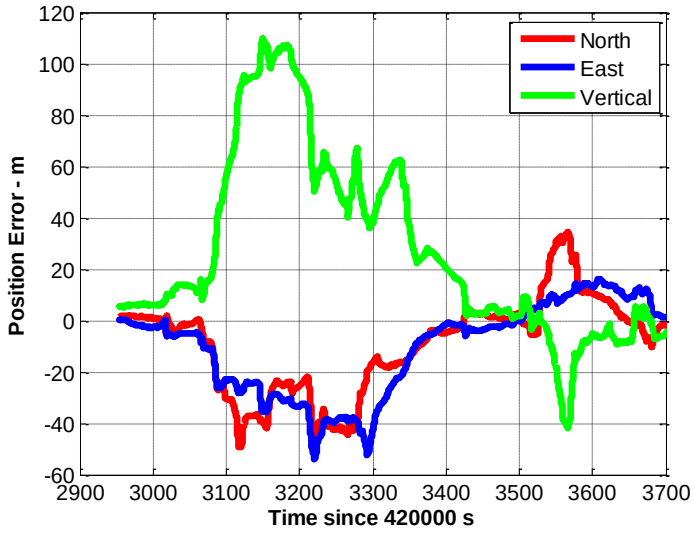

Figure 5.6: Position Performance for 200 ms Coherent Integration of the Dominant Peak Strategy using Kalman Filter

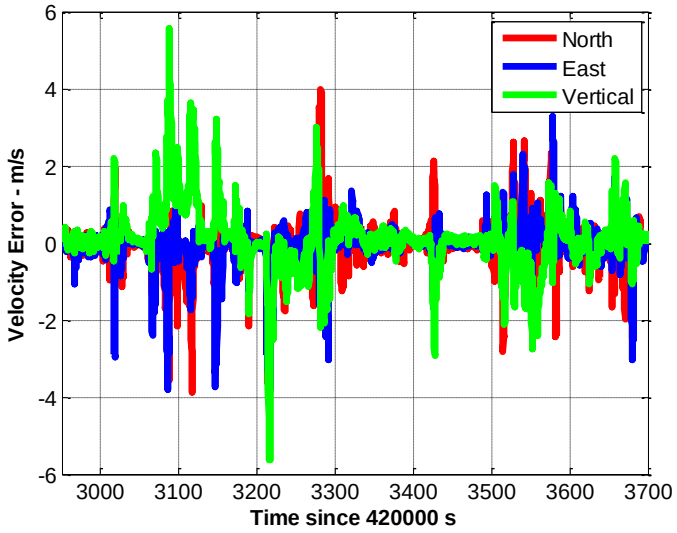

Figure 5.7: Velocity Performance for 200 ms Coherent Integration of the Dominant Peak Strategy using Kalman Filter

A high and low elevation satellite are selected here to show the NCO errors during the test performed. Remember that the NCO errors indicate the search space quality as mentioned in section 2.4.2. Figure 5.8 shows the NCO code phase and frequency errors of PRN 4, whose elevation and azimuth are 50 degree and 153 degree, respectively. It is observed that the NCO frequency errors (in terms of the absolute value) are less than 10 Hz most of the time, and jump to 20 to 30 Hz in extreme cases. Also, the NCO code phase errors are generally less than 0.1 chips and jump to 0.15 chips for some epochs.

This is also the case for PRN 28 with a 24 degree elevation and 114 degree azimuth. These results suggest that the larger search space is sufficient to tolerate the receiver anomalies. Nevertheless, the resulting position and velocity solutions may not be ideal.

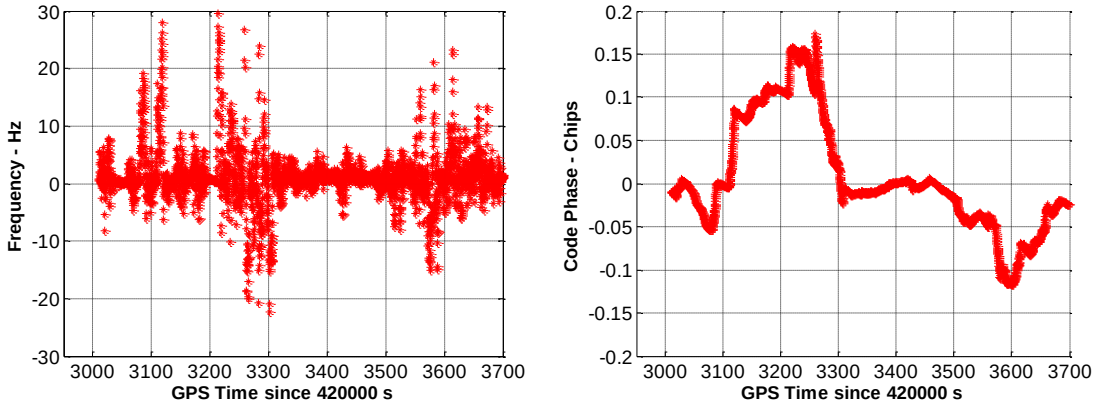

Figure 5.8: PRN 4 NCO Frequency and Code Phase Errors

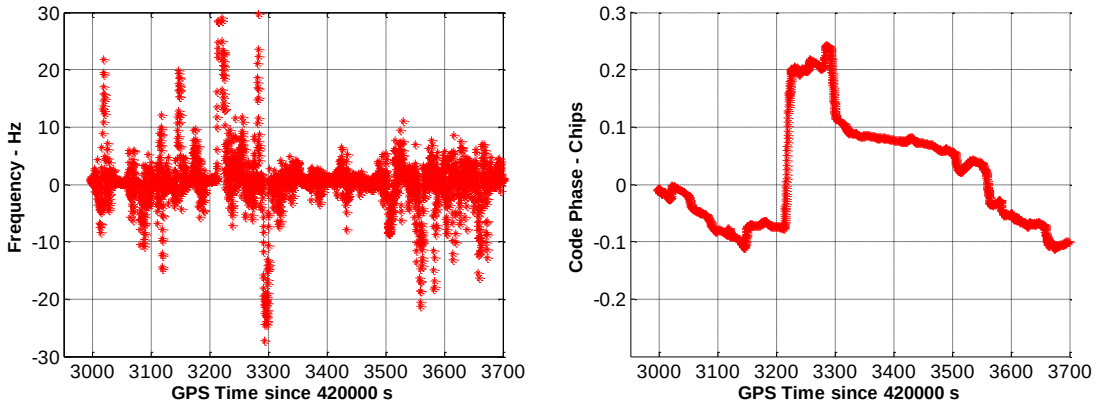

Figure 5.9: PRN 28 NCO Frequency and Code Phase Errors

To evaluate the pseudorange quality in a more efficient manner, the least-squares (LS) method is utilized in the navigation solution to evaluate the measurements quality. Note that a Kalman filter is still used within the receiver when operating in vector mode, however, the measurements are processed separately using LS. The reason for this is that LS is more sensitive to variations in the location of identified LOS peak. In other words, if a multipath peak is falsely identified as a LOS peak, the position errors from the LS method will be more adversely affected than the

Kalman filter. As such, the LS approach is useful for assessing the overall performance of the tracking algorithm without additional filtering of the resulting measurements.

Figure 5.10 shows the performance of the LS method (blue dot), indicating that the pseudorange errors are quite large; producing position errors of over 100 m in some cases (the reference trajectory is shown in red). Position errors are more than 100 m during the period of 423186.8 s to 423220.0 s (which corresponds to 600 m East and 420 m North in Figure 5.10, and this position variation can also be observed in Figure 5.5). This is due to strong multipath peaks observed for several satellites and identified as the LOS peaks.

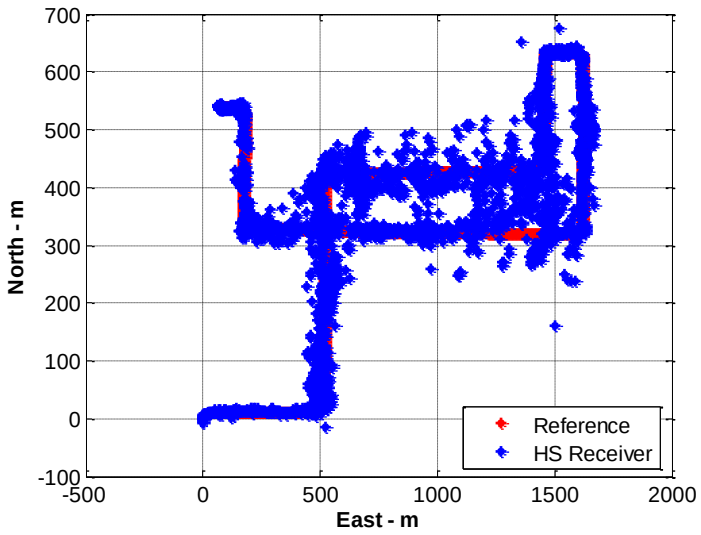

Figure 5.10: Position Performance for 200 ms Coherent Integration Time using Least-Squares Estimation

Figure 5.11 shows the correlation map from PRN 28 at the epoch of 423186.8 s where several signal peaks are observed (see projection onto frequency axis in red). The multipath peak (*i.e.*,

strongest peak, with -0.17 code phase offset) is utilized in the dominant scheme, and consequently, more than 100 m position error is introduced in the receiver.

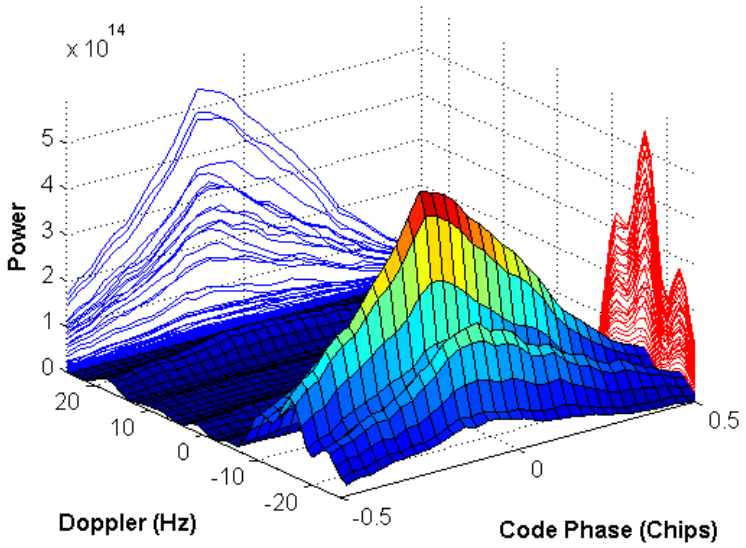

Figure 5.11: Correlation Map of PRN 28 at the epoch of 423186.8 s

Now the method introduced in section 5.2 is applied to assess the pseudorange and Doppler measurement qualities. Figure 5.12 shows the Doppler errors and pseudorange errors of PRN 4. Doppler errors are generally close to zero and pseudorange errors are generally less than 10 m, however, in extreme epochs these reach 40 Hz and 150 m respectively. When traveling North-South (e.g., from 423100 s to 423160 s), measurements errors are smaller than when traveling East-West (e.g., from 423180 s to 423270 s). This can be explained by satellite azimuth being close to 180 degrees, causing the LOS signal to be largely blocked or attenuated by high buildings when travelling in an East-West direction. In some cases, the pseudorange error is observed to be as large as 150 m when the receiver is close to high buildings. In the dominant peak strategy, all of these multipath peaks are used in the navigation filter. As a result, large position and velocity variations are expected.

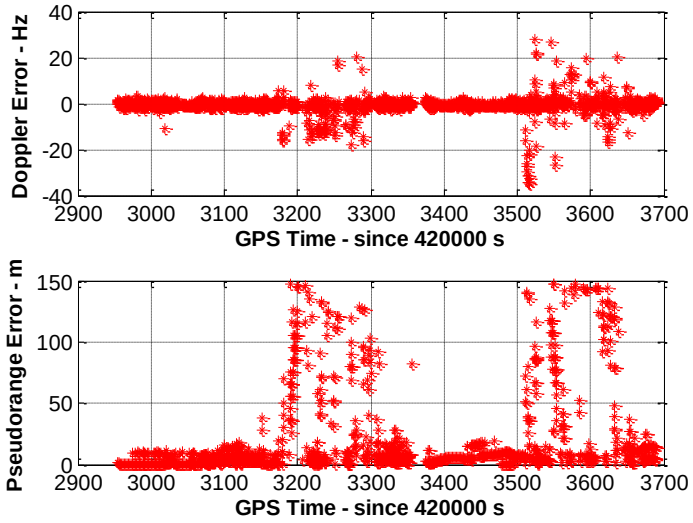

Figure 5.12: PRN 4 Pseudorange and Doppler Errors for 200 ms Coherent Integration Time by using Dominant Peak Strategy

Figure 5.13 shows the pseudorange and Doppler errors of PRN 28. Large pseudorange errors were observed more uniformly throughout the dataset as the satellite azimuth is 114 degrees. Specifically, the LOS signals were blocked by buildings most of the time as the majority of traveling was done in West-East and South-North directions. During the period from 423020 s to 423060 s the Doppler errors were close to zero, in contrast, the pseudorange errors were around 50 m to 70 m. This is caused by the receiver being static during that time period. In this case, the multipath peak has exactly the same Doppler as the LOS peak.

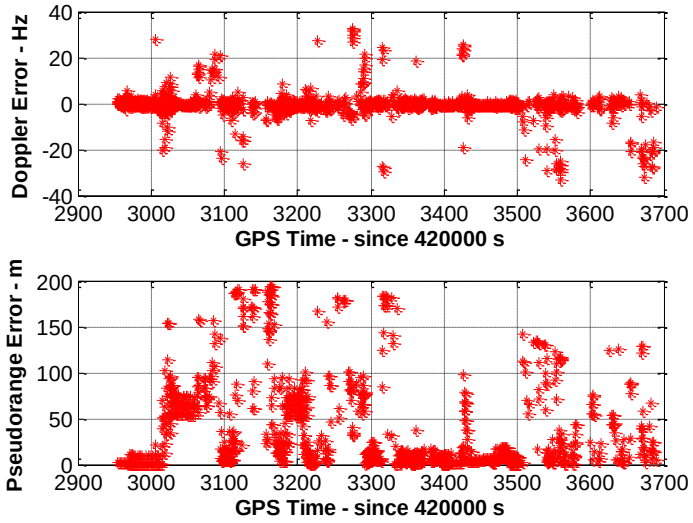

Figure 5.13: PRN 28 Pseudorange and Doppler Errors for 200 ms Coherent Integration Time by using Dominant Peak Strategy

Figure 5.14 shows the cumulative histogram of pseudorange errors (in terms of absolute value) for each satellite. Low elevation satellites (*i.e.*, PRN 12 and PRN 28) are more vulnerable to the multipath sources, and 20 percent of the pseudorange measurement errors are more than 50 m. Figure 5.15 shows the cumulative histogram of Doppler errors (in terms of absolute value) for each satellite. Usually the Doppler errors are less than 10 Hz and have less variation than the pseudorange errors. This is caused by the vehicle being static for some periods of time which produces high accuracy Doppler measurements.

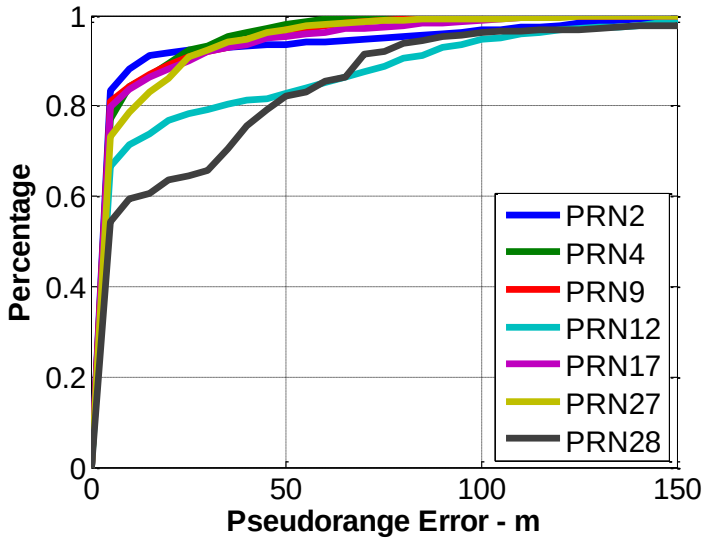

Figure 5.14: Cumulative Histogram of Pseudorange Errors for 200 ms Coherent Integration Time by using Dominant Peak Strategy

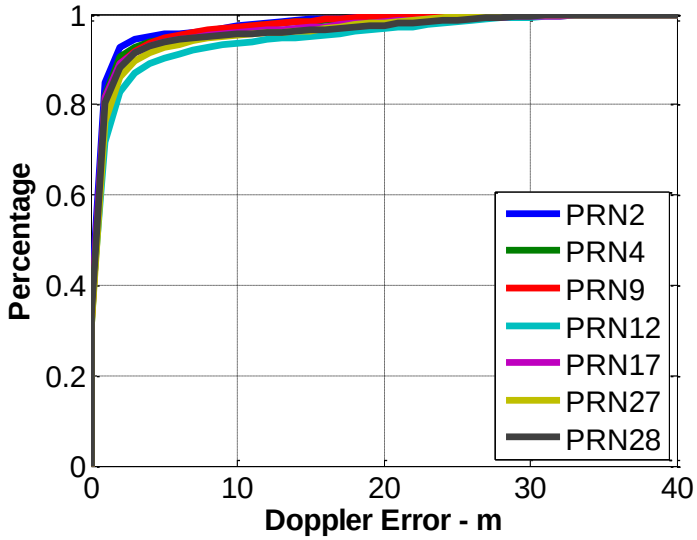

Figure 5.15: Cumulative Histogram of Doppler Errors for 200 ms Coherent Integration Time by using Dominant Peak Strategy

Table 5.3 shows the availability and reliability of measurements when using the dominant peak method. Low elevation satellites generally have poor measurement qualities (e.g., PRN 12 and PRN 28) with relatively large pseudorange errors and Doppler errors. The availability for PRN 12 is 59%, which means that only 59 percent of time the signal (either LOS signal or multipath signal) is present in the correlation map. Only 54 percent of these signal peaks are actually the LOS signals. In contrast, for the high elevation satellites (e.g., PRN 4 and PRN 17), the availability is more than 80 percent, and around 80 percent of them are the LOS signals.

Table 5.3: Measurement Quality from the Dominant Peak Strategy

Satellite	Elevation (Degree)	Pseudorange Error		Doppler Error		Availability	Reliability
		Mean (m)	STD (m)	Mean (Hz)	STD (Hz)		
PRN 2	22	-6.0	30.6	-0.4	3.4	77%	83%
PRN 4	50	-0.8	15.4	0.2	2.6	92%	80%
PRN 9	54	-0.5	18.6	-0.4	3.3	83%	78%
PRN 12	30	-26.7	45.3	0.2	5.9	59%	54%
PRN 17	53	-0.0	21.3	0.5	4.8	91%	78%
PRN 27	53	-3.6	20.6	-1.0	4.6	73%	70%
PRN 28	24	-23.4	45.0	-0.3	4.9	61%	62%

Different coherent integration times were also used and the results are summarized in Table 5.4. It is observed that 200 ms coherent integration time yields the best performance in terms of the position and velocity accuracy. It is noticed that 500 ms has degraded performance compared to the 200 ms coherent integration time, which again, demonstrates that the long coherent integration performance is degraded by the receiver dynamics and/or oscillator stability. 40 ms and 1000 ms coherent integration times also introduce large positioning errors and can be explained by the fact that for 40 ms integration time, most of the multipath signals are

overlapped with the LOS signal, thus increasing the multipath errors in the receiver. For the 1000 ms integration time, the integration performance is degraded by the receiver dynamics.

Table 5.4: Summarized RMS Position and Velocity Errors for Different Coherent Integration Times by using Dominant LOS Peak Strategy

Coherent Integration Time	Position (m)			Velocity (m/s)		
	North	East	Vertical	North	East	Vertical
40 ms	116.3	92.6	118.6	1.95	1.21	2.51
100 ms	58.4	98.0	72.9	1.45	1.29	1.51
200 ms	26.7	27.7	61.2	1.58	1.17	1.36
500 ms	76.3	135.5	113.6	1.55	1.19	1.40
1000 ms	138.5	67.6	93.9	2.01	1.62	1.51

5.4 Assumed LOS Peak Strategy

The limitations of the dominant peak strategy were shown in the previous section. Although multipath peaks can possibly be excluded by a narrow search space size, the receiver diverges due to the receiver anomalies. A wide search space size strategy can avoid the receiver divergence phenomenon, however, relatively large position and velocity errors are observed due to more multipath peaks being included in the search space. In this section, the assumed LOS peak strategy is employed to better identify the LOS peaks.

To recall, the idea behind the algorithm is to use a relatively narrow LOS region (predicted from Kalman filter covariance matrix) if no receiver anomaly is present, and a wider LOS region if an anomaly occurs. Note that the search space size remains fixed; only the LOS region is adaptively changed. Different coherent integration times are also considered in this section to assess their ability to separate LOS peak and multipath peaks.

5.4.1 200 ms Coherent Integration Time

To begin, a 200 ms coherent integration is applied to assess the assumed LOS peak strategy performance. The processing parameters used are summarized in Table 5.5.

Table 5.5: Block Processing Strategy for the Assumed LOS Peak Strategy using 200 ms Coherent Integration Time

Integration Time	200 ms	
Search Space	Doppler Domain	±30 Hz
	Code Phase Domain	±150 m
Search Step	Doppler Domain	2 Hz
	Code Phase Domain	10 m

To begin the analysis, Figure 5.16 shows the number of satellites used in the navigation filter from the GSNRx-hs™ receiver (blue) and the commercial high sensitivity receiver (red). Figure 5.17 shows the dilution of precision (DOP) calculated in the GSNRx-hs™ receiver. Most of the time the DOP values are reasonable, but increased values are periodically observed. These correspond to locations within the trajectory where satellite obscuration is most severe. GSNRx-hs™ receiver tracks more satellite than the commercial high sensitivity receiver due to different receiver strategies being applied. Usually seven to nine satellites are used in the GSNRx-hs™ receiver, but this drops to between two to four satellites where the LOS signals are highly attenuated and/or corrupted by multipath. Note that at the beginning a total of seven satellites are tracked by the GSNRx-hs™ receiver once the block processing strategy is applied, and increased to nine around the epoch 423720 s. The observations were removed in the navigation filter due to the LOS signals being absent (assumed) from these satellites. This is why the number of satellites dropped to two to four for some extreme cases, however, still seven to nine satellites were tracked by the receiver.

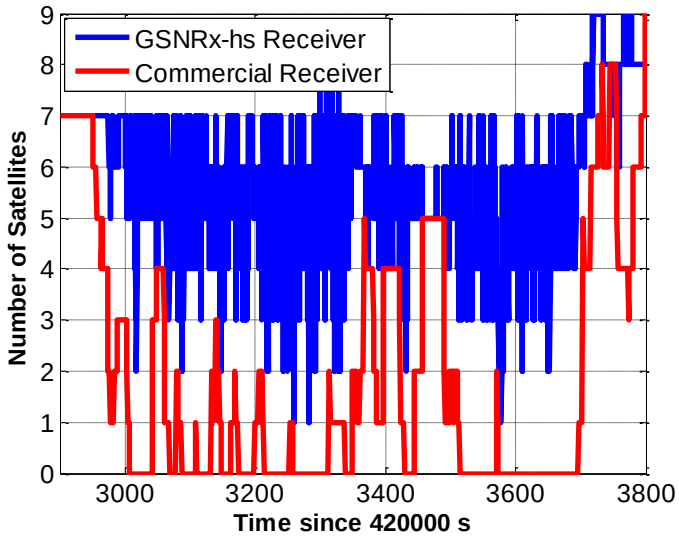

Figure 5.16: Number of Satellites used in the Navigation Filter for August 16, 2012 Data

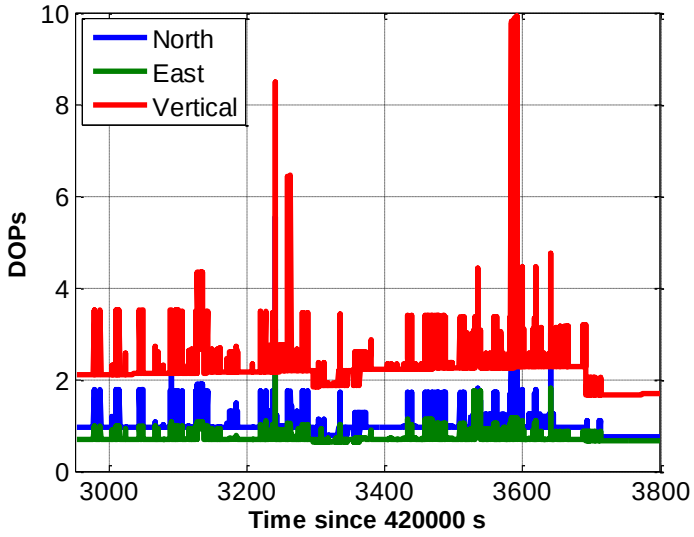

Figure 5.17: DOPs Calculated in the GSNRx-hs™ Receiver for August 16, 2012 Data

The position performance is shown in Figure 5.18 and Figure 5.19. As expected, the assumed LOS peak strategy (green line) has better performance than the dominant peak strategy (recall Figure 5.5 and Figure 5.6). The position error in the North direction reaches as much as 60 m for

the dominant peak approach but remains less than 30 m for the assumed LOS peak approach. Two other data sets show similar results, as will be shown in section 5.5. This suggests that the proposed approach successfully removes multipath peaks much of the time. In addition, the position performance from a commercial high sensitivity receiver is included for comparison purposes (yellow line), which is summarized in Table 5.6.

Figure 5.18: Position Performance of the Assumed LOS Peak Strategy for 200 ms Coherent Integration by Employing Kalman Filter (Red: Reference, Green: GSNRx-hs™ Receiver, Yellow: Commercial High Sensitivity Receiver)

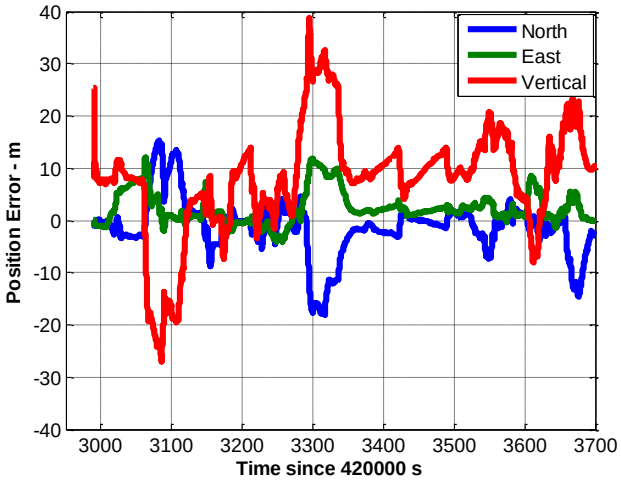

Figure 5.19: Position Performance of the Assumed LOS Peak Strategy for 200 ms Coherent Integration by Employing Kalman Filter

Figure 5.20 shows the velocity errors from the assumed LOS peak strategy. Large velocity biases (*i.e.*, receiver anomalies) are observed for several epochs, which suggests that false identification occurs (*i.e.*, multipath peak was falsely identified as the LOS peak in the receiver).

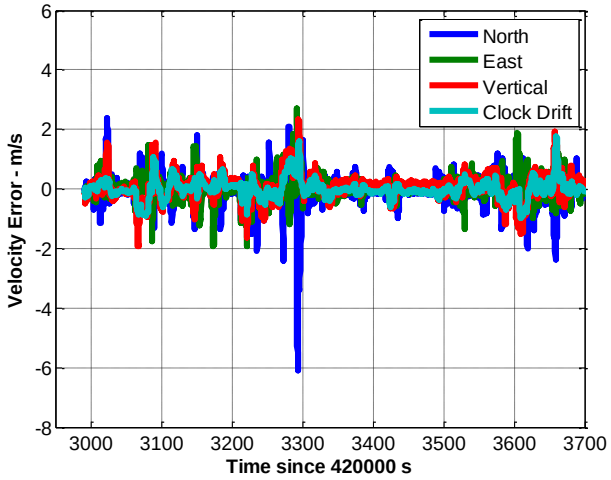

Figure 5.20: Velocity Performance of the Assumed LOS Peak Strategy for 200 ms Coherent Integration by Employing Kalman Filter

Table 5.6 summarizes the position and velocity error statistics for 200 ms coherent integration time. The performance of the commercial high sensitivity receiver and GSNRx-hs™ using the dominant peak strategy (200 ms coherent integration time) are also shown for comparison. It is observed that the position accuracy is improved substantially after using the assumed LOS peak strategy.

Table 5.6: Summarized RMS Position and Velocity Errors for 200 ms Coherent Integration Time using Assumed LOS Peak Strategy

Receiver Type	Position (m)			Velocity (m/s)		
	North	East	Vertical	North	East	Vertical
Commercial	34.9	43.4	32.3	3.32	2.92	0.65
GSNRx-hs™ Dominant Peak	26.7	27.7	61.2	1.58	1.17	1.36
GSNRx-hs™ Assumed LOS	4.1	5.6	18.5	0.44	0.37	0.46

After assessing the receiver performance in the positioning domain, more details in the tracking domain are shown in following sub-sections.

5.4.1.1 NCO Errors before Receiver Anomaly Checking

This section presents the NCO errors along with the predicted LOS regions for the comparison purposes. To address the importance of the receiver anomaly check, the LOS region predicted solely based on the Kalman filter variance-covariance matrix is shown, even though that may later be scaled as part of the LOS identification algorithm. PRN 4 and PRN 28 are selected to illustrate the predicted LOS region quality from the receiver.

Figure 5.21 shows the NCO errors and LOS regions of PRN 4 in the Doppler domain and code phase domain. The blue dots represent the predicted LOS region. The red dots show the actual

NCO errors. The latter also represent the Doppler offset and code phase offset of the LOS peak, if present. Note that true NCO values from GSNRx-ss™ receiver are utilized to generate the actual NCO errors. It is observed that NCO errors are generally smaller than the LOS region, which suggests that the variance-covariance matrix from the Kalman filter is a reasonable approximation of the position and velocity accuracy.

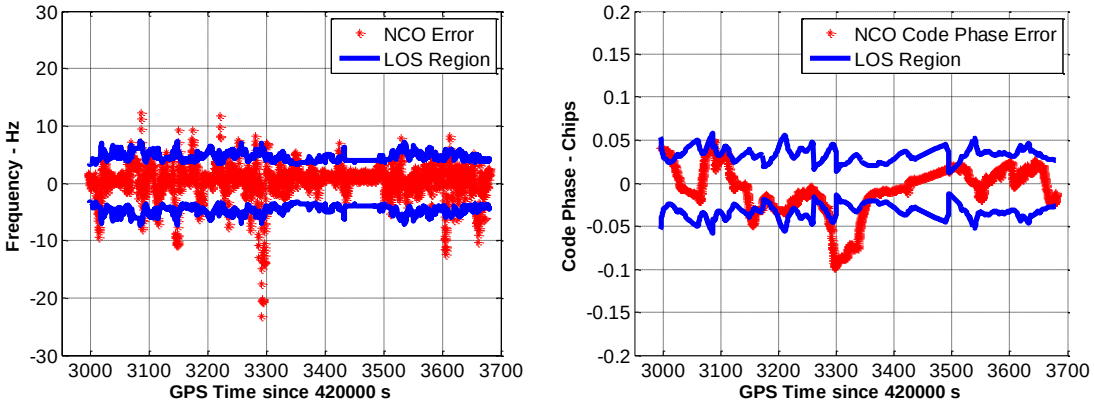

Figure 5.21: PRN 4 NCO Errors and Associated Receiver LOS Region

That said, the NCO errors are outside of the LOS region for some epochs because of receiver anomalies. This can be observed at the epoch 423293.6 s, where the North velocity error reaches 6 m/s (refer to Figure 5.20). Consequently, a 24 Hz NCO frequency error is observed for PRN 4. In other words, the LOS peak is outside of the LOS region in the Doppler domain. Thus, the LOS peak is excluded from the receiver (*i.e.*, mis-detection). This explains why it is crucial to expand the LOS region. Obviously, once the receiver anomaly is identified in the receiver, the LOS signal availability may potentially be improved.

Similar to the NCO frequency case, position errors also drive the NCO code phase outside of the LOS region in the code phase domain for some epochs. Again, it is also important to expand the

LOS region in the code phase domain to accommodate this. Note that only the LOS signal can be employed to check for a position anomaly (recall Figure 4.4 in section 4.3.1), which is different from the velocity anomaly check, where both LOS signal and multipath signals can potentially be utilized. To this extent, it is more challenging to detect the position anomaly in the receiver.

Figure 5.22 shows the NCO errors and associated LOS region in the frequency and code phase domain for PRN 28. Most of the NCO errors fall into the predicted LOS regions.

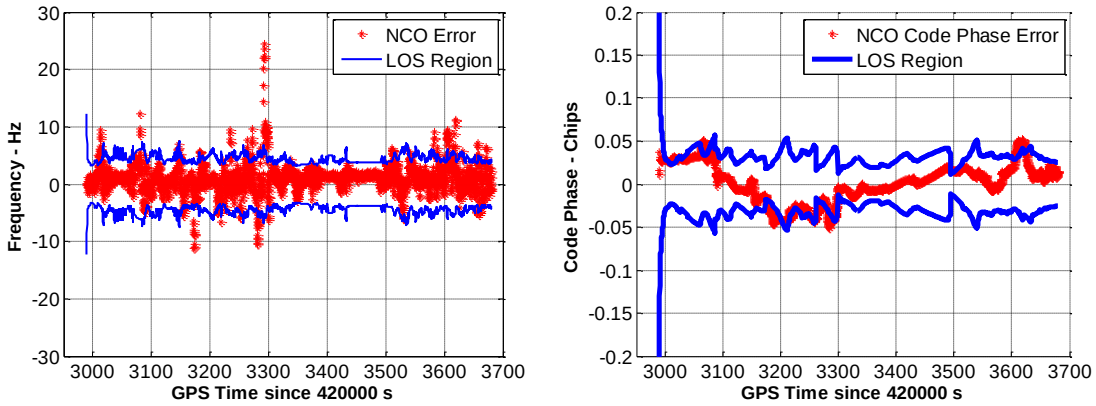

Figure 5.22: PRN 28 NCO Errors and Associated Receiver LOS Region

The predicted LOS region shown above is generally smaller than 5 Hz in the Doppler domain, and 0.05 chips in the code phase domain. In Chapter Three it was shown that only 40 percent of the multipath Doppler offsets are smaller than 5 Hz during the dynamic period. Certainly, if the predicted LOS region is implemented in the receiver, most of the multipath peaks can be removed during the peak selection process (*i.e.*, any peak outside the LOS region will be considered as a multipath peak).

Table 5.7 summarizes the number of NCO anomaly occurrences on each satellite before receiver anomaly checking is applied.. Here, the occurrence of an anomaly is determined after comparing

the receiver NCO values with the reference values (i.e., from GSNRx-ss™ receiver) in post processing. In other words, these are not the anomalies reported by the receiver itself. Totally, 3547 epochs were processed. Receiver velocity anomalies have varied effects on each satellite. NCO frequency anomalies are observed at more than 200 epochs for PRN 2, PRN 12, and PRN 28. However, they are observed fewer than 100 epochs for the rest of the constellation. This is because the satellite geometry is different for each satellite. Also, from this table it is observed that NCO code phase anomalies occur less frequently than NCO frequency anomalies.

Table 5.7: Receiver Anomalies before the Receiver Anomaly Detection

Satellite	Frequency Anomaly	Code Phase Anomaly
PRN 2	227	53
PRN 4	97	0
PRN 9	61	0
PRN 12	264	263
PRN 17	80	0
PRN 27	53	0
PRN 28	233	14

5.4.1.2 Performance of Receiver Anomaly Check

After applying the position and velocity anomaly check in the receiver, the number of remaining (or undetected) NCO frequency anomalies drops substantially. Specifically, Figure 5.23 shows the predicted LOS region of PRN 4 after the receiver anomaly check, including a rescaled version of the LOS region. Notice that the number of receiver anomaly drops due to LOS region being expanded and not due to the velocity errors being reduced. Figure 5.24 shows a zoomed-in version during the period of 423170 s to 423180 s where it is observed that after the receiver anomaly check, the LOS signals (if present) can be observed in the LOS region.

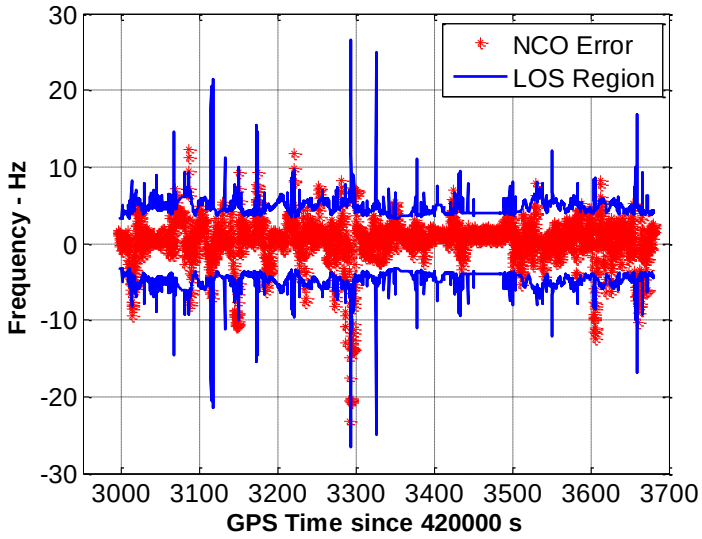

Figure 5.23: PRN 4 NCO Frequency Errors and Associated Receiver LOS Region after the Receiver Anomaly Check

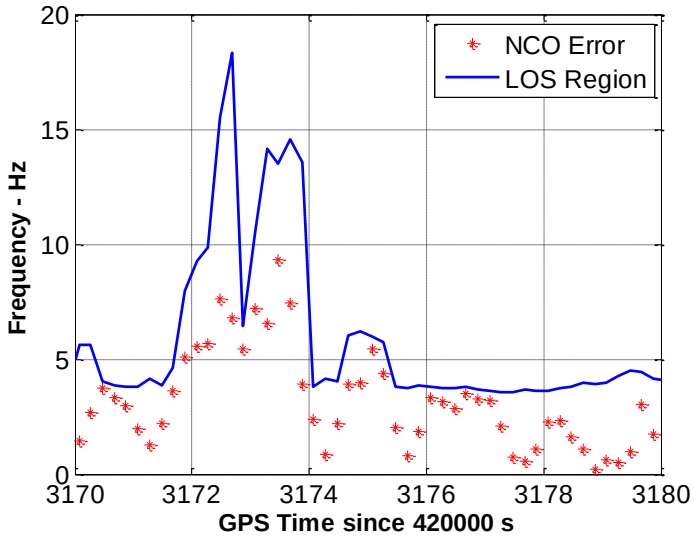

Figure 5.24: PRN 4 NCO Frequency Errors and Associated Receiver LOS Region after the Receiver Anomaly Check Zoomed-In

Figure 5.25 shows the predicted LOS region of PRN 28 after the receiver anomaly check, and Figure 5.26 shows a zoomed-in version during the period of 423075 s to 423085 s. In the latter figure, it is observed that the proposed method cannot remove the receiver anomaly completely (*i.e.*, the NCO errors were still outside of the LOS region for four epochs). This is due to the proposed method strongly relying on the satellite geometry and the observed LOS peak and multipath peaks. If the satellite geometry is not well distributed and the directional-dependence of multipath is weak, the receiver anomaly cannot be detected as reliably by this method.

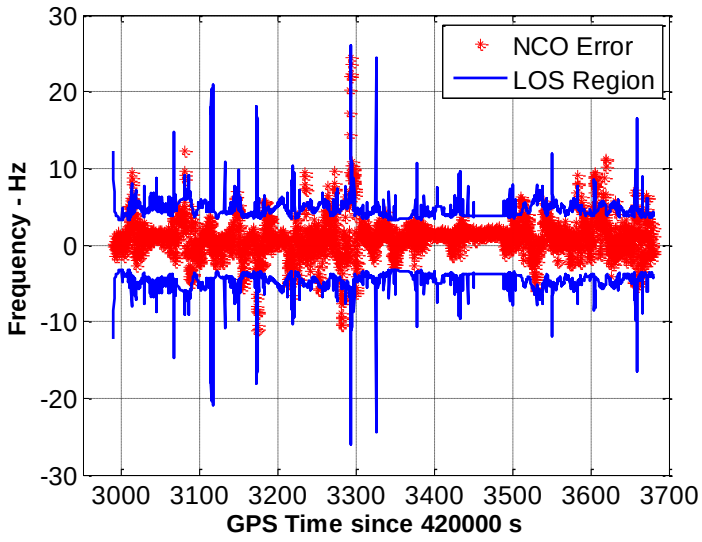

Figure 5.25: PRN 28 NCO Frequency Errors and Associated Receiver LOS Region after the Receiver Anomaly Check

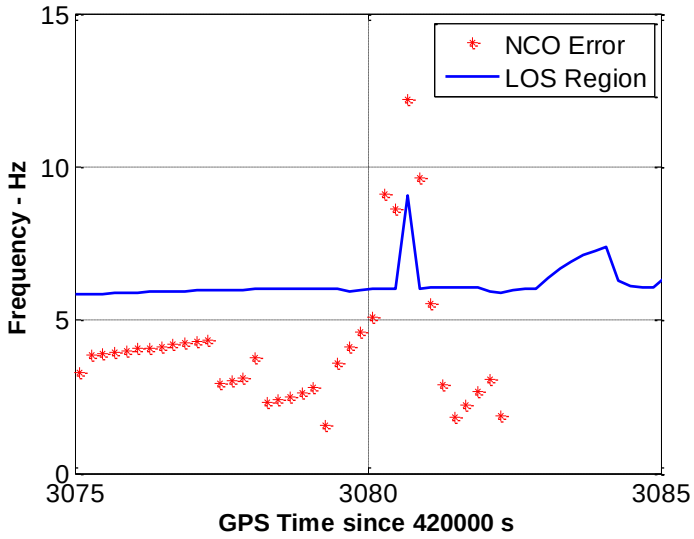

Figure 5.26: PRN 28 NCO Frequency Errors and Associated Receiver LOS Region after the Receiver Anomaly Check Zoomed-In

The reduction in the number of receiver anomalies after applying the anomaly check (i.e., un-detected receiver anomalies) is summarized in Table 5.7. It is observed that the receiver anomalies are reduced substantially. The NCO frequency anomaly for PRN 4 is decreased from 93 to 43, and for PRN 28 it is decreased from 233 to 142. Again, the receiver anomaly cannot be removed completely. No position anomaly has been reported in the receiver, thus no improvement is shown in this table in the code phase domain. There may be two reasons for this; first, only LOS peak (*i.e.*, C/N_0 is larger than 42 dB-Hz) can be utilized to check the position anomaly in the algorithm, and; position anomaly is only observed from three satellites, with 53, 263, and 14 anomalies respectively. Thus, the probability of detecting the position anomaly is low, which again, addresses the difficulty to detect the position anomaly in the receiver.

Table 5.8: Receiver Anomalies before and after the Receiver Anomaly Detection

Satellite	Frequency Anomaly		Impro-vement	Code Phase Anomaly		Impro-vement
	Before	After		Before	After	
PRN 2	227	112	51%	53	53	0%
PRN 4	97	43	54%	0	0	0%
PRN 9	61	26	57%	0	0	0%
PRN 12	264	192	27%	263	263	0%
PRN 17	80	42	48%	0	0	0%
PRN 27	53	15	72%	0	0	0%
PRN 28	233	142	39%	14	14	0%

Figure 5.27 shows the Doppler and pseudorange errors after employing the assumed LOS peak strategy for PRN 4. Compared with the dominant peak strategy case (Figure 5.12), both Doppler errors and pseudorange errors are reduced substantially. The maximum pseudorange error is reduced from 150 m to 25 m. Note that the pseudorange and Doppler measurements are not available during some periods (e.g., between 423350 s to 423375 s), because no LOS signals are identified during this period, *i.e.*, the received detects a "no signal" or a "multipath-only" epoch. Still, the Doppler errors reach as high as 15 Hz during the period 423200 s to 423210 s due to false-detection occurring.

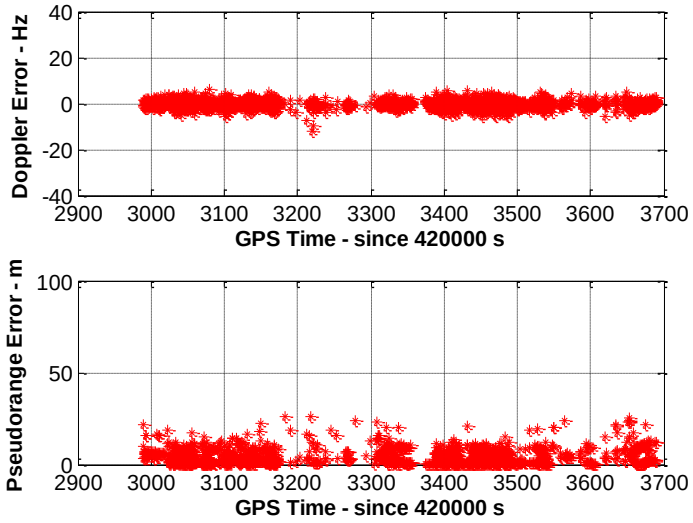

Figure 5.27: PRN 4 Pseudorange and Doppler Errors for 200 ms Coherent Integration Time by using Assumed LOS Peak Strategy

Figure 5.28 shows the Doppler and pseudorange errors after employing the assumed LOS peak strategy for PRN 28. Both accuracy and availability are degraded compared to PRN 4. This is due to PRN 28 experiencing more multipath signals and the receiver cannot reliably separate LOS and multipath peaks (*i.e.*, more multipath peaks were overlapped with the LOS peak), thus the number of measurement errors grows. Also, as with PRN 4, the results are dramatically better than in the dominant peak case (Figure 5.13).

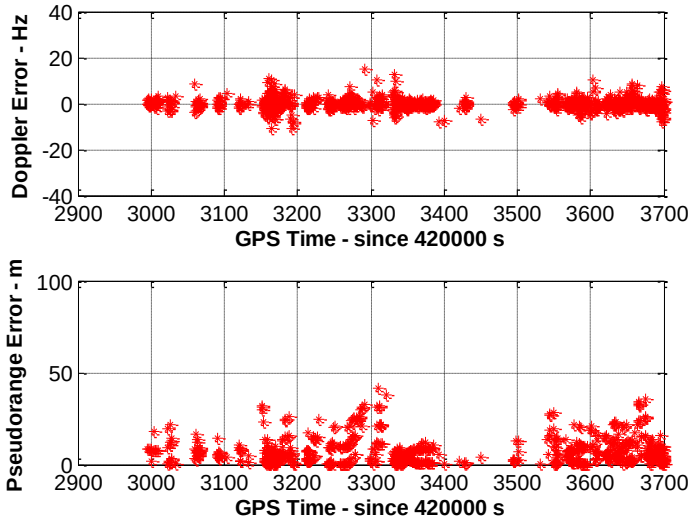

Figure 5.28: PRN 28 Pseudorange and Doppler Errors for 200 ms Coherent Integration Time by using Assumed LOS Peak Strategy

Figure 5.29 and Figure 5.30 show the cumulative histograms of the pseudorange and Doppler errors from the assumed LOS peak strategy on a per-satellite basis. Compared to the equivalent dominant peak strategy results in Figure 5.14 and Figure 5.15, the pseudorange and Doppler accuracies are improved significantly. For example, the pseudorange accuracies are improved to be less than 20 m for more than 80 percent of time for the whole constellation.

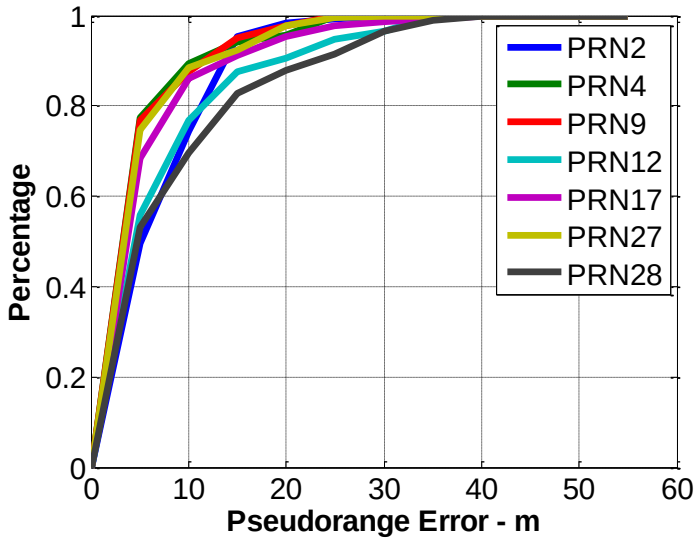

Figure 5.29: Cumulative Histogram of Pseudorange Errors for 200 ms Coherent Integration Time by using Assumed LOS Peak Strategy

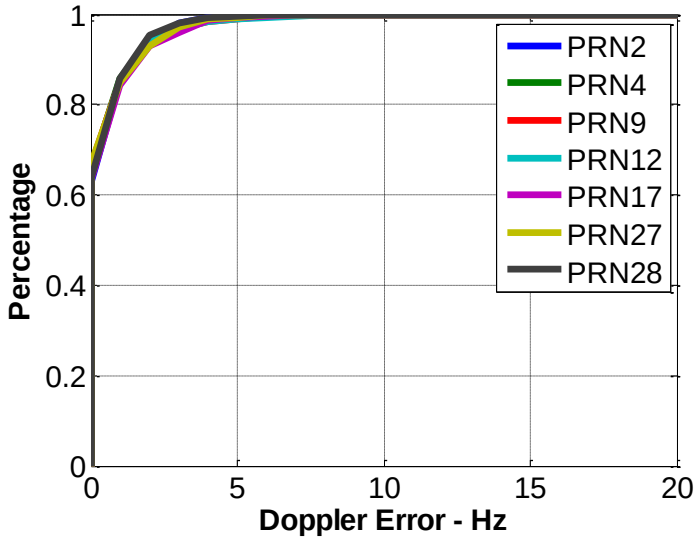

Figure 5.30: Cumulative Histogram of Doppler Errors for 200 ms Coherent Integration Time by using Assumed LOS Peak Strategy

Table 5.9 shows the peak identification performance for each satellite. Several conclusions can be drawn from this table. First, the availability is reduced substantially for low elevation satellites compared to the dominant peak strategy (recall Table 5.3). Second, as expected, high elevation satellites generally have better availability than low elevation satellite. The availability is 83% for PRN 4 with an elevation of 50 degrees, and 35% for PRN 28 with an elevation of 24 degrees. Third, the reliability of the approach is high with at least 90% of the multipath peaks being removed.

Table 5.9: Measurement Qualities from the Assumed LOS Peak Strategy

Satellite	Elevation (Degree)	Pseudorange Error		Doppler Error		Availability	Reliability
		Mean (m)	STD (m)	Mean (Hz)	STD (Hz)		
PRN 2	22	-0.6	5.8	0.0	1.3	63%	98%
PRN 4	50	-1.4	8.0	-0.1	1.7	83%	94%
PRN 9	54	-1.3	7.2	0.0	1.7	74%	94%
PRN 12	30	-1.6	9.9	0.1	1.7	33%	90%
PRN 17	53	-2.4	6.9	0.2	1.5	80%	95%
PRN 27	53	-0.3	8.4	0.0	1.6	60%	93%
PRN 28	24	0.7	8.2	0.0	1.5	35%	91%

Figure 5.31 compares the dominant peak strategy performance and the assumed LOS peak strategy performance in terms of availability and reliability percentages. Again, the reliabilities are improved significantly after employing the assumed LOS peak strategy.

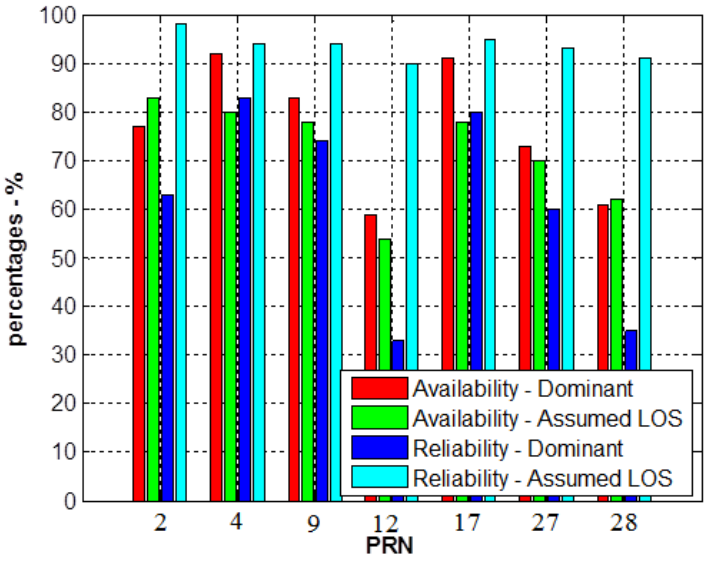

Figure 5.31: Dominant Peak Strategy and the Assumed LOS Peak Strategy Availability and Reliability Comparison

Note that although a small LOS region is applied in the assumed LOS peak strategy most of the time (recall Figure 5.23 and Figure 5.25), it is more robust than the dominant peak strategy when using a narrow search space scheme. This is because the LOS region could be expanded in the assumed LOS peak strategy.

5.4.2 Different Search Strategies

This section analyzes the high sensitivity receiver performance as a function of the coherent integration time and search space size. Table 5.10 summarizes the RMS position and velocity errors as a function of coherent integration times for a fixed search space of ±30 Hz in the Doppler domain and ±150 m in the code phase domain. As shown, 200 ms and 500 ms coherent integration times return compatible receiver performance even though 500 ms coherent integration time can potentially separate more peaks. 100 ms coherent integration has worse

performance as 60 percent of multipath peaks are overlapped with the LOS peak. Also for 1 s coherent integration time, the correlation performance is degraded by the receiver dynamics.

Table 5.10: Summarized RMS Position and Velocity Errors for Different Coherent Integration Times by using Assumed LOS Peak Strategy

Coherent Integration Time	Position (m)			Velocity (m/s)		
	North	East	Vertical	North	East	Vertical
40 ms	56.4	93.3	179.4	0.99	0.78	1.43
100 ms	24.2	7.4	58.4	0.63	0.55	0.92
200 ms	4.1	5.6	18.5	0.44	0.37	0.46
500 ms	5.2	4.7	23.0	0.53	0.49	0.47
1000 ms	30.4	19.1	55.5	1.03	1.13	0.77

Table 5.11 shows the effect of different search space sizes in the Doppler domain for 200 ms coherent integration time, note that the search space size in the code phase domain is kept to be ±150 m. Presumably, a larger search space size would have better performance as more multipath peaks can be observed to diagnose receiver anomaly. However, this is not the case for search space sizes larger than 50 Hz. This is because after expanding the search space in the Doppler domain, more cross-correlation peaks were observed in the receiver. Since the receiver was not able to remove them completely due to velocity anomalies, the cross-correlation peaks cannot be reliably predicted. ±100 Hz search space size has worse performance in terms of the position accuracy. In contrast, ±40 Hz search space has slightly better performance than the ±30 Hz case.

Table 5.11: Summarized RMS Position and Velocity Errors for Different Search Space Sizes using Assumed LOS Peak Strategy

Search Space	Position (m)			Velocity (m/s)		
	North	East	Vertical	North	East	Vertical
30 Hz	4.1	5.6	18.5	0.44	0.37	0.46
40 Hz	4.7	4.3	18.4	0.46	0.49	0.62
50 Hz	6.8	6.1	24.3	0.50	0.50	0.67
100 Hz	8.8	6.2	28.2	0.53	0.51	0.66

5.5 March 3, 2011 and August 19, 2011 Data Sets Assessment

Based on the assessment above, 200 ms coherent integration time and ±30 Hz search space size in the Doppler domain are considered reasonable settings in the assumed LOS peak strategy. Note that ±150 m search space size in the code phase domain is applied.

To further support these conclusions, a similar navigation domain analysis as shown above is also applied for the March 3, 2011 and August 19, 2011 data sets. The same strategy shown in Table 5.5 is applied. Again, a commercial high sensitivity receiver is used for comparison purposes. Position and velocity accuracies are used as a metric to assess the receiver performance.

5.5.1 March 3, 2011 Data Set

More than one hour data was collected on March 3, 2011 in downtown Calgary. The trajectory was mainly in a rectangle area and was repeated six times. The sky plot is shown in Figure 5.32, it is observed that most of the satellites were at the East-West direction. Figure 5.33 shows the receiver performance, again, the red line shows the reference trajectory, the green line shows the GSNRx-hs™ receiver performance, and the yellow line shows the commercial high sensitivity

receiver performance. High sensitivity receiver (using the assumed LOS peak strategy) outputs are almost overlapped with the reference trajectory, which suggests that the selected search space and coherent integration time work well in the urban canyon area (position and velocity performance are summarized in Table 5.12). Degraded performance is observed for the commercial high sensitivity receiver, with large variations near the high buildings when experienced vehicle dynamics.

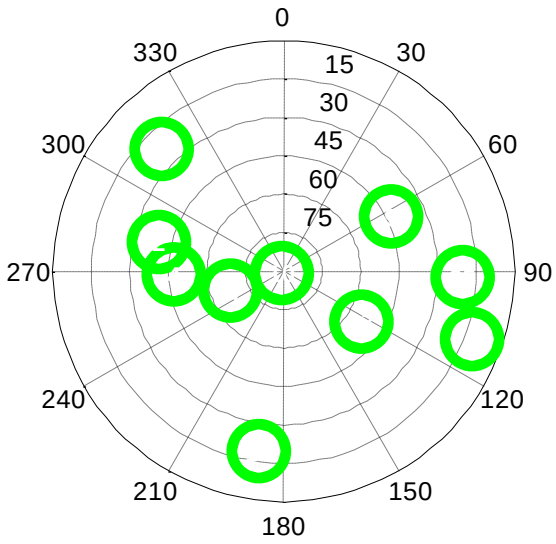

Figure 5.32: Sky-Plot of March 3, 2011 Data Set at the Start of Test

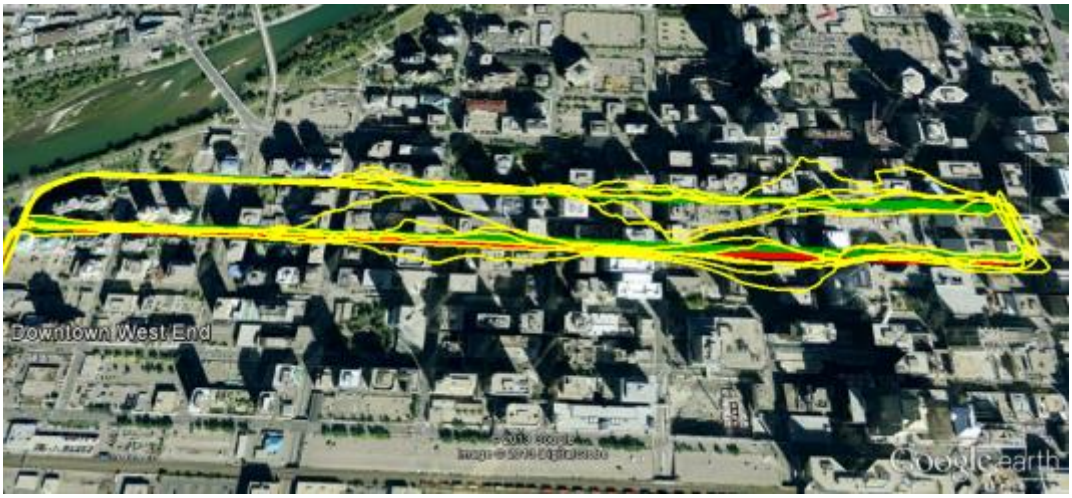

Figure 5.33: Position Performance Comparison for March 3, 2011 Data Set in the Downtown Calgary (Red: Reference, Green: GSNRx-hs™ Receiver, Yellow: Commercial HSGPS)

Figure 5.34 shows the number of satellites used in the navigation filter from the GSNRx-hs™ receiver and the commercial high sensitivity receiver. Figure 5.35 shows the DOP calculated in the GSNRx-hs™ receiver, the North DOP values are generally larger than the East DOP values as most of the satellites were distributed at East-West direction (see Figure 5.32). For the GSNRx-hs™ receiver generally six to ten satellites are used in the navigation filter. This number drops to three to four satellites where the LOS signals are highly corrupted by the surrounding buildings. A total of ten satellites are tracked by the GSNRx-hs™ receiver. Some observations are removed in the navigation filter when the LOS signals are deemed absent, so the number of satellites drops to three to four in some cases. A similar trend can also be observed from the commercial high sensitivity receiver.

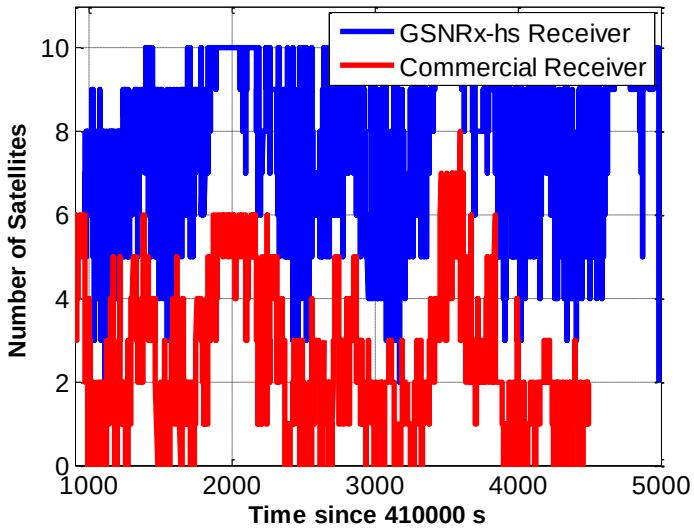

Figure 5.34: Number of Satellites used in the Navigation Filter for March 3, 2011 Data

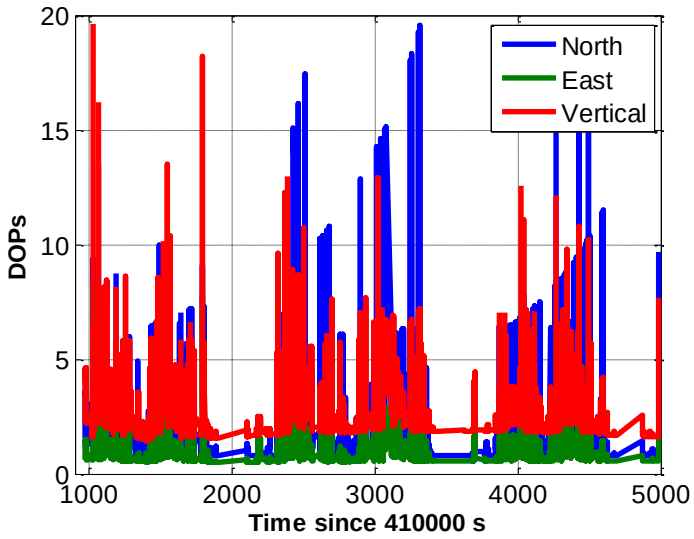

Figure 5.35: DOPs Calculated in the GSNRx-hs™ Receiver for March 3, 2011 Data

Position and velocity errors of the high sensitivity receiver using 200 ms coherent integration time is shown in Figure 5.36. The position errors are generally less than 20 m, and increased to more than 40 m for some extreme epochs. Velocity errors are generally less than 1 m/s, and jump

to 2 m/s to 8 m/s. The East direction outperformed North direction as most traveling was done in East-West direction, thus there is a higher probability of tracking the LOS signal in East-West direction.

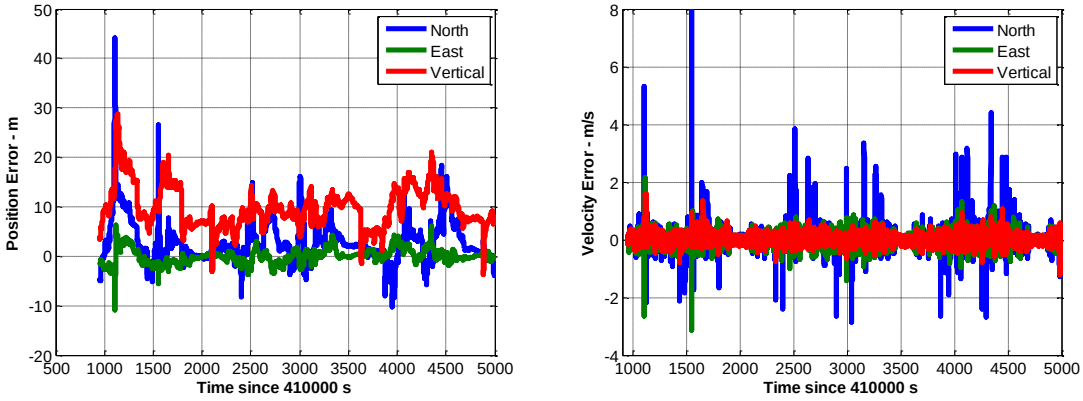

Figure 5.36: Position and Velocity Performance of 200 ms Coherent Integration Time for March 3, 2011 Data

Table 5.12: Summarized RMS Position and Velocity Errors for 200 ms Coherent Integration Time by using Assumed LOS Peak Strategy

	Position (m)			Velocity (m/s)		
	North	East	Vertical	North	East	Vertical
Commercial	18.2	7.0	13.9	1.21	0.73	1.01
GSNRx-hs™ Assumed LOS	7.2	1.6	13.9	0.47	0.21	0.20

It is worth noting that the large velocity bias in the GSNRx-hs™ receiver (*i.e.*, North velocity bias) was repeated six times in the same area. As shown in Figure 5.37, the vehicle turned a corner during these periods manoeuvring from East to South. Meanwhile, the vehicle was surrounded by high buildings blocking most of the LOS signals, thus only two to four satellites were used in the navigation filter of the GSNRx-hs™ receiver. As there were less than four

satellites used in the navigation filter, biased receiver estimates were obtained. The receiver anomaly check was applied in the receiver to expand the LOS regions and more satellites were included in the navigation filter (as more LOS signals were deemed present).

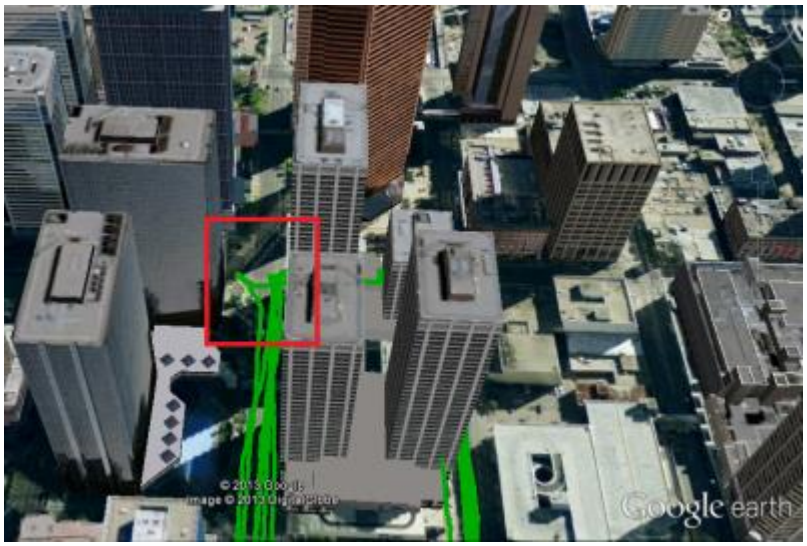

Figure 5.37: The Most Challenging Area for March 3, 2011 Data Set (shown in the red rectangle) (from Google Earth™)

Again, different coherent integration times were utilized to assess the positioning performance for this data set. The results are summarized in Table 5.13. 200 ms coherent integration time returns best performance in terms of the position and velocity accuracy. It is also acknowledged that different oscillator qualities may affect the optimal coherent integration time selection (Gaggero, 2008).

Table 5.13: Summarized RMS Position and Velocity Errors for Different Coherent Integration Times by using Assumed LOS Peak Strategy

Coherent Integration Time	Position (m)			Velocity (m/s)		
	North	East	Vertical	North	East	Vertical
40 ms	48.7	25.9	37.8	0.65	0.33	0.61
100 ms	20.8	24.8	21.2	0.42	0.29	0.39
200 ms	7.2	1.6	13.9	0.47	0.21	0.20
500 ms	18.5	5.3	18.2	0.69	0.29	0.22
1000 ms	16.5	5.3	13.5	0.83	0.99	0.26

Table 5.14 shows the performance of different search space sizes. Again, a large search space does not return better positioning performance. In this case it is because the cross-correlation peaks cannot be removed completely in the correlation map, which could be falsely identified as a LOS signal and/or a multipath signal.

Table 5.14: Summarized RMS Position and Velocity Errors for Different Search Space Sizes by using Assumed LOS Peak Strategy

Search Space	Position (m)			Velocity (m/s)		
	North	East	Vertical	North	East	Vertical
30 Hz	7.2	1.6	13.9	0.47	0.21	0.20
40 Hz	10.5	3.9	18.2	0.44	0.23	0.24
50 Hz	10.0	4.0	17.8	0.44	0.24	0.24
100 Hz	9.6	3.8	18.8	0.46	0.25	0.25

5.5.2 August 19, 2011 Data Set

Another GPS data set was collected in downtown Calgary on August 19, 2011. This data set is more challenging than the other two as the vehicle passed under more elevated pedestrian crossings (between buildings) compared to the previous two data sets. When under one of these crossings, nearly the entire sky was obscured, which is as shown in Figure 5.38.

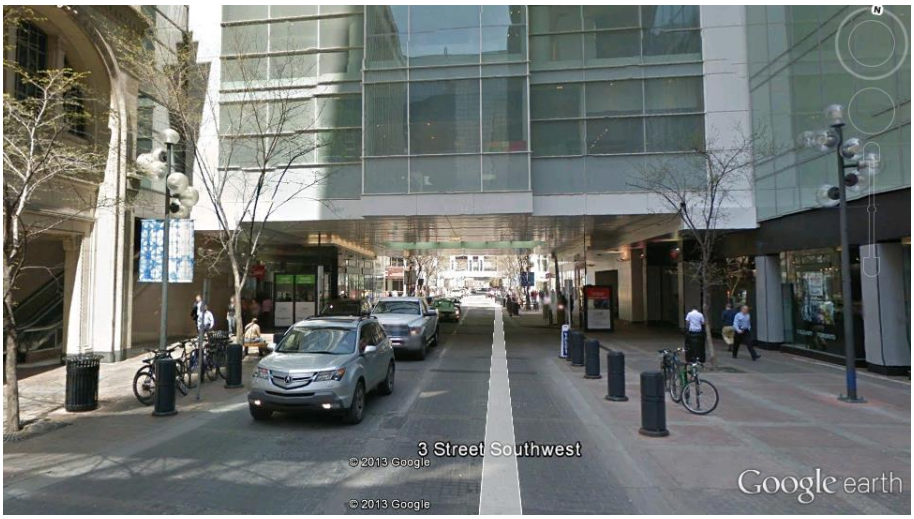

Figure 5.38: Elevated Pedestrian Crossing where Nearly the Entire Sky was Obscured (from Google Street View)

Figure 5.39 shows the high sensitivity receiver performance. As before, the red line shows the reference trajectory, the green line shows the GSNRx-hs™ high sensitivity receiver performance, and the yellow line shows the commercial high sensitivity receiver performance.

Figure 5.39: Position Performance Comparison for August 19, 2011 Data Set in the Downtown Calgary (Red: Reference, Green: GSNRx-hs™ Receiver, Yellow: Commercial HSGPS)

Position and velocity performance of high sensitivity receiver using 200 ms coherent integration time and ±30 Hz search space is shown in Figure 5.40, degraded performance is observed compared to the previous two data sets in that the vertical position error increased to 80 m for some extreme epochs. At these times the vehicle was under the elevated pedestrian crossing and no LOS signals were available, thus the receiver solely relied on the prediction in the Kalman filter and large position and velocity errors were obtained (*i.e.*, receiver anomaly introduced). Table 5.15 summarizes the position and velocity errors for the GSNRx-hs™ receiver and the commercial high sensitivity receiver.

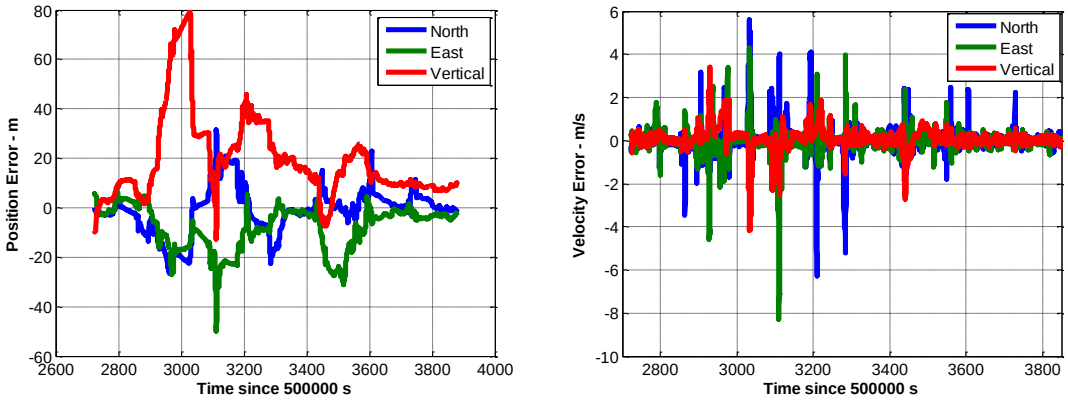

Figure 5.40: Position Performance of August 19, 2011 Data Set, 200 ms Coherent Integration, 30 Hz Search Space

Table 5.15: Summarized RMS Position and Velocity Errors for 200 ms Coherent Integration Time using Assumed LOS Peak Strategy

	Position (m)			Velocity (m/s)		
	North	East	Vertical	North	East	Vertical
Commercial	19.0	12.2	36.3	0.89	0.58	0.18
GSNRx-hs™	10.2	17.0	36.4	0.76	0.67	0.62

5.6 Dense Foliage and Sub-urban Areas

As shown in the previous sections, improved performance was obtained in the urban canyon environment after applying the assumed LOS peak strategy in the high sensitivity receiver. In this section, data sets collected under dense foliage and in sub-urban areas are used to verify the effect of the assumed LOS peak strategy in more benign environments. Different coherent integration times are also employed. Figure 5.41 shows the dense foliage and suburban test environments. During the dense foliage period the signal was degraded by the tree crowns, and for the suburban area the signal was affected by the commercial three- to four-story buildings.

Figure 5.41: Dense Foliage (left) and Suburban (Right) Test Environments

5.6.1 Dense Foliage

Figure 5.42 shows the sky plot during the dense foliage data collection where a total of eight satellites were tracked. Figure 5.43 shows the signal tracking performance in the dense foliage area, as well as the cumulated carrier to noise ratio (C/N_0) (selected six satellites were shown). Four satellites have high elevation angles and the other two satellites have low elevation angles.

The C/N_0 estimates from high elevation satellites are much stronger than the urban canyon area, which is normal as the dense foliage cannot block signals completely.

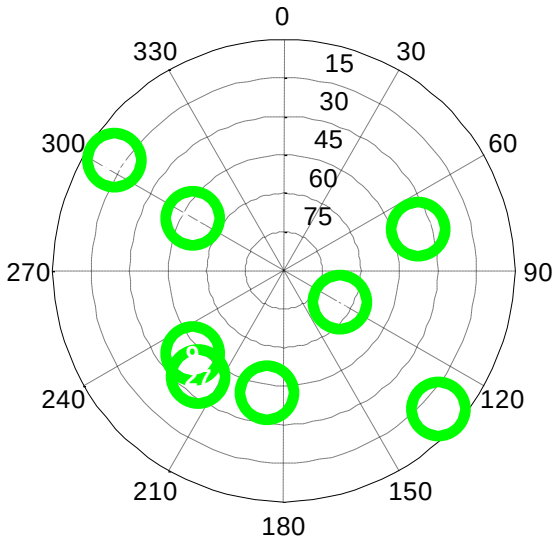

Figure 5.42: Sky Plot at the Start of the Dense Foliage Period

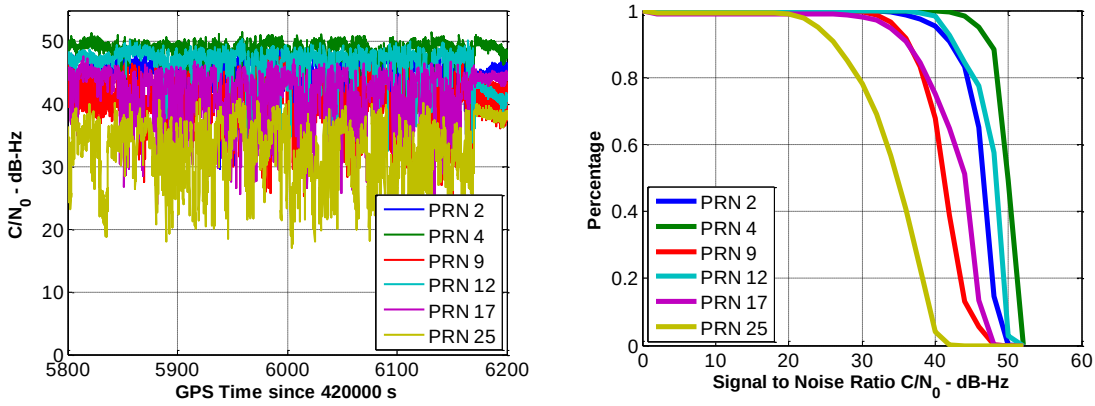

Figure 5.43: C/N_0 Estimates during the Dense Foliage Environment from the High Sensitivity Receiver

Multipath distribution in the dense foliage is also evaluated as shown in Figure 5.44. The multipath code phase offsets are smaller than the urban canyon area (revisit Figure 3.9). This can be explained by the fact that the reflectors are leaves, branches and low buildings surrounding the vehicle close to the receiver. In this regard, the long path delay (e.g., longer than 0.2 chip) is very rare.

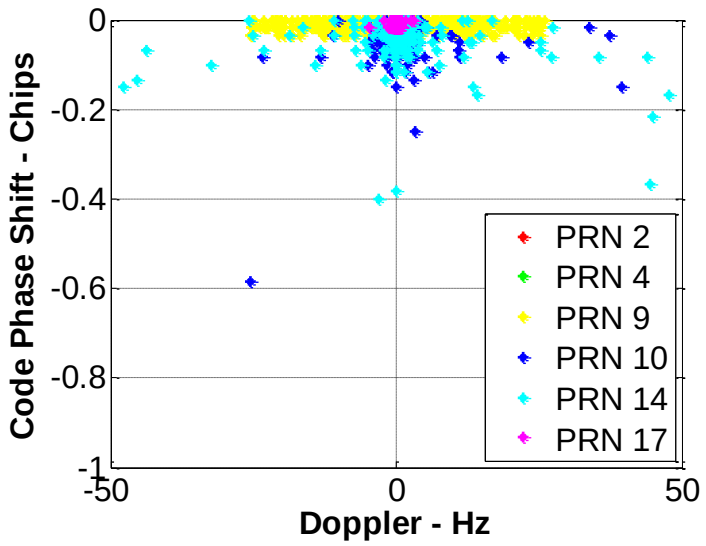

Figure 5.44: Multipath Distribution in the Dense Foliage Area

Figure 5.45 shows the high sensitivity receiver performance; the red line shows the reference trajectory, the green line shows the GSNRx-hs™ high sensitivity receiver performance, and the yellow line shows the commercial high sensitivity receiver performance. GSNRx-hs™ outputs are almost overlapped with the reference trajectory, which suggests that the assumed LOS peak strategy works well in the dense foliage area. The commercial high sensitivity receiver experienced large position variations. The position and velocity errors of the GSNRx-hs™ high sensitivity receiver are shown in Figure 5.46.

Figure 5.45: Position Performance Comparison for Dense Foliage Data Set (Red: Reference, Green: GSNRx-hs™ Receiver, Yellow: Commercial High Sensitivity Receiver)

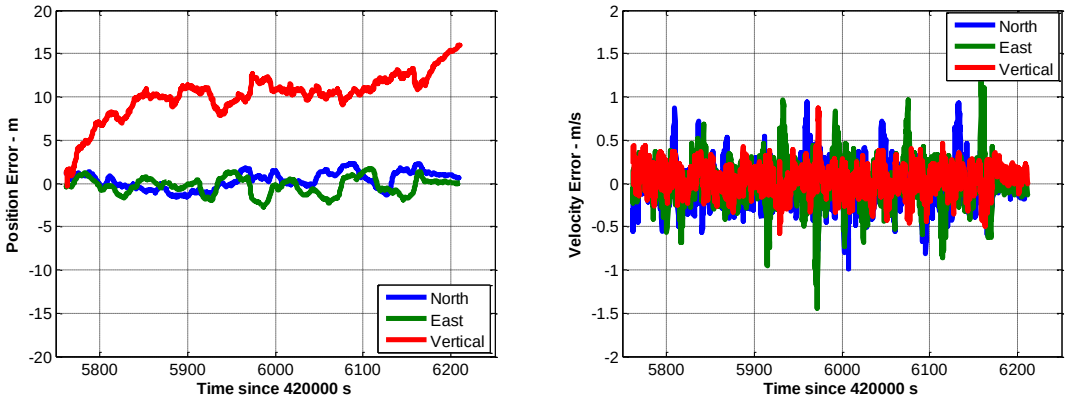

Figure 5.46: Receiver Performance of the Assumed LOS Peak Strategy for 200 ms Coherent Integration by Employing Kalman Filter

Table 5.16 summarized the position and velocity errors for the GSNRx-hs™ receiver and the commercial high sensitivity receiver. The GSNRx-hs™ receiver outperforms the commercial high sensitivity receiver in terms of the position and velocity accuracies.

Table 5.16: Summarized RMS Position and Velocity Errors for Dense Foliage Environment

	Position (m)			Velocity (m/s)		
	North	East	Vertical	North	East	Vertical
Commercial	46.7	26.5	43.5	0.91	0.72	0.58
GSNRx-hs™ Assumed LOS	1.3	0.7	12.7	0.23	0.26	0.21

Figure 5.47 shows the NCO frequency and code phase errors during the dense foliage area for a high elevation satellite (PRN 4) and a low elevation satellite (PRN 17). It is observed that the NCO frequency errors for both PRN 4 and PRN 17 are less than 5 Hz for the whole period, and the NCO code phase errors are less than 0.05 chips (~15 m), which is much less than in the urban canyon environment. These results are expected as the velocity errors are less than 0.5 m/s most of the time and the position accuracies are better than 10 m. However, it is also observed that the NCO frequency errors jump to 10 Hz for over three to four seconds for PRN 17. Again, this is due to the velocity anomalies inducing biases in the nominal parameters.

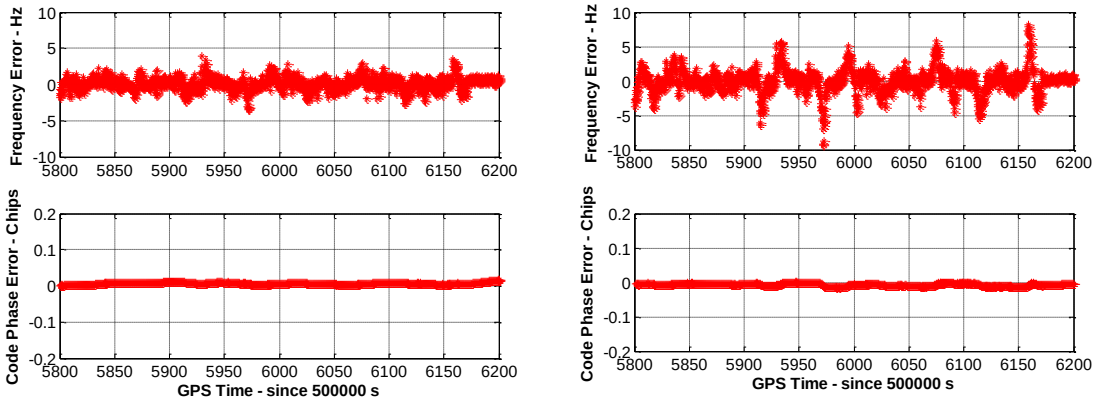

Figure 5.47: NCO Errors of PRN 4 (Left) and PRN 17 (Right) during the Dense Foliage Period

Table 5.17 shows the position and velocity performance for varied coherent integration times. 200 ms and 500 ms coherent integration times return compatible performance in terms of the

RMS accuracy. However, longer the coherent integration time does not guarantee the better the navigation performance, which is consistent with earlier results.

Table 5.17: Summarized RMS Position and Velocity Errors for Different Coherent Integration Times by using Assumed LOS Peak Strategy

Coherent Integration Time	Position (m)			Velocity (m/s)		
	North	East	Vertical	North	East	Vertical
40 ms	3.1	6.4	21.3	0.26	0.40	1.35
100 ms	2.6	7.5	29.3	0.22	0.25	0.29
200 ms	1.3	0.7	12.7	0.23	0.26	0.21
500 ms	2.2	3.3	12.2	0.35	0.40	0.13
1000 ms	5.1	4.1	11.8	1.14	1.15	0.51

5.6.2 Suburban

Twenty minutes data were collected from the outside of urban canyon to the University of Calgary, most of the surrounding objects were low buildings of less than three floors, and residential communities. Figure 5.48 shows the sky plot during the dense foliage data collection (a total of nine satellites were tracked).

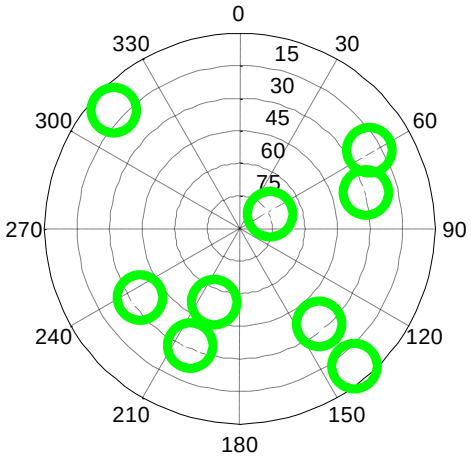

Figure 5.48: Sky Plot at the Start of the Suburban Period

Figure 5.49 shows the signal tracking performance in the suburban area, as well as the cumulative histogram of carrier to noise ratio (C/N_0) (selected four satellites were shown). The signal power is higher than the dense foliage environment due to the low buildings having less effect on the LOS signals compared to the canopies, thus LOS signals are tracked most of the time.

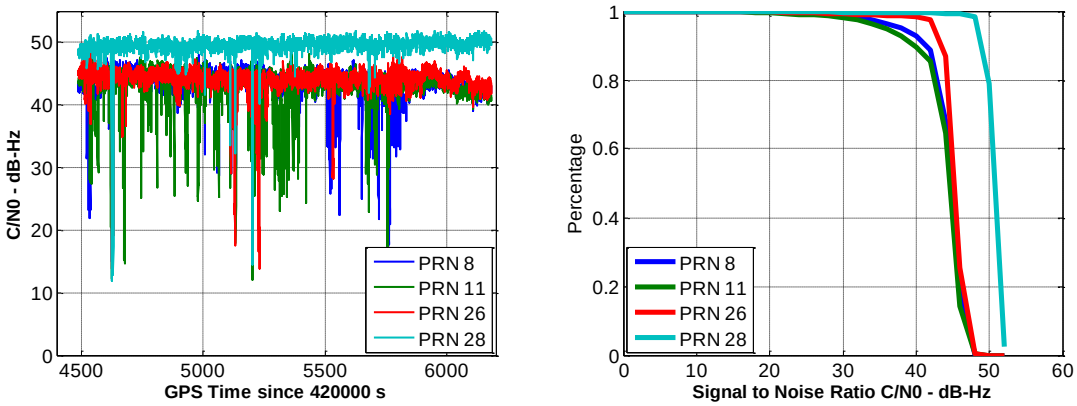

Figure 5.49: C/N_0 Estimates during the Suburban Environment from the High Sensitivity Receiver

As shown in Figure 5.50 the position errors are generally less than 8 m, and the velocity errors are less than 0.5 m/s and jump to 1.5 m/s when passing under the bridges. Table 5.16 summarizes the position and velocity errors for the GSNRx-hs™ receiver and the commercial high sensitivity receiver. GSNRx-hs™ receiver and the commercial high sensitivity receiver have compatible performance.

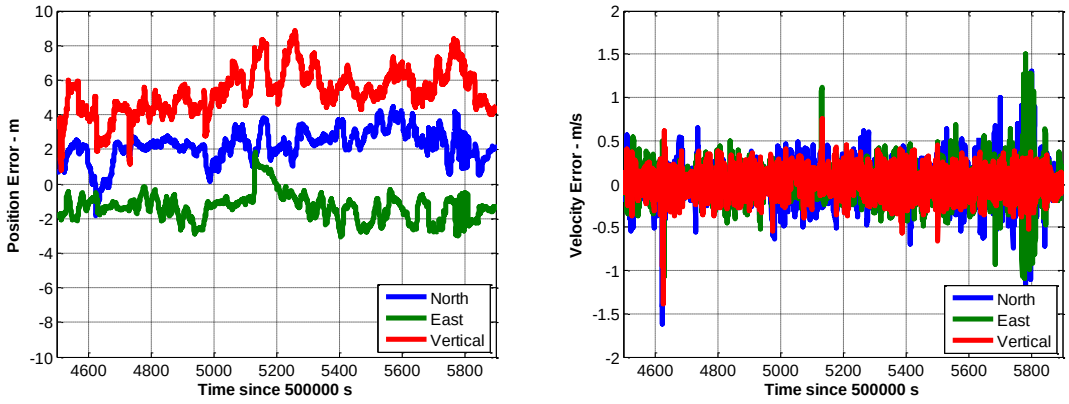

Figure 5.50: Position Performance of the Assumed LOS Peak Strategy for 200 ms Coherent Integration by Employing Kalman Filter

Table 5.18: Summarized RMS Position and Velocity Errors for Dense Foliage Environment

	Position (m)			Velocity (m/s)		
	North	East	Vertical	North	East	Vertical
Commercial	4.2	2.6	7.7	0.32	0.12	0.21
GSNRx-hs™ Assumed LOS	3.1	2.1	6.6	0.22	0.18	0.15

As position and velocity performance are better than in the dense foliage environment, the NCO errors are also smaller as shown in Figure 5.51.

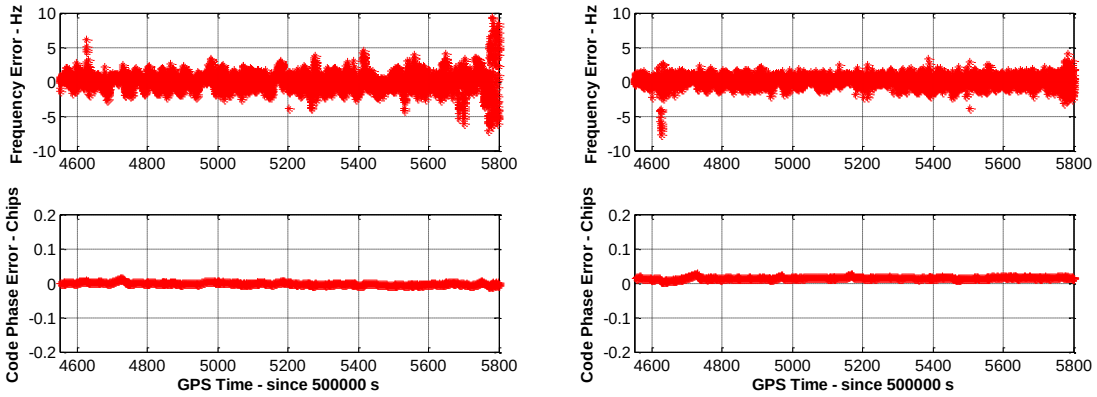

Figure 5.51: NCO Errors of PRN 8 and PRN 28 during the Dense Foliage Period

Table 5.19 shows the position and velocity performance for varied coherent integration times. 200 ms and 500 ms coherent integration times return compatible performance in terms of the RMS accuracy.

Table 5.19: Summarized RMS Position and Velocity Errors for Different Coherent Integration Times by using Assumed LOS Peak Strategy

Coherent Integration Time	Position (m)			Velocity (m/s)		
	North	East	Vertical	North	East	Vertical
40 ms	5.8	2.4	5.3	0.34	0.29	0.31
100 ms	2.5	2.2	7.6	0.17	0.11	0.15
200 ms	3.1	2.1	6.6	0.22	0.18	0.15
500 ms	3.6	2.5	6.3	0.33	0.31	0.10
1000 ms	4.9	3.6	7.5	0.84	0.89	0.22

5.7 Summary

Different receiver architectures are applied and compared in this chapter, including the standard receiver, high sensitivity receiver using dominant peak strategy, and high sensitivity receiver using the assumed LOS peak strategy. Different search strategies are applied. It is shown that the standard receiver architecture using a maximum 20 ms coherent integration time has limited

capabilities for urban canyon navigation, as expected. The dominant peak strategy using a narrow search space diverged in the urban canyon area. A wider search space offers better performance than the narrow search space strategy, but still, large position and velocity variations are observed.

High sensitivity receiver using the assumed LOS peak strategy returns better positioning performance. An empirically-optimal search strategy has been developed in this thesis for the high sensitivity receiver applications. 200 ms and ±30 Hz search space size had the best performance in terms of the position and velocity accuracies. Two data sets collected in the downtown Calgary were assessed to enhance this selection. Furthermore, the assumed LOS peak strategy works for both urban canyon and dense foliage scenarios, as well as the suburban areas.

Chatper Six: Conclusion and Future Works

This chapter provides the conclusions of the research presented in this thesis, focused on the multipath distribution calibration and high sensitivity receiver design. Recommendations for possible future work that can complement the presented results are provided.

6.1 Conclusions

6.1.1 Multipath Distribution in the Urban Canyon Environment

Multipath signals are characterized in an urban canyon scenario with application to vehicular navigation, described in Chapter Three and Chapter Four. This includes identifying the various peaks in the correlator outputs and then assessing the Doppler offsets and path delays of all LOS and multipath signals. The availability of LOS and multipath signals are also assessed. Furthermore, the multipath peaks are characterized as a function of vehicle speed and carrier to noise ratio (*i.e.*, C/N_0). Also, the directional-dependence phenomenon of multipath signals is proposed and verified by real data, and its application to detect the receiver anomaly is discussed. The main conclusions are as follows:

- The effective peak identification method introduced in this work provides reasonable performance. LOS signal and multipath signals can be identified on the correlation map.
- Higher vehicle speed can better separate the LOS peak and multipath peaks. Also, longer coherent integration time has better peak separation performance, verified by Figure 3.16.
- Multipath peak signal power can be stronger than the LOS peak, yet, most of the multipath peak powers are lower than 42 dB-Hz. Thus, an assumption is made in this research that if a signal peak power is more than 42 dB-Hz, it is a LOS peak.

- Multipath peaks are direction-dependent, so given the satellite geometry, vehicle velocity and its uncertainty, the multipath region can be predicted.
- The dominant peak and the most accurate peak are introduced in the measurement domain, and it is demonstrated that the dominant peak is not always the most accurate peak, with a percentage from 20 to 80.
- Availability of multipath peaks grows when increasing the search space size. It is more likely to obtain multipath peaks by selecting a wider search space.

6.1.2 High Sensitivity Receiver Performance

This research aims to obtain better position performance for vehicle-based high sensitivity receivers in urban canyons. Different receiver architectures are applied and compared, including the standard receiver, high sensitivity receiver using dominant peak strategy, and high sensitivity receiver using the assumed LOS peak strategy. Also, different search space strategies are applied. Conclusions from the high sensitivity receiver performance assessment are as follows:

- Standard receiver architecture using maximum 20 ms coherent integration time has limited capabilities for urban canyon navigation (less than 10 percent). This is because standard tracking loops are unable to maintain lock of the LOS signal in the urban canyon area.
- The dominant peak strategy (*i.e.*, high sensitivity receiver) using narrow search space diverged due to the search space size is not sufficiently wide to tolerate the large navigation errors to maintain a reliable tracking. A wider search space offers better performance than the narrow search space strategy, but still, large position and velocity variations are observed. It is shown that the position RMS error is close to 70 m and the velocity RMS error is close to 2 m/s.

- Using the proposed assumed LOS peak strategy returns better positioning performance. It is shown that the position RMS error is close to 20 m and the velocity RMS error is close to 0.6 m/s. A LOS region is proposed in this architecture to better identify the LOS signals from the correlation map, specifically, the LOS region is adaptively changed between a narrow size to a wide size to improve the reliability of signal tracking. It is shown that the reliability for a low elevation satellite is improved from around 60% to 90%; and for a high elevation satellite, it is improved from around 75 % to 95%. Most of the multipath signals are removed from the receiver.
- The receiver anomaly detection scheme is proposed in this research to detect receiver estimates biases based on the Doppler and code phase offsets of LOS signal and multipath signals. Improvements are shown in this thesis after applying the receiver anomaly check in the high sensitivity receiver. The undetected receiver velocity anomaly is dropped around 30% to 70%.
- Empirically-optimal search strategy has been developed in this research for the high sensitivity receiver applications. 200 ms and ±30 Hz search space size has the best performance in terms of the position and velocity accuracies. Three data sets collected in the downtown Calgary were assessed to enhance this selection. Moreover, the assumed LOS peak strategy works for both urban canyon and dense foliage scenarios, as well as the suburban areas.

6.2 Future Work

Based on the assessment and the results shown in this research, the following recommendations can be made:

- More GNSS systems can be applied in the high sensitivity. As mentioned in Chapter Two the main challenge in the urban canyon navigation is lack of satellites, thus it will be beneficial to add GLONASS, COMPASS, and Galileo in the high sensitivity receiver to improve the availability and accuracy of the GSNRx-hs™ receiver.
- Satellites with no LOS signals were removed during the LOS signal selection process, which led to less than four satellites in the navigation filter for some extreme case resulting in large solutions biases, as shown in Chapter Five. It is worth to assess performance of different navigation filter designs, e.g., keep at least four satellites in the navigation filter.
- The measurement extraction strategy can be improved as currently the Doppler and code phase are extracted from the assumed LOS peak directly. However, the measurement quality can be improved through a fitting process to better estimate the location of the LOS signal.
- This research primarily concentrated on the peak separation in the Doppler domain, and less work was done to improve the receiver performance when the LOS peak and multipath peak overlapped in the code phase domain. It is worth improving receiver performance under these conditions when those peaks overlapped in the code phase domain.
- Optimization of the proposed high sensitivity receiver can be applied to achieve the real-time applications, as currently more than 200 correlators are applied for each satellite, which cannot be fulfilled by a commercial hardware receiver design, or may require more power than would be practically feasible.

References

Ashman, B., and J. L. Garrison (2013) "Tracking of Direct and Reflected Global Navigation Satellite System (GNSS) Signals in Hubble Servicing Mission 4", in the Proceedings of the ION Pacific PNT 2013, Honolulu, Hawaii, April 23-25, 2013

Balaei, A. T., and D. M. Akos (2011) "Cross Correlation Impacts and Observations in GNSS Receivers", Journal of The Institute of Navigation, Vol. 58, No. 4, Winter 2011

Bartone, C. and F. Van Graas (1998) "Ranging Airport Pseudolite for Local Area Augmentation", in the Proceeding of IEEE PLANS, Palm Springs, CA, April 1998

Best, R. E. (2004) "Phase-Locked Loops: Design, Simulation, and Applications", 6th Edition, McGraw-Hill

Betz, J. W. and P. B. Fine (2000) "Effect of Narrow Correlator Spacing on Code Tracking Accuracy", in the Proceeding of ION NTM 2000, January 26-28, Anaheim, CA

Bhuiyan, M. Z., H., E. S. Lohan, and M. Renfors (2008) "Code Tracking Algorithms for Mitigating Multipath Effects in Fading Channels for Satellite-Based Positioning", EURASIP Journal on Advanced in Signal Processing, January 2008

Bickerstaff, J., R. Frayling-Cork, and T. Haddrell (2006) "Capture, Analysis and Mitigation of Multipath in a High Sensitivity GPS Receiver", in the Proceeding of ION/GNSS 2006, Fort Worth, TX, 26-29 September, 2006

Borio, D., C. O'Driscoll, and G. Lachapelle (2008) "Coherent, Non-Coherent and Differentially Coherent Combining Techniques for the Acquisition of New Composite GNSS Signals", IEEE Transaction on Aerospace and Electronic System, May 2008

Borio, D., C. O'Driscoll (2009a), ENGO638 Lecture Notes, Department of Geomatics Engineering, the University of Calgary

Borio, D. N. Sokolova, and G. Lachapelle (2009b) Doppler Measurements and Velocity Estimation: a Theoretical Framework with Software Receiver Implementation, in Proceeding of ION GPS GNSS, 23-25 September, Savannah, Georgia

Borre, K., D. M. Akos, N. Bertelsen, and P. Rinder (2006) "A Software-Defined GPS and Galileo Receiver", Birkhauser Boston

Brown, R. G., P. Y. C. Hwang (1996) "Introduction to Random signal and applied Kalman filtering", 3rd edition, Wiley Inc

Farrell, J. A. (2008) "Aided Navigation: with High Rate Sensors", McGraw-Hill Publications

Fenton, P., B. Falkenberg, T. Ford, K. Ng, and A. J. Van Dierendonck (1991) "NovAtel's GPS Receiver – the High Performance OEM Sensor of the Future," in Proceedings of ION GPS–91, Albuquerque, NM, September 1991, pp.49–58

Fenton, P. C. and J. Jones (2005) "The Theory and Performance of NovAtel Inc.'s Vision Correlator", ION/GNSS 2005, Long Beach, CA

Filippov, V., D. Tatarnicov, J. Ashjaee, A. Astakhov, I. Sutiagin (1998) "The First Dual-Depth Dual-Frequency Choke Ring", in the Proceeding of ION/GPS 1998

Gaggero, P. O. (2008) "Effect of Oscillator Instability on GNSS Signal Integration Time", Master Thesis, Faculty of Science Institute of Microtechnology, University of Neuchatel

Gaggero, P. O., and D. Borio (2008) "Ultra-stable Oscillators: Limits of GNSS Coherent Integration", in Proceedings of ION/GNSS 2008, September, Savannah, GA

Gardner, F. M. (2005) "Phaselock Techniques", Wiley Interscience

Garin, L., F. van Diggelen, and J. M. Rousseau (1996) "Strobe & Edge Correlator Multipath Mitigation for Code", in Proceedings of the ION GPS, September 1996, Kansa City, MO

Gelb, A. (1974) "Applied Optimal Estimation", The M.I.T. Press

Giremus, A, Tourneret, J-Y, and Calmettes, V, (2007) "A Particle Filtering Approach for Joint Detection/Estimation of Multipath Effects on GPS Measurements", IEEE Transactions on Signal Processing, Vol. 55, No. 4, April 2007

Irsigler, M. and B. Eissfeller (2003) "Comparison of multipath mitigation techniques with consideration of future signal structures," in Proceedings of the ION/GNSS, September 2003, Portland, OR

Izadpanah, A. (2009) "Parameterization of GPS L1 Multipath using a Dual Polarized RHCP/LHCP Antenna", Master Thesis, Department of Geomatics Engineering, the University of Calgary, Canada

Jones, J., P. Fenton, and B. Smith (2004) "Theory and Performance of the Pulse Aperture Correlator", NovAtel Document, 2004

Kaplan, E. D. and C. Hegarty (2006) "Understanding GPS: Principle and Applications", Second Edition, Artech House, Boston

Kiesel, S. (2008) "GNSS Receiver with Vector Based FLL-Assisted PLL Carrier Tracking Loop", in Proceeding of ION GNSS, 16-19, September, Savannah GA, pp. 197-203

Lentmaier, M., B. Krach, and P. Robertson (2008) "Bayesian Time Delay Estimation of GNSS Signals in Dynamic Multipath Environments", International Journal of Navigation and Observation, Vol. 2008, Article ID 372651

Langley, R. B. (1997) "GPS Receiver System Noise", GPS World, June 1997

Li, T., M. G. Petovello, G. Lachapelle, and C. Basnayake (2010) "Ultra-tightly Coupled GPS/Vehicle Sensor Integration for Land Vehicle Navigation", Journal of Institute of Navigation, 57, 4, 263-274

Lin, T., C. O'Driscoll, and G. Lachapelle (2011) "Development of a Context-Aware Vector-Based High-Sensitivity GNSS Software Receiver", ITM 2011, Session C4, San Diego, CA, January 2011

MacGougan, G., G. Lachapelle, R. Klukas, L.K Siu, L. J, Garin, J Shewfelt and G. Cox (2002) "Degraded GPS Signal Measurements with A Stand-Alone High Sensitivity Receiver", Proceedings of ION National Technical Meeting (NTM) 2002, January 28-30, San Diego, CA, pp 191 – 204

McGraw, G. A. and M. S. Braasch (1999) "GNSS Multipath Mitigation Using Gated and High Resolution Correlator Concepts", in Proceedings of the National Technical Meeting of the Institute of Navigation, San Diego, California, January 1999

Misra, P. and P. Enge (2006) "Global Positioning System: Signals, Measurements and Performance", 2nd Edition, Ganga-Jamuna Press

Moelker, D. J. (1997) "Multiple Antennas for Advanced GNSS Multipath Mitigation and Multipath Direction Finding", in the Proceeding of ION/GPS 97, September, Kansas City

Niu, X., S. Nasser, C. Goodall, and N. El-Sheimy (2007) "A Universal Approach for Processing any MEMS Inertial Sensor Configuration for Land-Vehicle Navigation," the Journal of Navigation, vol 60, no 2, The Royal Institute of Navigation, pp.233-245

O'Driscoll, C., D. Borio, M.G. Petovello, T. Williams and G. Lachapelle (2009) "The Soft Approach: A Recipe for a Multi-System, Multi-Frequency GNSS Receiver", Inside GNSS Magazine, Volume 4, Number 5, pp. 46-51

O'Driscoll, C., G. Lachapelle, and M. Tamazin (2011) "Dynamic Duo: Combined GPS/GLONASS Receivers in Urban Environments", GPS World, January, 2011

Parkinson, B. W. and J. J. Spilker (1996) "Global Positioning System: Theory and Applications," Vol.1, American Institute of Aeronautics and Astronautics publication, Inc.

Petovello, M. G. and G. Lachapelle (2006) "Comparison of Vector-Based Software Receiver Implementations with Application to Ultra-Tight GPS/INS Integration", in Proceedings of ION GNSS, 26-29 September, Fort Worth TX, pp.2977-2989

Petovello, M.G., C. O'Driscoll and G. Lachapelle (2008) "Weak Signal Carrier Tracking Using Extended Coherent Integration with an Ultra-Tight GNSS/IMU Receiver", European Navigation Conference 2008, Toulouse, France, 23-25 April

Phelts, R. E., and P. Enge (2000) "Multipath Mitigation for Narrowband Receivers", IEEE Position Location and Navigation Symposium, 13-16 March, San Diego, CA

Ray, J. K., M. E. Cannon, and P. Fenton (1998) "Mitigation of Static Carrier Phase Multipath Effects Using Multiple Closely-Spaced Antennas", in Proceedings of the Institute of Navigation (ION-GPS '98), Nashville, September 1998

Ray, J. K. (2000) "Mitigation of GPS Code and Carrier Phase Multipath Effects Using a Multi-Antenna System", PhD Thesis, Geomatics Engineering, University of Calgary

Ray, J. K. (2006) "What receiver technologies exist for mitigating GNSS pseudorange and carrier phase multipath", GNSS Solution

Sharp, I., K. Yu, and Y. J. Guo (2008) "Performance Analysis of Bandlimited TOA Estimation Using Peak Tracking", IEEE Vehicular Technology Conference, 2008

Sharp, I., K. Yu, and Y. J. Guo (2009) "Peak and Leading Edge Detection for Time-of-Arrival Estimation in Band-Limited Positioning Systems", The Institution of Engineering and Technology Communications, 2009

Spangenberg, M., J. Y. Tourneret, V. Calmettes, and G. Duchateau (2008) "Detection on Variance Changes and Mean Value Jumps in Measurement Noise for Multipath Mitigation in Urban Navigation", Signals, Systems and Computers, 42nd Asilomar Conference, 26-29 October, 2008

Soloviev, A and F. van Graas (2008) "Utilizing Multipath Reflections in Deeply Integrated GPS/INS Architecture for Navigation in Urban Environments", in Proceedings of ION/IEEE PLANS 2008, May 5-8, Monterey, CA

Soloviev, A., C. Toth, D. Grejner-Brzezinska (2011) “Performance of Deeply Integrated GPS/INS in Dense Forestry Areas”, in proceeding of ION/GNSS 2011, September 20-23, Portland, Oregon

Spilker, J. J. (1994) “Fundamentals of Signal Tracking Theory in Global Positioning System: Theory and Applications”, vol. I, B. W. Parkinson and J. J. Spilker, Jr., Eds.: American Institute of Aeronautics and Astronautics, Inc., 1994, pp. 245-327.

Spilker, J. J. (1996) “GPS Signal Structure and Theoretical Performance. In Parkinson, B. W., editor, Global Positioning System: Theory and Applications”, Volume 1, volume 163 of Progress in Astronautics and Aeronautics, chapter 3. American Institute of Aeronautics and Astronautics, Washington, DC.

Townsend, B. R. and P. Fenton (1994) “A Practical Approach to the Reduction of Pseudorange Multipath Errors in a L1 GPS Receiver,” in Proceedings of the 7th International Technical Meeting of the Satellite Division of the Institute of Navigation (ION-GPS ’94), vol. 1, pp. 143–148, Salt Lake City, Uyah, USA, September 1994

Townsend, B. R., D. J. R. van Nee, P. C. Fenton, and K. J. Van Dierendonck (1995) “Performance Evaluation of the Multipath Estimating Delay Lock Loop”, Navigation 42, No. 3, Fall 1995, 503 – 514

Tsui, J. (2005) “Fundamentals of Global Positioning System Receivers: A Software Approach”. Wiley, 2005

Van Dierendonck, A. J., P. Fenton, and T. Ford (1992) “Theory and Performance of Narrow Correlator Spacing in a GPS Receiver”, Navigation: Journal of The Institute of Navigation, Vol.39, No.3, Fall 1992

Van Dierendonck, A. J. (1996) “GPS Receivers,” Chapter 8: Global Positioning System: Theory and Applications, Volume 1, B. W. Parkinson & J. J. Spilker Jr., ed., American Institute of Aeronautics and Astronautics, Inc., Washington D. C.

Van Dierendonck, A.J. and M. S. Braasch (1997) “Evaluation of GNSS Receiver Correlation Processing Techniques for Multipath and Noise Mitigation”, Proceedings of the ION National Technical Meeting, Santa Monica, January 1997

Van Diggelen, F. (2009) “A-GPS: Assisted GPS, GNSS, and SBAS”, Artech House, Boston

Van Graas, F., A. Soloviev, M. Uijt de Haag, S. Gunawardena, and M. Braasch (2005) “Comparison of Two Approaches for GNSS Receiver Algorithms: Batch Processing and Sequential Processing Considerations”, in the Proceeding of ION/GPS, September, Long Beach, CA

Van Graas, F., A. Soloviev, M. Uijt de Haag, and S. Gunawardena (2009) “Closed Loop Sequential Signal Processing and Open Loop Batch Processing Approaches for GNSS Receiver Design,” IEEE Journal of Selected Topics in Signal Processing, Vol. 3, Issue 4, August 2009

Van Nee, R. D. J. (1992) “The Multipath Estimating Delay Lock Loop”, Proceedings of the IEEE 2nd Int. Symp. On Spread Spectrum Techniques and Applications, Yokohama, 1992

Van Nee, R. D. J., J. Siereveld, P. C. Fenton, and B. R. Townsend (1994) “The Multipath Estimating Delay Lock Loop: Approaching Theoretical Accuracy Limits”, IEEE Position Location and Navigation Symposium, 1994

Ward, P. W., J. W. Betz, and C. J. Hegarty (2006) “Understanding GPS: Principle and Applications”, Second Edition, Chapter 4: Interference, Multipath, and Scintillation, Artech House, Boston

Weill, L. R. (1995) “Achieving Theoretical Accuracy Limits for Pseudoranging in the Presence of Multipath”, in the Proceeding of ION/GPS, September, Palm Springs, CA

Weill, L. R. (1997) “Conquering Multipath: The GPS Accuracy Battle”, GPS World, Advanstar Communications, Eugene, OR, April 1997

Weinbach, U. N. Raziq, and P. Collier (2009) “Mitigation of Periodic GPS Multipath Errors using a Normalised Least Mean Square Adaptive Filter”, Journal of Spatial Science, 54:1, 1-13

Xie, P., M. G. Petovello, and C. Basnayake (2011) “Multipath Signal Assessment in the High Sensitivity Receivers for Vehicular Applications”, Proceedings of ION/GNSS 2011, September 18-22, Portland, OR

Xie, P. and M. G. Petovello (2012) “Improving High Sensitivity Receiver Performance in Multipath Environment for Vehicular Applications”, Proceedings of ION/GNSS 2012, September 17-21, Nashville, TN

u-blox (2010) “Dead Reckoning for Automotive Applications: Intelligent Solutions for Modern Urban Navigation”

Zarchan, P. (2005) “Fundamentals of Kalman Filtering: A Practical Approach”, Second Edition, American Institute of Aeronautics and Astronautics, Inc

APPENDIX A: Multipath Distribution of March 3, 2011 Data Set

The multipath distributions of August 16, 2012 data were shown in Chapter Three. Further to this, the data collected on March 3, 2011 is utilized to verify Equations (3.1) and (3.2) in this section. Figure A.1 shows the peak distribution in the code phase domain.

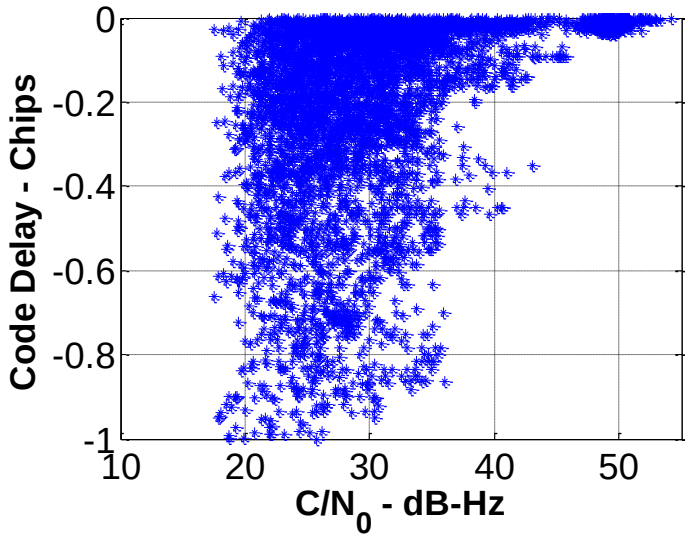

Figure A.1: Peak Code Phase Offset for Different Signal Power, March 3, 2011 Data Set

Figure A.2 shows the Doppler offsets for different signal powers of the March 3, 2011 data set, totally 12976 peaks are observed.

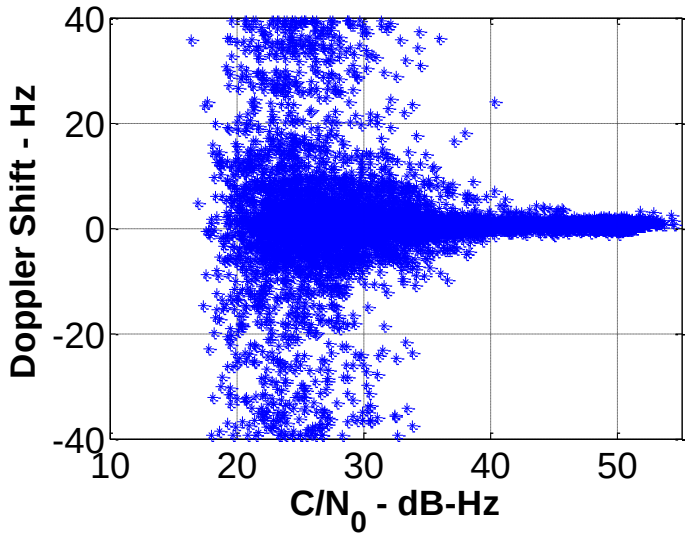

Figure A.2: Peak Doppler offset for Different Signal Power, March 3, 2011 Data Set

Figure A.3 shows the standard deviation of Doppler offsets, the same model is applied to this data set.

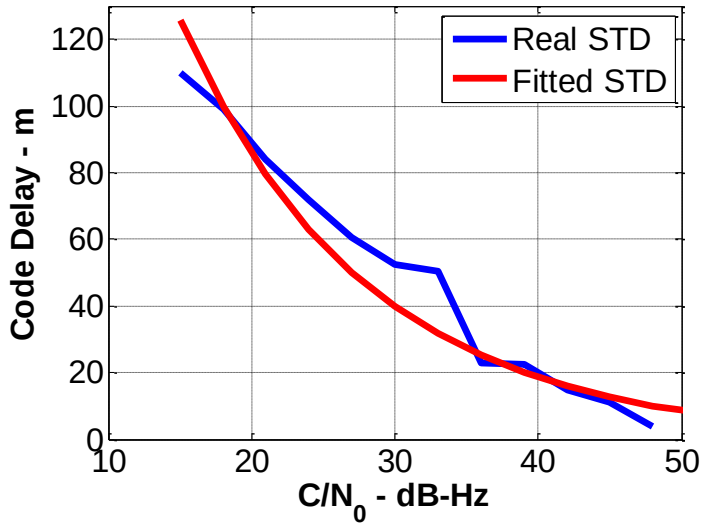

Figure A.3: Peak Code Phase Offset Standard Deviation Fitting Performance, March 3, 2011 Data Set

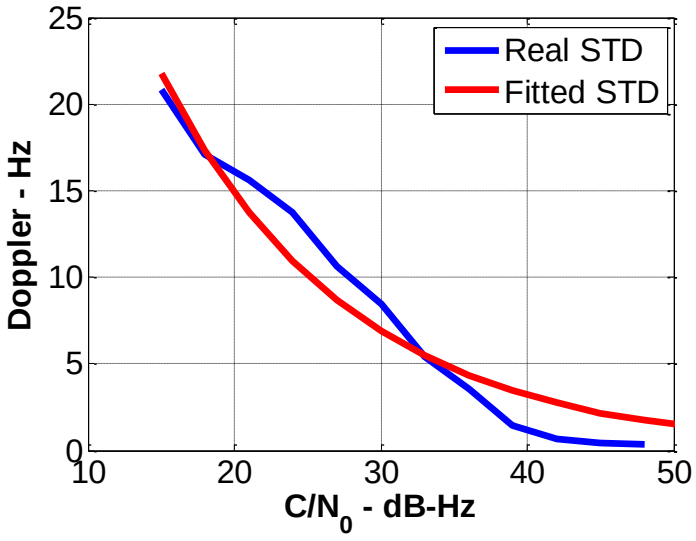

Figure A.4: Peak Doppler Offset Standard Deviation Fitting Performance, March 3, 2011 Data Set

APPENDIX B: Navigation Filter Used In The Vector-Based Strategy

The navigation filter used to close the tracking loop in the vector-based architecture, which is shown in this section. Generally, least-squares estimation technique and Kalman filter technique could be employed. However, only Kalman filter is introduced in this section, more specifically, the dynamic model and measurement model are introduced.

Dynamic model

The dynamic model is assumed to have the following model (Petovello et al 2006)

$$\begin{bmatrix} \dot{p} \\ \dot{v} \\ \dot{b} \\ \dot{d} \end{bmatrix} = \begin{bmatrix} 0_{3\times3} & I_{3\times3} & 0_{3\times1} & 0_{3\times1} \\ 0_{3\times3} & 0_{3\times3} & 0_{3\times1} & 0_{3\times1} \\ 0_{1\times3} & 0_{1\times3} & 0_{1\times1} & I_{1\times1} \\ 0_{1\times3} & 0_{1\times3} & 0_{1\times1} & 0_{1\times1} \end{bmatrix} \cdot \begin{bmatrix} p \\ v \\ b \\ d \end{bmatrix} + \begin{bmatrix} 0_{3\times3} & 0_{3\times1} & 0_{3\times1} \\ I_{3\times3} & 0_{3\times1} & 0_{3\times1} \\ 0_{1\times1} & I_{1\times1} & 0_{1\times1} \\ 0_{1\times1} & 0_{1\times1} & I_{1\times1} \end{bmatrix} \cdot \begin{bmatrix} (\omega_v)_{3\times1} \\ (\omega_b)_{1\times1} \\ (\omega_d)_{1\times1} \end{bmatrix} \tag{B.1}$$

where p : Vehicle position vector

v : Vehicle velocity vector

b , d : Clock bias and drift, respectively

I , 0 : Identity matrix and zero matrix, respectively

ω_v : Velocity process noise

ω_b : Clock bias process noise

ω_d : Clock drift process noise

The subscripts indicate the dimension of the quantity. This model assumes the velocity is a random walk process, however, higher order models may be selected for other applications.

Measurement model

The pseudorange and Doppler errors are used as the measurements in the navigation filter. The pseudorange is given by

$$\rho_i = \left(\vec{P}_S - \vec{P}_R\right)\vec{H}_{LOS} + b_R \tag{B.2}$$

The Doppler is given by

$$f_i = \frac{\left(\vec{V}_S - \vec{V}_R\right)\vec{H}_{LOS} + d_R}{\lambda} \tag{B.3}$$

The design matrix can be obtained by expanding the observation Equations (B.2) and (B.3) in a Taylor series as given by

$$H_{2i-1} = \frac{\partial z_i}{\partial P_R}, H_{2i} = \frac{\partial z_i}{\partial V_R} \tag{B.4}$$

where i is from 1 to N (the total satellite number), and z_i is either pseudorange observation ρ_i or Doppler observation f_i.